Dynamic behaviour of brain and surrogate materials under ballistic impact

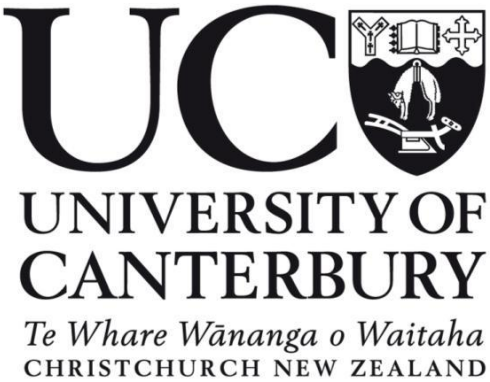

Milad. Soltanipour. Lazarjan

A thesis submitted for the degree of Doctor of Philosophy

in Mechanical Engineering

at the University of Canterbury

Christchurch, New Zealand

2015

To my parents and my brother

Acknowledgements

I would like to thank my supervisor Associate Professor. Mark Jermy for giving me the opportunity to study in such a beautiful country, it was just not possible to do all of this hard work without his guidance and positive energy. I thank my co-supervisor Dr. Michael Taylor for his support and help during the course of this study. I would also like to thank Dr. Patrick Geoghegan for his support from the first day to the last day of this research.

I would like to thank University of Canterbury Doctoral Scholarship for giving me the opportunity to study in New Zealand.

My gratitude to academic staff and technicians of the University of Canterbury at the Department of Mechanical Engineering. Special thanks to Eric Cox, Garry Cotton, and Julian Phillips for their technical assistance.

To all my friends and family all around the world. Especial thanks to Ghasem Soltanipour, Hamid Soltanipour, Hadi Irannejad, and Somam Askari, Roxana Irannejad, Razieh Ghorbani, Padina Suky, Payman Alinaghi, Nicolas Babot, Ali Nazmi for their positive energy and support. Special thanks to Dr. Pavlo Vynogradskyy from Ukraine, who taught me how to study and live.

Special thanks to my parents Abbas Soltanipour Lazarjan and Shahnaz Irannejad Rankouhi and my brother Mamad Soltanipour Lazarjan for all of their support and love in all my life.

Abstract

In the last several decades the number of the fatalities related to criminally inflicted cranial gunshot wounds has increased (Aarabi et al.; Jena et al., 2014; Mota et al., 2003). Back-spattered bloodstain patterns are often important in investigations of cranial gunshot fatalities, particularly when there is a doubt whether the death is suicide or homicide. Back-spatter is the projection of blood and tissue back toward the firearm. However, the mechanism of creation of the backspatter is not understood well. There are several hypotheses, which describe the formation of the backspatter. However, as it is difficult to study the internal mechanics of formation of the backspatter in animal experiments as the head is opaque and sample properties vary from animal to animal. Performing ballistic experiments on human cadavers is rarely not possible for ethical reasons. An alternative is to build a realistic physical 3D model of the human head, which can be used for reconstruction of crime scenes and BPA training purposes. This requires a simulant material for each layer of the human head. In order to build a realistic model of human head, it is necessary to understand the effect of the each layer of the human head to the generation of the back-spatter. Simulant materials offer the possibility of safe, well-controlled experiments. Suitable simulants must be biologically inert, be stable over some reasonable shelf-life, and respond to ballistic penetration in the same way as the responding human tissues. Traditionally 10-20% (w/w) gelatine have been used as a simulant for human soft tissues in ballistic experiments. However, 10-20% of gelatine has never been validated as a brain simulant. Moreover, due to the viscoelastic nature of the brain it is not possible to find the exact mechanical properties of the brain at ballistic strain rates. Therefore, in this study several experiments were designed to obtain qualitative and quantitative data using high speed cameras to compare different concentrations of gelatine and new composite material with the bovine and ovine brains. Factors such as the form of the fragmentation, velocity of the ejected material, expansion rate, stopping distance, absorption of kinetic energy and effect of the suction as well as ejection of the air from the wound cavity and its involvement in the generation of the backspatter have been investigated. Furthermore, in this study a new composite material has been developed, which is able to create more realistic form of the fragmentation and expansion rate compared to the all different percentage of the

gelatine. The results of this study suggested that none of the concentrations the gelatine used in this study were capable of recreating the form of the damage to the one observed from bovine and ovine brain. The elastic response of the brain tissue is much lower that observed in gelatine samples. None of the simulants reproduced the stopping distance or form of the damage seen in bovine brain. Suction and ejection of the air as a result of creation of the temporary cavity has a direct relation to the elasticity of the material. For example, by reducing the percentage of the gelatine the velocity of the air drawn into the cavity increases however, the reverse scenario can be seen for the ejection of the air. This study showed that elastic response of the brain tissue was not enough to eject the brain and biological materials out of the cranium. However, the intracranial pressure raises as the projectile passes through the head. This pressure has the potential of ejecting the brain and biological material backward and create back-spatter. Finally, the results of this study suggested that for each specific type of experiment, a unique simulant must be designed to meet the requirements for that particular experiment.

Publications Arising from this Research

Journal Papers

Published

1. Experimental investigation of the mechanical properties of brain simulants used for cranial gunshot simulation. **Lazarjan MS**, Geoghegan PH, Jermy MC, Taylor M (2014) Forensic science international Volume 239 (0):73-78. Presented in chapter 4.

2. Visualisation of the air ejected from the temporary cavity in brain and tissue simulants during gunshot wounding. **Lazarjan MS**, Geoghegan PH, Taylor MC, Jermy MC, Forensic Science International Volume 246, Pages 104–109. Presented in chapter 7.

In preparation

1. Validation of a new brain simulant material in ballistic penetration. **Lazarjan MS**, Geoghegan PH, Taylor MC, Jermy MC Presented in chapter 3.
2. Stopping distance, form and size of the permanent cavity in gelatine and bovine brain. **Lazarjan MS**, Geoghegan PH, Taylor MC, Jermy MC Presented in chapter 5.

Conference Proceedings

1. Formation of Back-Spattered Bloodstain Patterns: Air flow Visualisation and form of the Damage in a Brain Tissue Simulant (**M.S. Lazarjan**, P.H. Geoghegan, M.C. Jermy, and M.C. Taylor) 19th Australasian Fluid Mechanics Conference Melbourne, Australia 8-11 December 2014. Presented in chapter 5, 7.

2. Realistic simulant for human brain at ballistic range of impact (**M.S. Lazarjan**, P.H. Geoghegan, M.C. Jermy, and M.C. Taylor) 22nd International Symposium on the Forensic Sciences. Adelaide Australia 31th Aguest-4th Dec 2014. Presented in chapter 3, 4.
3. Feature tracking to estimate the velocity of air ejected from the temporary cavity during gunshot wounding (M.S. Lazarjan , P.H. Geoghegan , M.C. Jermy , and M.C. Taylor)17th International Symposium on Applications of Laser Techniques to Fluid Mechanics, At Lisbon, Portugal, 07-10 July, 2014. Presented in chapter 6.

4. Experimental investigation into the mechanical properties of brain simulants used for cranial gunshot simulation, and airflow ejection during collapse of the temporary cavity (M.S. Lazarjan, P.H. Geoghegan, M.C. Jermy, and M.C. Taylor) 2013 IABPA San Diego, CA, USA. Training conference October 1-4 2013. Presented in chapter 4, 6.

5. Developing a realistic simulant for human brain for cranial gunshot reconstruction Lazarjan M.S., Geoghegan P.H., Jermy M.C. Taylor M (ESR 7th Science conference 3-4 December 2013 Lincoln New Zealand). Presented in chapter 4.

6. Developing a realistic simulant for human brain during gunshot wounding. Lazarjan M.S., Geoghegan P.H., Jermy M.C. Taylor M (3rd Annual Forensic Biology Symposium G10 Frederick Street Dunedin New Zealand 13March 2013). Presented in chapter 4.

Table of Contents

List of the Figures

List of tables

1 Literature review

This chapter includes an introduction and literature review on Blood Pattern Analysis (BPA). The hypothetical mechanisms which are thought to be important to the formation of the backspatter were discussed. Moreover, fundamental theories that could help to understand the behaviour of the material at high velocity impact are presented.

1.1 Introduction

1.2 Blood stain pattern analysis and type of the blood stain pattern:

In investigation at crime scenes, an important factor to determine the scenario leading to fatality is the formation of the back-spatter and blood stain pattern (Bevel et al., 2012; Davidson et al., 2012; Kunz et al., 2013). This analysis is performed by the BPA experts at the crime scene and laboratory. Blood stain pattern can be divided in six essential types such as: dripped and splashed blood, projected blood, impact patterns, cast-off stains, expirated and transferred bloodstains (Peschel et al., 2011).

1.2.1 Essential types of the blood stain pattern:

Figure 1-1 shows different types of the blood stain pattern. Figure 1-1(A) shows an example of trail of drip stains. This indicates the direction and movement of the wounded person. Impact pattern is shown in Figure 1-1 (B), the elliptical stains shows the location of the blow. An example of the swing cast-off can be seen at the Figure 1-1(C), which shows the direction and number of the blows. Figure 1-1(D) presents blood stain pattern as a result of the gunshot. Form and size of the expirated blood stain pattern is very similar to the one generated by the gunshot.

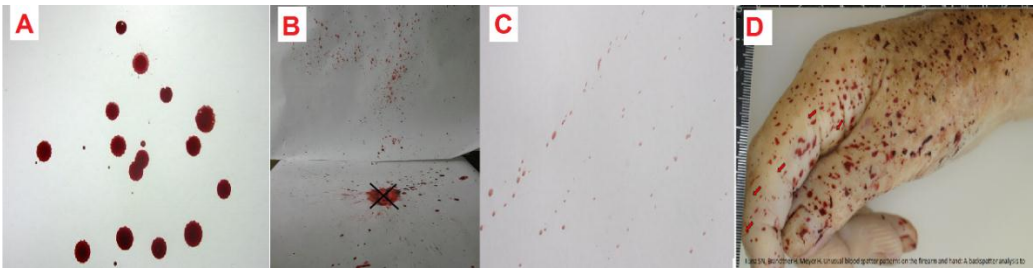

Figure 1-1: Essential types of the blood stain pattern; A-Trail of drip stain B- Impact pattern C- Swing cast-off D-Gunshot pattern (D-adapted from (Kunz et al., 2013) with permission)

Therefore, it is often possible to identify the weapon used at the scene by analysing the form, size and direction of the blood stain pattern. Also this helps to distinguish between accident, homicide and suicide (Peschel et al., 2011). All the evidence collected by the BPA experts and police which is subsequently presented at the court and must have high level of reliability, so it is really important to understand the mechanical behaviour of the material and their introduction into the formation of the back-spatter and blood stain pattern. Particularly in this study, the effect of the deformation and failure

of the brain tissue to the generation of the back-spatter as a result of cranial gunshot is studied. For ethical reasons it is obviously impossible to obtain in vivo human data from cranial gunshot wounding. It is also difficult to observe the internal mechanics in experiments with post mortem human or animal samples as the head is opaque. Therefore, it is important to replicate the human head experimentally to provide a better understanding of the mechanical response to a cranial ballistic impact .This type of information will help to build a realistic 3D model of the human head, which can be used for reconstruction of the complicated scenarios of incidents.

1.3 Hypothesised mechanisms of formation of the back-spatter:

There are three mechanisms hypothesised for the formation of the back spatter; tail splash, subcutaneous gas effect and collapse of the temporary cavity. All mechanisms are the result of the interaction of the bullet and tissues. The first mechanism is tail splash (Figure 1-2-A) as the bullet impacts the tissue, material flows in the opposite direction to the bullets penetration. This happens before the generation of the temporary cavity (Davidson et al., 2012). The second mechanism is the subcutaneous gas effect, in this mechanism occurs when the gun barrel is in contact with the target (Figure 1-2-B). As the bullet penetrates subcutaneous gas will move between skin and tissue create a cavity in between layer causing the skin to bulge. This cavity collapses in a couple of milliseconds and can move biological material towards the firearm (Davidson et al., 2012) .

The third mechanism (Figure 1-2-C) is collapse of the temporary cavity as the bullet passes through the target it creates a temporary cavity, by collapse of this cavity biological materials move towards the firearm.

Figure 1-2: A-Tail splash B-Subcutaneous gas effect C- Collapse of the temporary cavity

1.4 Background of high velocity of impact and failure of soft targets:

The damage and failure of the material under high velocity impact involves several disciplines such as: plasticity and elasticity theory, hydrodynamics, fracture mechanics, materials response to high strain rate of impact and high pressure physics (Rosenberg et al., 2012). The discipline, which covers the high velocity impacts and interaction between various types of targets and projectiles is called terminal ballistics (Rosenberg & Dekel, 2012). However, as the failure mechanism of the projectile and target depends on the velocity of the impact, some classification is required. Rosenberg and Dekel (Rosenberg & Dekel, 2012) classified the velocity into three sections: "The low velocity range (below 500 m/s), the ordnance velocity range (between 500 and 2,000 m/s) and the hypervelocity range (above 2,000 m/s)''.One of the subsection of terminal ballistics is wound ballistics, which is the study of the behaviour and effect of the bullet in a person or an animal (Kneubuehl et al., 2012). Kneubuehl et al. divided wound ballistics into three areas: hand gun bullets, bullets from long weapons and fragments, as they have different fundamental structure and energy. Fragmenting bullets are also known as hollow point or frangible bullets. This type of bullet is designed in a way that the projectile expands upon impact and stopping distance in the muscle is less compare to the rifle projectile. The form of the damage caused by the different types of the bullets are varied. Energy of the projectile can be divided into two essential types: kinetic energy and thermal energy. Kinetic energy of the projectile is the result of bullets flight energy and energy of the rotation, energy of the motion of the gases and recoil energy of the weapon (Rosenberg & Dekel, 2012). Thermal energy is the result of the heat transferred to the cartridge, friction between bullet and bore and internal energy of the gases. The literature shows that there is a complex behaviour of the material at high velocity impact and it is required to highlight that the focus of this study is on low velocity range of impact with non-deformable projectile to the soft target, which is gelatine in this section of the study. Gelatine is known to be a viscoelastic material with a shear thinning properties at room temperature. It means viscosity of the material decreases by increasing the shear strain rate. The physical response of a soft target (e.g. skin, muscle, brain or gelatine or some other tissue simulant) can be divided into four essential sections: shock wave, pressure wave, compression and tension zone and temporary and permanent cavity.

1.4.1 Shock wave, pressure wave and zone of compression and tension:

When the bullet hits the target it creates a shock wave, which passes through the target in a couple of milliseconds (yellow dots in Figure 1-3). The shock wave doesn't have a major effect compared to the damage caused by the temporary cavity. The radial displacement of the tissues at the tip of the bullet creates a pressure wave, which propagates through the tissues (Kneubuehl et al., 2012) (green section in Figure 1-3). Compression of the material happens mostly in front of the bullets path. Figure 1-3 shows the mechanical reaction of the target assuming the bullet is not experiencing any deformation. The red section in Figure 1-3 shows the zone of compression of the material as the bullet impacts. The blue section shows the section of the target, which is under tension. It must be noted that a large impact force appears as the bullet hit the target (Rosenberg & Dekel, 2012). This force first stretches the material in a radial direction relative to the bullet path, then overcomes the strength of the material and causes the material to fail and separate.

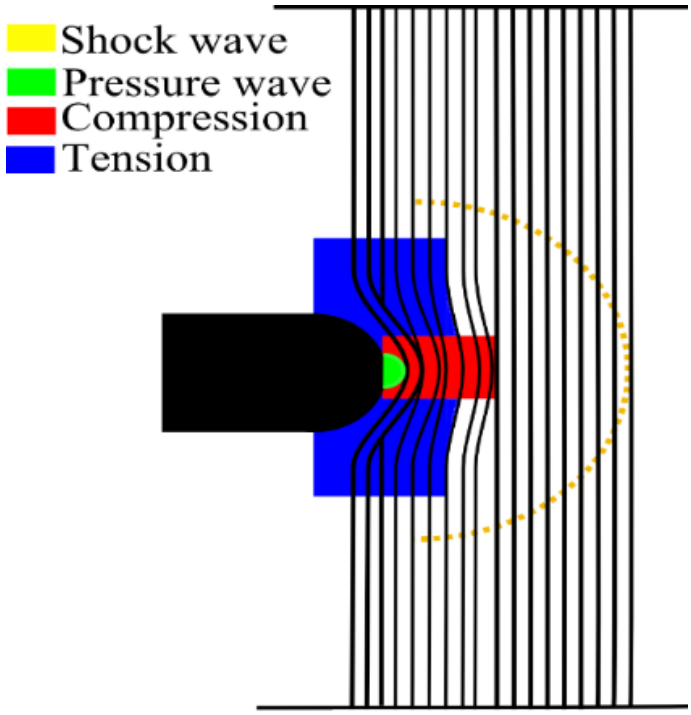

Figure 1-3: Mechanical reaction of the target: Red-compression Blue-tension

1.4.2 Formation of the temporary cavity:

Figure 1-4 (A) shows the formation of the temporary cavity in schematic form and Figure 1-4 (B) is the image of the 9 mm bullet as the bullet penetrates 10 % gelatine (w/w). When the bullet penetrates a soft target, extremely high pressure is created at the tip of the projectile. Material starts to flow towards the bullet. ‘‘The viscosity and inertia of the medium cause the flow to break away from the surface of the bullet at an early stage. It means that only a small part of the bullet’s tip is in contact with the medium’’(Kneubuehl et al., 2012). As can be seen from Figure 1-4 material flows around the bullet, and only a small part of the tip of the bullet is in contact with the material. As mentioned before gelatine is a shear thinning material and at high strain rate of deformation it become less elastic.

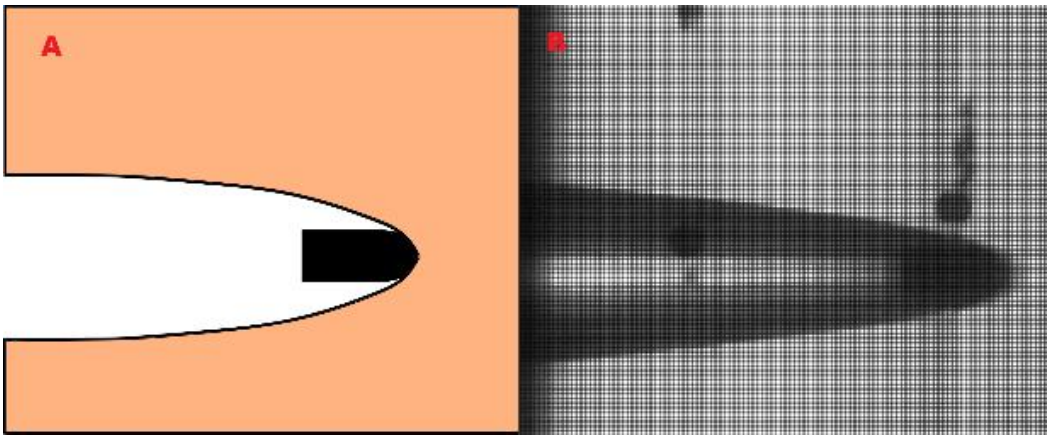

Figure 1-4: Material flows around the bullet A- sketch b- 9 mm bullet in 10% gelatine

1.4.3 Formation of the permanent cavity:

Figure 1-5 shows the schematic reaction of the 10 % gelatine as the bullet passes through a sample. The yellow section is the temporary cavity, the brown section is that part which is compressed and the temporary cavity forms and the red section is the unrecoverable material (crushed or cut). Wilson first characterised the damage caused by projectiles after the First World War He describes that the wounding effect of the projectile depends on amount of the energy transmitted to the tissue as well as the velocity of this transition and density of the tissue (Bellamy et al., 1991). However, Fackler’s (M. Fackler et al., 1984) research on 10% gelatine later shows that the form of the damage caused by the projectile depends on additional factors such as type of the bullet and form of the fragmentation of the projectile. The permanent cavity or wound track is the results of crushing and cutting the target as the

bullet passes through a soft target. The form and size of the permanent cavity depends on bullet energy, tumbling, expansion and fragmentation (M. L. Fackler, 1988; Martin L. Fackler et al., 1988). Disruption of the material depends on the elastic response of the material the size and form of the permanent cavity varies in different types of tissue. More elastic tissues such as lung, bowel wall and muscles, with elastic modulus at the higher end of the range exhibited by soft tissue, are more likely to return to their original shape as the bullet passes. A smaller fraction of the tissues will be crushed and cut compared to non-elastic solid like liver (Martin L. Fackler et al., 1988) . Also, the form of the damage in the air-filled cavities such as lung, gut and upper airway will be different due to the differences in the tissue construction. For example, the damage caused by AK-47 rifle in liver is much higher than lung and bowel (Martin L. Fackler et al., 1988). Failure behaviour of the material can be described as cutting and crushing of material. Material is cut when the total stress applied overcomes the strength of the material. The process involves in cutting can be divided in two mechanically: compression and shearing. Compression of the material can be quantified using bulk modulus (see section 1.6) and shearing properties of the material can be quantified using shear modulus (see section 1.6).

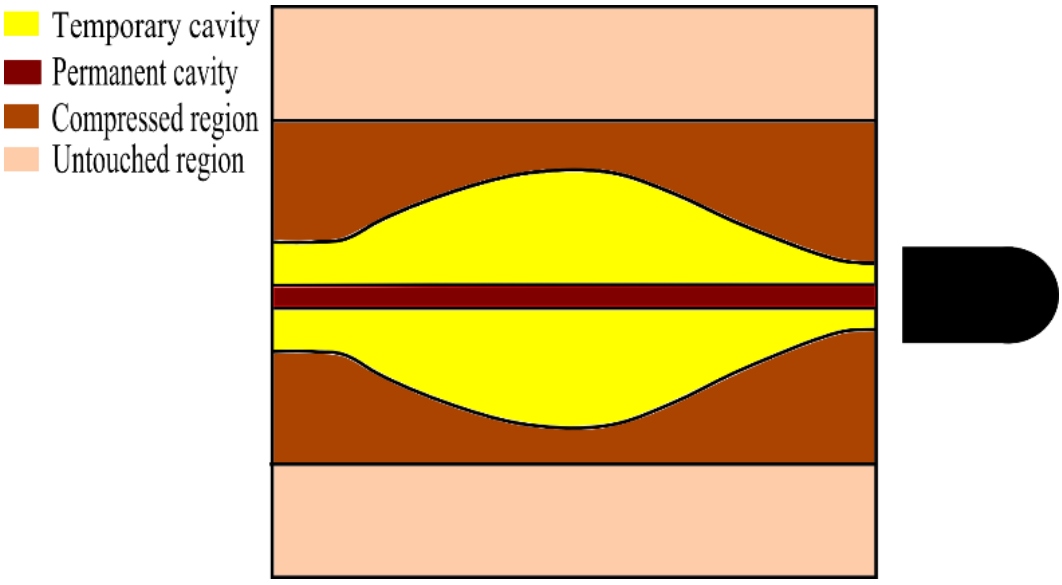

Figure 1-5: Bullets passage scheme

1.5 Anatomy of the human head:

The human head can be divided in four sections from the point of view of backspatter generation. Figure 1-6 shows the different layers of the human head from the cadaver. Scalp, Skull, Dura mater and Brain. Each of these materials has their own mechanical properties and failure mechanism.

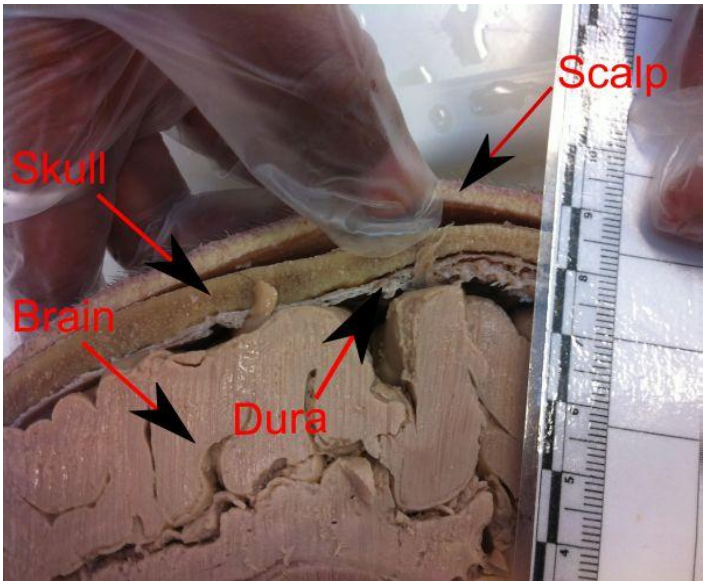

Figure 1-6: Different layers of human head (from an embalmed cadaver)

In order to find a realistic simulant to replicate the human brain at high velocity impact, it is important to know its mechanical properties and its anatomy. Like most biological tissues, brain is a viscoelastic material, which means that it exhibits both viscous and elastic properties. Its mechanical moduli are dependent on strain rate and time. As shown in Figure 1-7 from the point of view of physiology, human brain is divided in 29 sections each section has its own responsibility to control the body. The brain is one of the largest organs of human body, it composed of about 100 billion neurons and 1000 billion neuroglia. The average weight of the adult brain is about 1.3 kg (Tortora et al., 1996). The brain can be divided into four main parts: brain steam, cerebellum, diencephalon and cerebrum. The brain stem consists of the medulla oblongata, pons and midbrain, and it is connected to the spinal cord. Above the brain stem is the cerebrum, which covers the diencephalon like a cap. The cerebrum occupies most of the volume of the cranium. It has two halves (termed hemispheres), left and right (Tortora & Grabowsk, 1996). The focus of this research is on the dynamic behaviour of the cerebrum as it occupies the greater part of the cranium.

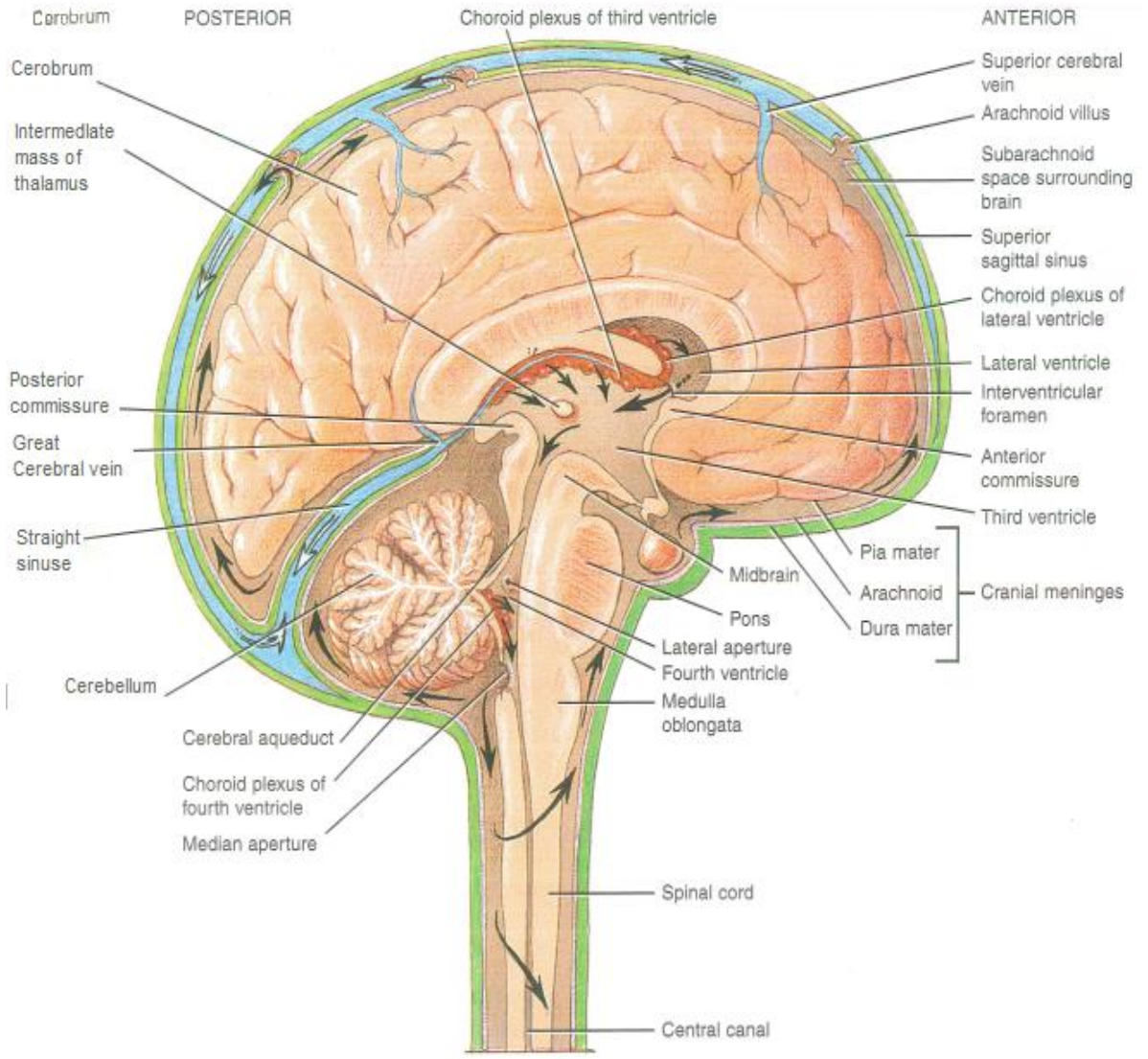

Figure 1-7: Anatomy of human brain (adapted from Tortora and Grabowski (Tortora & Grabowsk, 1996))

The cerebrum consists mostly of white matter and grey matter as shown in Figure 1-8. The white matter has a fibrous nature and the grey matter consists of concentrated neurons (Werner, 2003). As shown in Figure 1-8 the grey matter lies on the outer margin and creates the cortex, whereas white matter lies inside. Within the cortex are the ventricles, which are mainly responsible for maintaining and storing the cerebrospinal fluid (Faller et al., 2004).

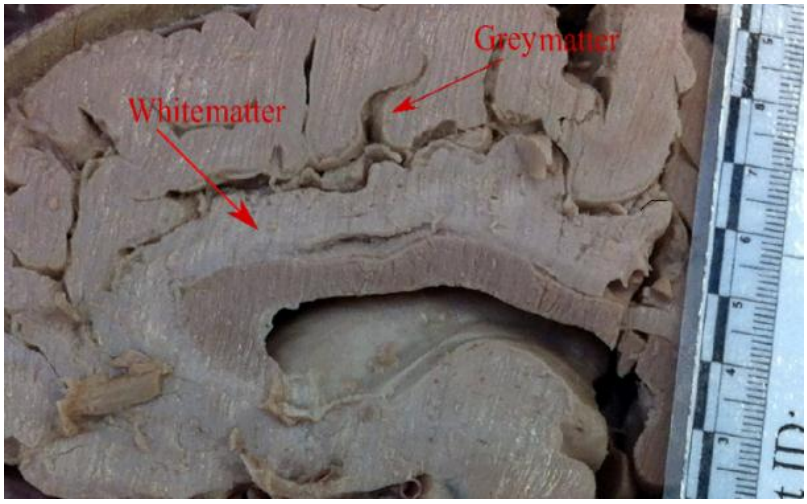

Figure 1-8: White and grey matters (from an embalmed cadaver)

1.6 Fundamental mechanical terminology:

This part of the thesis presents some of the fundamental relations which are necessarily for understanding the behaviour of the material during high velocity impact.

Shear stress

$$\boldsymbol{\tau = \frac{F}{A}} \qquad \text{Equation 1}$$

Shear stress is the force divided by area used to describe relation between the force parallel to the cross section area and change of original form of material (Chi and Pagano, 1967).

$$F = \text{Force}$$

$$A = \text{Area}$$

Bulk Modulus

$$\boldsymbol{E = \delta P \Big/ \left(\frac{\delta V}{V}\right)} \quad \text{Or} \quad \boldsymbol{E = \delta P \Big/ \left(\frac{\delta \rho}{\rho}\right)} \qquad \text{Equation 2}$$

Bulk modulus is the change of the pressure divided by change in volume and determines the compressibility of the material (Munson et al., 2006).

$E = bulk\ modullus\ elasticity$

$\delta P = differential\ change\ in\ pressure\ on\ the\ object$

$\delta V = differential\ change\ in\ volume\ on\ the\ object$

$V = initial\ volume\ of\ the\ object$

$\delta\rho = \ differential\ change\ in\ density\ on\ the\ object$

$\rho = initial\ density\ of\ the\ object$

Young's modulus

$$\mathbf{E} = \frac{\textbf{tensile stress}}{\textbf{tensile strain}} = \frac{\boldsymbol{\sigma}}{\boldsymbol{\varepsilon}} = \frac{\mathbf{F/A_0}}{\mathbf{\Delta L/L_0}} = \frac{\mathbf{FL_0}}{\mathbf{A_0 \Delta L}} \qquad \text{Equation 3}$$

Young's modulus describes the elasticity of the material and called modulus of elasticity.

$E =$ is the Young′s Modulus(modulus of elastisity)

$F =$ force appiled on an object under tension

$A_0 =$ cross section which force is applied

$\Delta L =$ is the length changes

$L_0 =$ orginal length

Elastic Modulus

$$\boldsymbol{\lambda} = \frac{\textbf{stress}}{\textbf{strain}} = \frac{\boldsymbol{\sigma}}{\boldsymbol{\varepsilon}} \qquad \text{Equation 4}$$

The elastic modulus is the restoring force in the deformation process divided by the area over which the force applied divided by the change caused by the stress to the original dimension of material.

Kinematic viscosity:

$$\boldsymbol{\nu} = \frac{\boldsymbol{\mu}}{\boldsymbol{\rho}} \qquad \text{Equation 5}$$

Kinematic viscosity is equal to dynamic viscosity divided by density (Munson et al., 2006).

$\mu =$ is the proportionality factor called dynamic viscosity

Shear stress for Newtonian fluid:

$$\boldsymbol{\tau}(\mathbf{y}) = \boldsymbol{\mu}\frac{\mathbf{du}}{\mathbf{dy}} \qquad \text{Equation 6}$$

$\mu =$ dynamic viscosity of fluid

$u =$ velocity of the fluid along the boundary

$y =$ high above the boundary

Dynamic pressure:

$$\boldsymbol{P = \frac{1}{2}\rho v^2} \qquad \text{Equation 7}$$

$P = presure$

$\rho = density$

$v = velocity$

$$\mathbf{E = \frac{1}{2}mV^2} \qquad \text{Equation 8}$$

Kinetic energy is the energy associated with the motion and is half mass multiplied to the square of velocity (Almansa et al., 1999).

Material type and viscoelasticity:

Pure solid materials are those in which the molecules are strongly bonded, so that the solid can retain its shape and exhibit an elastic response to stress and it can support a shear stress without motion. In a liquids the intermolecular bonding is weaker, the material takes the shape of its container, and shear stresses always induce internal motion. Shear-thinning viscoelastic materials act like solid under small load forces and act like fluid when a large force are applied on the material or over long timescales (Munson et al., 2006).

Figure 1-9 shows the stress strain curve for a metal such as steel. The curve can be divided in to four regions. The linear elastic region lies between points A to C in Figure 1-9. In this region the material deforms linearly and by removing the stress, the material will go back to its original shape. By removing stress from point B to C material is also will take its original shape but the relation between stress and strain is not linear. This point is called neck and at this point the cross sectional area of a tensed specimen become smaller. By increasing the stress form point C to D material will experience plastic deformation. At this stage by removing the stress material will not have its original shape and deformations are unrecoverable. Point D is the fracture or failure point which is indicate that material is broken.

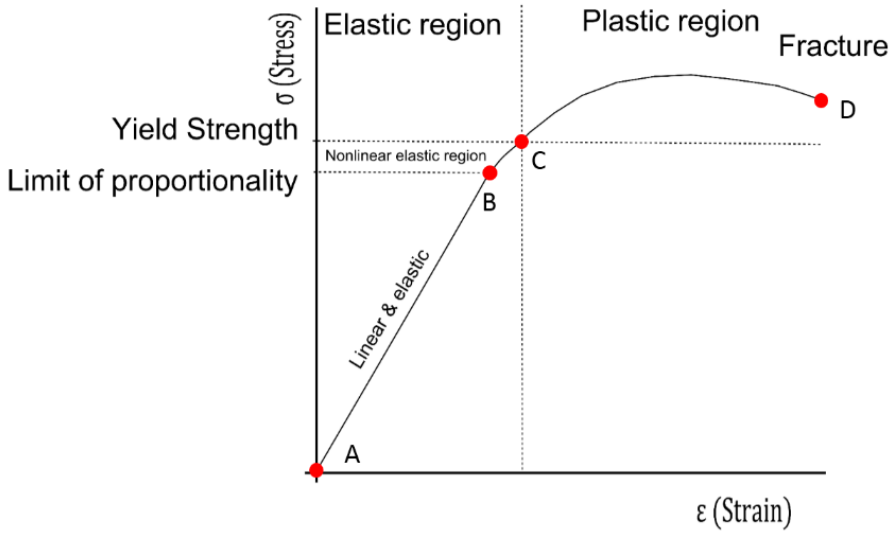

Figure 1-9: Stress-strain curve

Viscoelastic behaviour may be time dependent, so it is really important to know the time over which a force applied to the area. In viscoelastic phenomena, three important behaviours are known: namely viscoelastic creep, by applying constant stress to the material strain increases. Elastic recovery, by removing the load material will recover it its original shape. Plastic recovery by removing the load material will be experience permanent deformation. The strain- time profile applied to obtain the response of the material is shown in Figure 1-10 (Szabo, 2005).

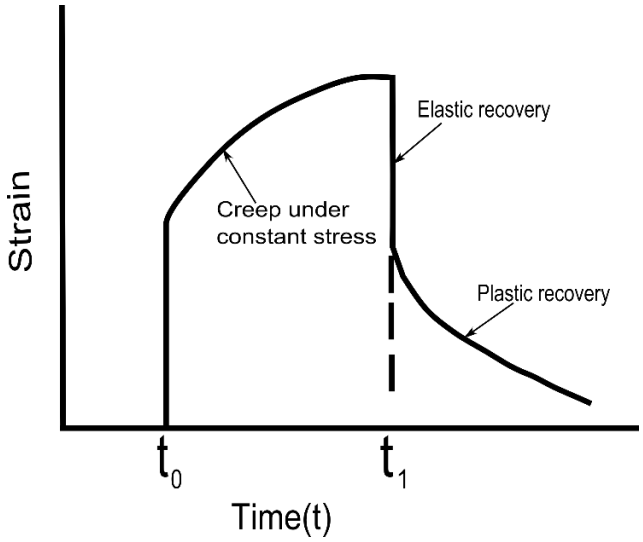

Figure 1-10: Stress time profile

The Maxwell model of a viscoelastic material is shown in Figure 1-11 represents a Newtonian damper for viscous behaviour of material and a Hookean spring as an elastic behaviour (Chen et al., 2012).

k_1 = stiffness of spring

ε = strain,

σ = stress

μ = viscosity

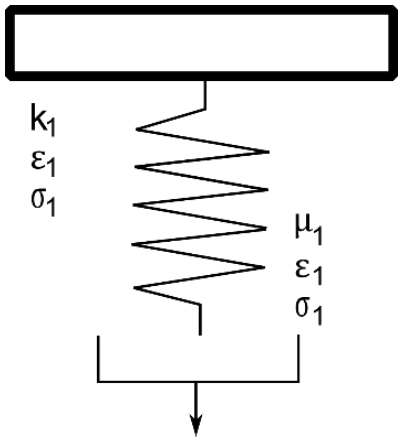

Figure 1-11: Maxwell model

$$\sigma = \sigma_1 = \sigma_2$$

$$\varepsilon = \varepsilon_1 + \varepsilon_2$$

$$\dot{\boldsymbol{\varepsilon}} = \frac{\dot{\boldsymbol{\sigma}}}{\boldsymbol{k}} + \frac{\boldsymbol{\sigma}}{\boldsymbol{\mu}} \qquad \text{Equation 9}$$

Equation (9) can be used to predict strain for viscoelastic material in Maxwell model.

Figure 1-12 shows the Kelvin-Voigt model of viscoelastic material. This model consists of purely viscous damper and purely elastic spring connected in parallel.

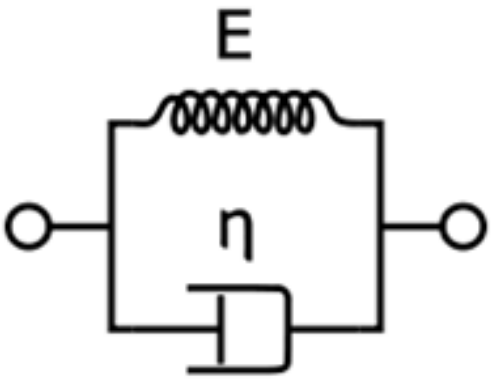

Figure 1-12: Kelvin-Voigt model

In this model strain and stress is identical for both damper and spring as they are connected in parallel.

$$\varepsilon_{total} = \varepsilon_{Damper} = \varepsilon_{Spring}$$

$$\sigma_{total} = \sigma_{Damper} = \sigma_{Spring}$$

From equation 10 it is possible to calculate shear stress or normal stress of the material with the respect to time.

$$\boldsymbol{\sigma(t) = E_{\varepsilon}(t) + \eta \frac{d_{\varepsilon}(t)}{dt}} \qquad \text{Equation 10}$$

It is possible to predict the behaviour of viscoelastic material using viscoelastic models such as Maxwell and Kelvin-Voigt model. The main differences between these two models are; the damper and spring connected in series in Maxwell model, however, they are connected in parallel in Kelvin-Voigt model. This indicate the stress and strain in Maxwell model can be different in damper and spring. However, in Kelvin-Voigt model stress and strain in both damper and spring are identical. It must be noted that there is a lack of information to validate such models for the brain tissues at ballistic range of impact. Thus, using the mathematical model to predict the behaviour of the material at ballistic range of impact is not possible yet.

1.7 A review of mechanical properties of the brain reported in the literature:

A huge discrepancy in the published results occurs because of the variety of materials and methods used. Since the properties of a viscoelastic material are dependent on time (see 1.6), it is logical to expect different results from high strain rate analysis and low strain rate analysis. For clarity in this literature review, articles have been divided in to two groups such as high strain rate computational modelling (blast) and experimental measurement of the mechanical properties of the brain.

In order to have a reliable finite element model it is important to characterise the mechanical properties of the materials used in the model. For example brain tissue is assumed to be isotropic and homogenous viscoelastic material in the work by Li Tan et al (Li et al., 2010). In the study by Gu et al (Gu et al., 2012) a hyper viscoelastic model was used, which is a constitutive model for prediction of the behaviour

of the nonlinear elastic material. Mechanical properties of the brain assumed to be viscoelastic in shear with stress rate dependent on the shear relaxation modulus (L. Zhang et al., 2013) also they reported that the white matter had a shear modulus 25% higher than grey matter. The variety in the mechanical properties reported can be seen clearly in Table 1-1. Given this, all the differences in the input data for the finite element modelling will have substantial effect on the results. A summary of the most recent (at the time of writing) article related to high strain rate modelling of the human head can be found in section 1.7.1.

Most of the measurements of the mechanical properties of the brain were performed on animal brain such as bovine and porcine, and there is no reliable information on the differences between human and animal as different protocols and methods are used in the literature (Prange et al., 2000; Takhounts et al., 2003). However, for ethical reasons it is not possible to perform the experiment on the healthy human brain. As such the results of animal brain experiments can be accepted. Recent studies show there is no significant differences on the mechanical properties of the brain between the bovine, porcine and caprine, and also there is no differences between the male and female animals (Pervin et al., 2011). Therefore it is reasonable to assume that the mechanical properties of human white and grey matter are similar to those of other large mammals. Of course, the structure of the skull and brain differs significantly from mammal to mammal. A summary of most cited articles for mechanical properties of the brain can be found in chapter 1.7.2.

1.7.1 Mechanical properties reported for brain in blast wave finite element modelling:

It should be noted that data presented in this section relates to blast waves, which have lower strain rates compared to the gunshot. Data presented in this section of the thesis are intended to illustrate the discrepancies between different sources in the literature. In the study by Taylor and Ford (Taylor et al., 2009) a finite element model of the human head was used to analyse the effect of the blast induced wave on traumatic brain injury. They considered that the grey matter and white matter were compressible viscoelastic materials. Also mechanical properties of the head were obtained from the

published work by Zhang et al. (L. Zhang et al., 2001). Mechanical properties of the materials used in their work can be found in Table 1-1 They reported that ‘‘significant levels of pressure, volumetric tension, and shear stress can occur in focal areas of the brain, dependent on the orientation of the blast wave and the complex geometry of the skull, brain, and tissue interfaces. The focal development of stress or strain energy could exceed the threshold for axonal injury and contribute to the development of Traumatic brain injury (TBI) and its neurological consequences’’.

In the study by Li et al. (Li et al., 2010) an isotropic homogeneous viscoelastic material was used as brain material (Table 1-1) in their finite element model to understand the effect of the helmet to the damages caused by the blast. They reported that the gap between head and helmet can amplify the blast over pressure.

In the work by Gu et al. (Gu et al., 2012) hyper viscoelastic material model used for the brain material at large strain/high frequency range. They formulated their model in term of large strain viscoelastic framework and considered linear viscous deformations in combination with hyperplastic behaviour. An example of the mechanical properties used for the head materials shown in Table 1-1.

The effect of a helmet in protection of the brain during blast wave impact was studied by Zhang et al (L. Zhang et al., 2013).They noted that traditionally brain is treated as a viscoelastic material and it can be approximated by the Kelvin viscoelastic model. The behaviour of the brain for Finite element modelling (FE) is assumed to be viscoelastic in shear with stress rate dependent on the shear relaxation modulus, and purely elastic for hydrostatic behaviour of the material. Due to the fibrous nature of the white matter, the shear modulus of the white matter was assumed to be 25% higher than grey matter. Mechanical properties of the brain used in this study can be found in Table 1-1 (L. Zhang et al., 2013). They reported that the biomechanical response of the human head to the blast is sensitive to the direction of the blast and geometry of the helmet. The peak intracranial pressure was reported to be in the range of 0.68-1.8 MPa in the coup cortical region (front section of the head).

Table 1-1: Mechanical properties of the brain reported in the literature

Material	Bulk Modulus	Shear Modulus (MPa)	Young's Modulus (MPa)	Poisson ratio	Density (g/cm^3)	Author
Brain	2.19 MPa	0.0068	NA	NA	1.04	(Li et al., 2010)
White matter Grey matter	2.37 GPa 2.37 GPa	NA	NA	0.49	1.04 1.04	(Taylor & Ford, 2009)
Brain	NA	NA	Hyper-viscoelastic	0.49	1.04	(Gu et al., 2012)
White matter Grey matter	NA	G_0 G_∞ 0.01 0.002 0.0125 0.0025	NA	NA	NA	(L. Zhang et al., 2013)

1.7.2 Experimental measurement of the mechanical properties of the brain:

The mechanical properties of the material are commonly characterized by their modulus, such as bulk modulus, Young's modulus and dynamic modulus. However, in the characterization of a material such as soft biological tissues, factors like frequency, temperature and strain rate will have severe effect on the results. For example Figure 1-13 adapted from Tamura et al. (Tamura et al., 2008) shows changes in Young's modulus in porcine brain, by increasing the strain rate and strain range. This graph clearly shows the sensitivity of the porcine brain tissue to both strain rate and strain range. By increasing strain rate and strain range the material becomes stiffer.

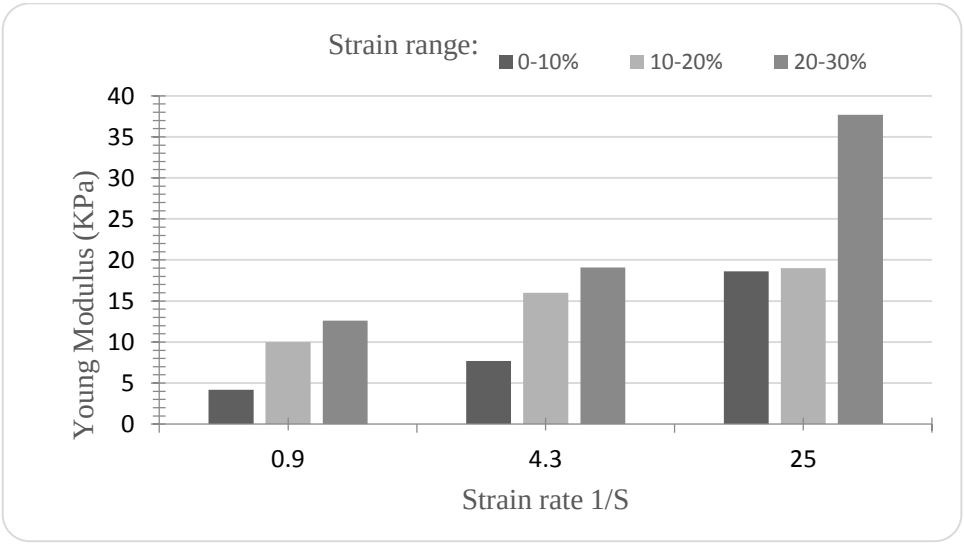

Figure 1-13: Young's modulus VS strain rate (adapted from Tamura at al (Tamura et al., 2008))

Figure 1-14 adapted from Zhang et al. (Jiangyue Zhang et al., 2011) shows the relation between tangent modulus (which is equivalent to the Young's modulus) and strain range. By increasing the strain range Young's modules increased. These results also indicate that temperature will have significant effect on the mechanical properties of the brain tissue.

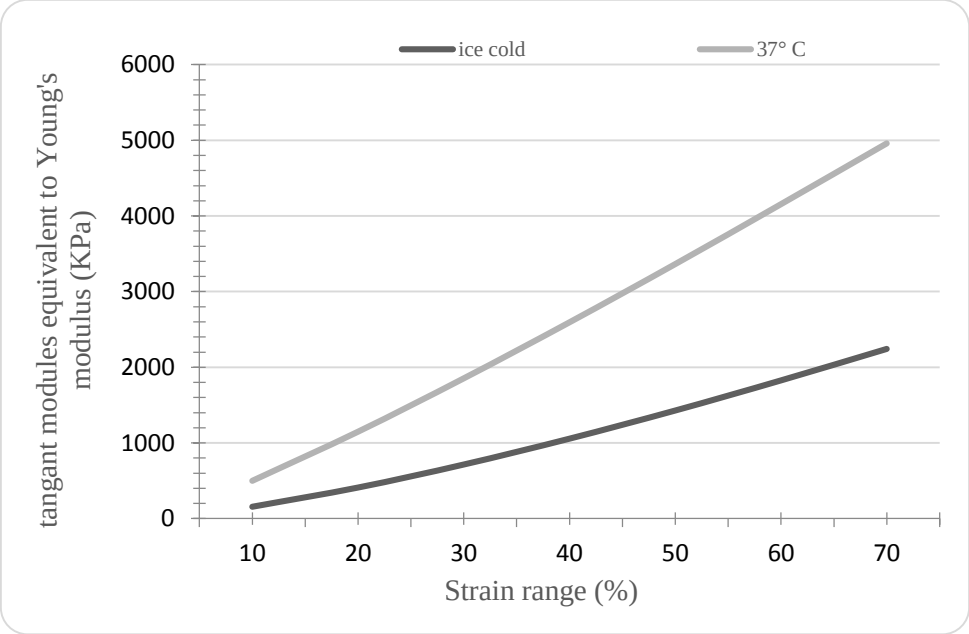

Figure 1-14: Tangent modulus VS Strain level (adapted from Zhang et al. (Jiangyue Zhang et al., 2011))

Figure 1-15 adapted from Samuel et al. (Samuel et al., 2004) shows changes in the Young's modulus by increasing frequency. This experiment was performed on lamb's brain at the strain rate of 0.1 MHz and 10 MHz. It can be seen that by increasing the frequency Young's modulus increases. Also Figure 1-16 adapted from Nicolle et al. (Nicolle et al., 2005) shows changes in the storage modulus and loss modulus in the porcine brain with the respect to frequency. As can be seen from Figure 1-15 and Figure 1-16 the mechanical properties of the brain changes with frequency (or timescale).

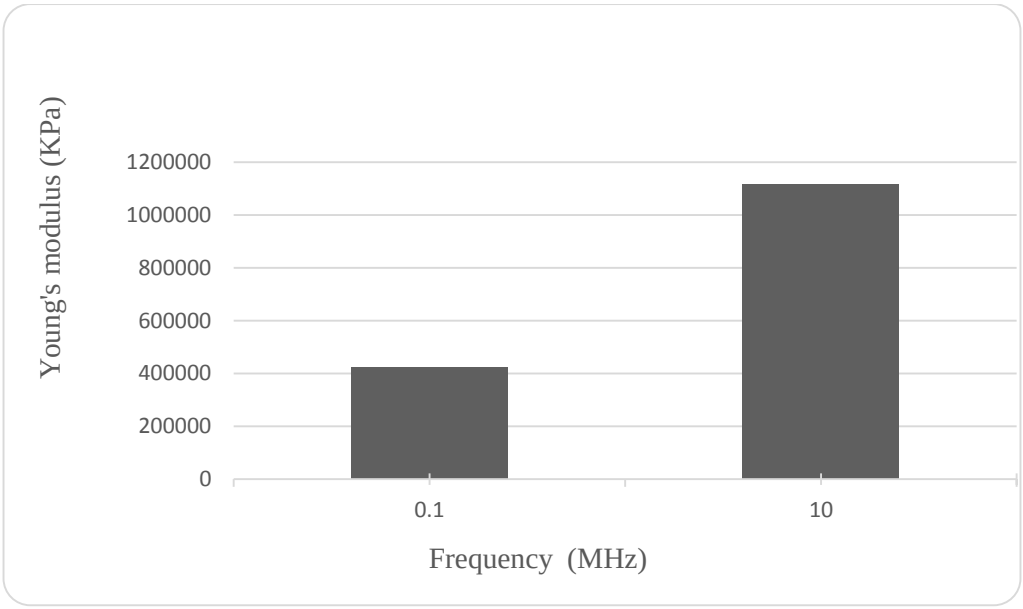

Figure 1-15: Young's modulus VS frequency (adapted from Samuel et al. (Samuel et al., 2004))

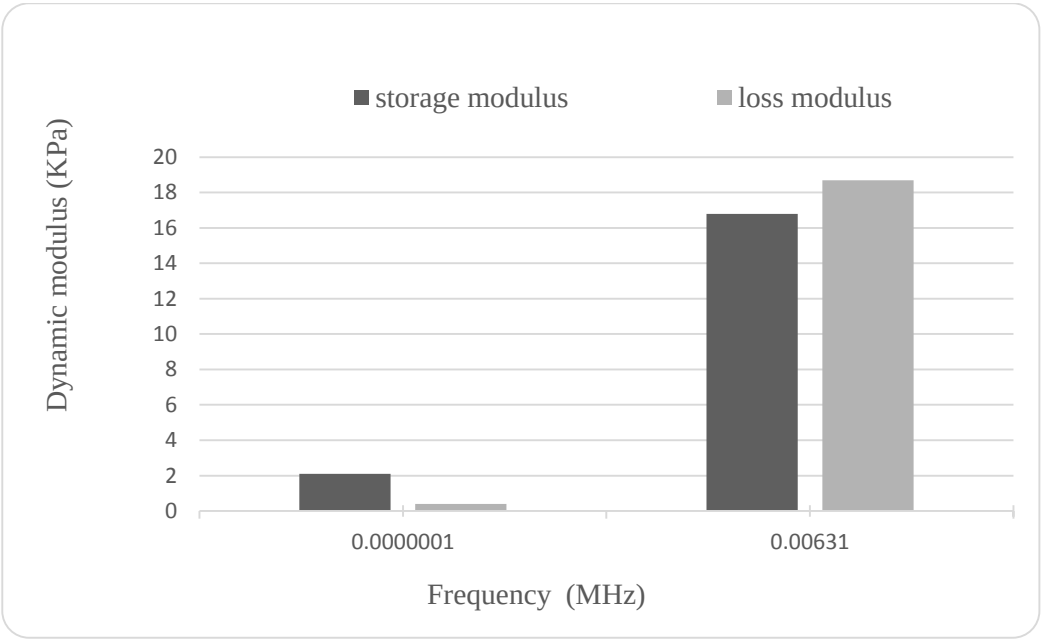

Figure 1-16: Dynamic modulus VS frequency (adapted from Nicolle et al. (Nicolle et al., 2005))

Figure 1-17 adapted from Pervin et al. (Pervin & Chen, 2011) shows that stress increases by increasing the strain rate from 1000 s^{-1} to 3000 s^{-1}.

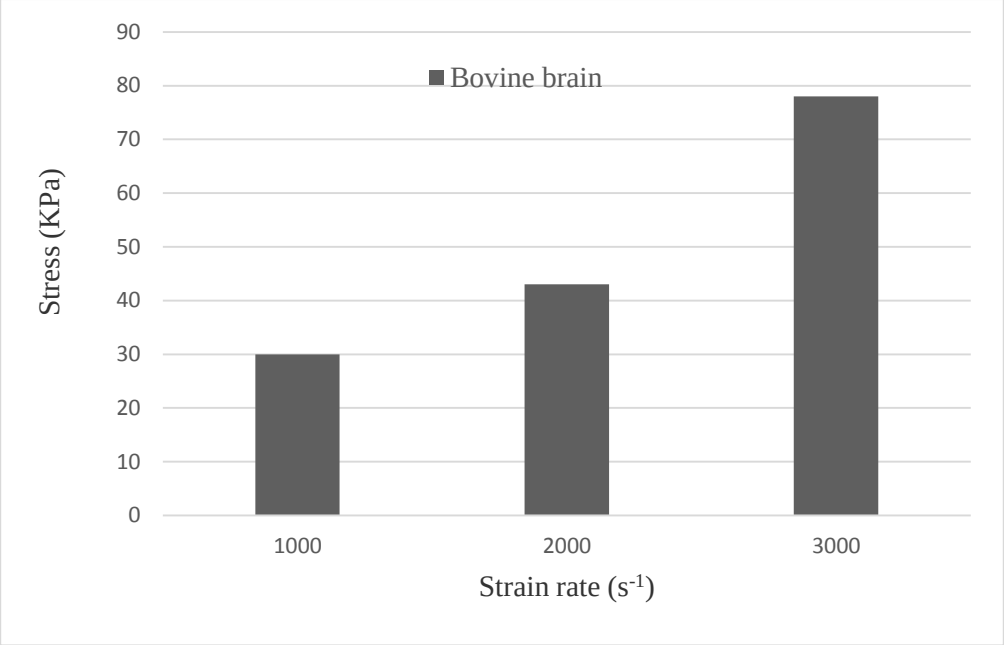

Figure 1-17: Stress VS strain rate (adapted from Pervin et al. (Pervin & Chen, 2011))

Given all the earlier information it is clear that mechanical properties of the brain tissue are very sensitive to frequency, strain rate (level). More detailed information on different mechanical properties of the brain reported in the literature are given in chapter 1.7.3.

1.7.3 Summary of reported mechanical properties of the brain:

A study was performed by Miller and Chinzei (Miller et al., 2002) on porcine brain at the strain rate of 0.64 and 0.64×10^{-2} s^{-1} at strains up to 30% . Cylindrical samples with a diameter of 30 mm and height of 10 mm were preserved in saline at 5° C. They reported that the behaviour of the brain is nonlinear and there is a strong dependency between stresses and strain rate. They proposed a new hyper-viscoelastic model, which performed well in compression and extension up to 30% strain. Also they noted that stiffer response can be found in the tissue by increasing the strain rate.

In the study by Samuel et al. (Samuel et al., 2004) fresh lambs brain was used to measure the high frequency properties of brain tissues using the ‘‘wave-in-a-tube’’ (Samuel et al., 2004) method. Brain tissues were tested at frequencies of 100 kHz up to 10 MHz at very low strain rate. Samples with diameter of the 12.7 mm were used at the same day as brain was removed from the skull. All samples were tested at the temperature of 25-27° C .They reported that complex ‘‘bulk modulus is fairly constant (2133 MPa) with the respect to the frequency’’. Complex shear and Young’s modulus are varied with

frequency. They found that Poisson ratio for white matter ranged from 0.467 at 100 kHz to 0.415 at 10 MHz and Young's modulus ranged from 422.1 MPa to 1153 MPa and complex shear modulus ranged from 143.9 MPa to 412.4 MPa (Samuel et al., 2004).

Samples of porcine brain were used by Nicolle et al. (Nicolle et al., 2005) to study the shear modulus of brain tissue using an original custom-designed oscillatory shear device. Samples were cut from the white matter into cylindrical shapes with diameter of 10 and 20 mm and a height of 2.5 mm. Samples were preserved in Ringer-lactate solution at 6 ° C. The result showed that the dynamic modulus of the brain tissue began to decrease for an applied strain value between 1 to 2%. Oscillatory tests were repeated on one sample after 24 hours and no significant difference was observed. ''Storage and loss moduli ranged from 2.1 to 16.8 kPa and 0.4 to 18.7 kPa respectively between 0.1 and 6310 Hz ''. They reported that a full non-linear model must be used for addressing the brain injury as the brain tissues are mechanically fragile and it has a very low limit of linearity.

Mechanical properties of the porcine brain at large shear deformation was characterized by Hrapko et al. (M. Hrapko et al., 2006). Porcine brain was kept in ice cold saline solution for two hours and then white matter was cut into cylindrical samples with a diameter of 7-10 mm and height of 1-3 mm. An ARES rotational rheometer with a 10GM RFT transducer with plate-plate configuration was used to determine the properties of the material. All samples were tested at 37° C. They reported that linear behaviour of the material occurs at strain rates of less than 0.01. Also the recovery time is 10 times more than loading time, which can be one of the reasons for the non-linear behaviour of the material.

Mechanical properties of the porcine brain have been characterised by Tamura et al. (Tamura et al., 2008) using tensile tests at strain rates of 0.9 to 25 s^{-1} with strain levels of 15 to 50%. Brain tissues were tested as bulk material consisting of grey matter and white matter. Samples were cylindrical with height and diameter of 14 mm and preserved at -20 ° C one hour before the test. They also reported that mechanical properties of the brain tissues are strongly dependent on the strain rate. The elastic modulus were reported to be 4.2, 7.7, and 18.6 kPa for strain rates of 0.9, 4.3, and 25 s^{-1} respectively.

Dynamic response of bovine grey and white matter under compression has been characterized by Pervin and Chen (Pervin et al., 2009). A modified split Hopkinson pressure bar was used at this study to find the mechanical properties of the soft tissue at the strain rate ranging from 0.01 to 3000 s^{-1}. Bovine brains were preserved in artificial cerebrospinal fluid at the temperature of 37 °C and all the experiments were performed less than four hours post-mortem. They reported significant rate dependency on both grey matter and white matter essentially for the strain rate above 100 s^{-1}. On increasing the strain rate, the material becomes stiffer even in the quasi-static range.

The effect of the gender and species on the mechanical properties of the brain has been characterized by Pervin and Chen (Pervin & Chen, 2011). A conventional material testing machine (MTS 810) and a Kolsky bar were used for quasi-static and high strain rate experiments respectively. The experimental setup and size of the samples were the same for both sets of experiments. Samples of bovine, porcine and caprine were kept in artificial cerebrospinal fluid at the temperature of 37 °C. Cylindrical samples from white matter and grey matter with the diameter of 10 mm and height of 1.7 mm were cut from one hemisphere of the brain and a hole with a diameter of 4.7 mm was punched at the centre of each sample before the experiment. They reported significant rate dependency on mechanical properties of the brain in all three species. At 15% strain and strain rate of 1000 s^{-1}, stress were 30, 35, 38 kPa and for the strain rate of 0.01 s^{-1} stress was below 0.5 kPa. This shows that the stress values at quasi-static strain rates are two order of magnitude lower than the corresponding dynamic stress value. At the strain level of 30% with the strain rate of 3000 s^{-1}, stress values were 5.5 and 2.7 times for the 1000 s^{-1} and 2000 s^{-1} strain rate respectively. Moreover, no significant differences were observed in grey and white matters between different species and gender (Pervin & Chen, 2011).

In the study by Zhang et al. (Jiangyue Zhang et al., 2011) a Hopkinson pressure bar was used to determine mechanical properties of the porcine bran. Porcine brain was cut in to 2 mm thick samples and divided in two groups. The first group was preserved in ice, and second group was warmed to 37 °C before the commencement of any tests. The mean strain rate was reported to be $2487 \pm 72\ s^{-1}$.The results showed significant difference between the first and second groups. The second group demonstrated stiffer response than the first group. Engineering stress for the first group were 8.4, 124.7,

436.4, and 995.9 kPa at the strain rate of 10%, 30%, 50%, and 70%. Engineering stress for the second group were 29.1, 351.1, 117.2 and 2394.4 kPa. They reported that stress level rises by increasing the strain level in both groups (Jiangyue Zhang et al., 2011).

High rate bulk and shear response of the brain has been studied by Nie et al. (Nie et al., 2012). A modified Kolsky compression bar with aluminium confinement collar was used to measure uniaxial strain (bulk response) and a Kolsky torsion bar was used to determined dynamic shear response of the bovine brain at the strain rate of 0.01-700 s^{-1}. Bovine brain was kept at 37 ° C in artificial cerebrospinal fluid. Cylindrical samples were cut from the brain with a diameter of 19 mm and height of 1.7 mm and a hole with a diameter of 14 mm was cut through the centre of the sample to create a ring for the test. They reported the dynamic bulk modulus is in the range of 1.68-2.33 GPa, close to the low rate values reported in the literature. The shear response is sensitive to the strain rate. The shear moduli with less than 5% shear strain are 5.9, 10.4, and 53.5 kPa for the strain rate of 0.01 s^{-1}, 1 s^{-1} and 700 s^{-1}.

Fresh porcine brain was used by Rashid et al. (Rashid et al., 2012) to determine the mechanical properties of the brain tissues using compression tests at 30, 60, 90 s^{-1} strain rate in up to 30% strain. They reported at the compressive stress at 30% strain were 8.83, 12.8, 3.10 kPa at the strain rate of 30, 60, 90 s^{-1}. They also performed numerical calculations to estimate the initial shear modulus by using a one term Ogden model. Initial shear modulus were 6.06, 9.44 and 12.64 kPa for 30, 60, 90 s^{-1} strain rate respectively. This results indicate rate dependency of the brain tissues and also shows that the brain exhibits stiffer response as the strain rate increases, indicating that hyperelastic models are not adequate for modelling high strain deformation of the brain (Rashid et al., 2012).

1.8 A review on ballistic impacts in simulants:

Fackler and Malinowski (1985) investigated the effect of different types of bullet on tissue using ballistic gelatine at 4°C with a concentration of 10% by weight of gelatine in water. They suggested that the shock wave did not cause substantial displacement or damage to the tissue and they noted that using a soft-nosed bullet can cause more damage as the bullet can expand up to 3 times of its original

diameter. Bullet fragmentation can also cause more damage as after impact the bullet can separate into several fragments.

Farjo et al. (1997), reviewed the literature on failure properties of human tissues and performed experiments on gelatine. Their work concluded that there were many important factors, which had an effect on the failure of tissue such as sonic waves, the temporary cavity, and the permanent cavity. All of these phenomena were influenced by the velocity and mass of the bullet. They noted that the damage caused depends on the bullet energy deposited, bullet rotation as it travels through the material, and bullet fragmentation.

In a study by Bradshaw and Ivarsson (2001), silicone gel (Sylgard 527) was used for cerebrum, liquid paraffin was used to simulate cerebrospinal fluid, and the sulci were modelled by 200μm thickness low density polyethylene sheet. The study used marker points to observe the motion of each section. The authors reported that the deceleration phase can be considered as equivalent to a second impact at the opposite side.

Temporary cavity pulsation caused by .25 calibre and 9 mm bullets was studied by Zhang et al. (Jiangyue Zhang et al., 2005) using silicone gel (Sylgard 527) with five pressure sensors and a high speed camera. The absorption of projectile kinetic energy (E_k) by the target for the .25 calibre bullet was 45.2 J and for the 9 mm calibre was 283.7 J. They reported that temporary cavity created by a 9 mm projectile was 1.5 times larger in size than that caused by a .25 calibre bullet. They also reported that the pressure in the central region of the model was higher than that in the surrounding regions by at least 1.4 times for the .25 calibre and 1.6 times for 9 mm bullet.

A skin-skull-brain model was studied by Thali et al. (2002). An artificial skin was built with an outer layer of silicone, and silicone with synthetic fibres was used to simulate the fat and collagen of the scalp. Layers of polyurethane and latex were used to simulate skull and elastic latex was used to illustrate fragmentation of bone after impact. Thali et al. (2002) used 10% gelatine as a brain simulant. They reported that the model of the fragmentation of the bone and damage of the skin substitutes compared well with morphology seen in real cases.

Zhang et al. (2007) studied the formation of the temporary cavity and wounding using acrylic globes with a wall thickness of 2 mm for the skull and 10 % concentration of silicone gel (Sylgard 527) and gelatine in different experiments for the brain. Four pressure sensors were used to analyse the pressure distribution. The dynamics of the temporary cavity was reported to differ between the silicone and gelatine models. In the gelatine model, the diameter of the temporary cavity at the entry remained constant for a period after projectile exit and its entry and exit size were similar. In the silicone model however, the size of the temporary cavity at entry decreased after projectile exit, and the maximum diameter of the temporary cavity at the exit increased to a size larger than at entry. Peak entry pressure was higher than peak exit pressure in the gelatine model but in the silicone model entry pressure was lower than exit pressure.

1.9 Ballistic gelatine:

1.9.1 Review of preparation of the ballistic gelatine

Ballistic gelatine is the most commonly used material as a simulant for soft tissue (Martin L. Fackler et al., 1988; M. L. Fackler et al., 1988; M. L. Fackler & Malinowski, 1985; Jussila, 2004; Jorma Jussila et al., 2005; J. Jussila et al., 2005; Korac, 2001; Nicolas et al., 2004; C. W. A. Schyma, 2010; Jiangyue Zhang et al., 2005; L. Zhang et al., 2013). Mechanical properties of the gelatine has been studied since 1921 by Sheppard et al (Sheppard et al., 1921) . However applying the mechanical properties of the gelatine for assessing the wound damage is not practical. Thus more qualitative and quantitative experiments were performed in field of study. The main differences in preparation of the ballistic gelatine can be divided in three sections; concentration of the gelatine, temperature of the mixing and temperature of the block of the gelatine during the experiment. Several examples of variety in the method of preparation and temperature can be found in the review by Jussila (Jussila, 2004). Bowyer et al. (Bowyer et al., 1996) used 20% concentration of gelatine at the temperature of 24 °C. In the work by Berlin et al. (Berlin et al., 1983) they used distilled water at 85-90° mixed with the 20% concentration of the gelatine, they kept the material for 72 hours in the refrigerator and during the experiment temperature of the sample was 20 °C. Ragsdale and Josselson (Ragsdale et al., 1988) used 20% concentration of the gelatine, mixed with the water at the temperature of 85 °C, the samples had the

temperature of 4 °C at the moment of experiment. 10% w/w concentration of the was used by Fackler and Malinowski they warmed up the solution up to 40 °C and kept in the refrigerator at 4 °C. Jussila (Jussila, 2004) also reported that Federal Bureau of Investigation (FBI) used gelatine with 10% concentration mixed with the water at 60° C and kept it for at least 36 hours at 4 °C prior to the experiment. The effect of different gelatine batches, acidity of the water and temperature of the water into the penetration depth of the gelatine has been studied by Jussila (Jussila, 2004). They reported that acidity of the water used for preparation of the samples does not have a significant effect on the penetration depth of the projectile. Also they reported that there is no significant difference between gelatine batches which were stored for three years in a dark, dry, and formaldehyde free room and fresh samples. By changing the temperature and concentration of the gelatine it is possible to change the properties of the material. By decreasing the temperature the material becomes stiffer. Also increasing the concentration of the material will increase the stiffness of the sample (Jussila, 2004). Therefore, the temperature of the preparation of the gelatine solution in this study was kept at 55 °C, and the effect concentration was tested and will be discussed in detail in the material and equipment chapter 2. Although10% gelatine has been validated against porcine muscle tissue, the validity of 10% gelatine as brain simulant is still questionable. Thus, in this study several sets of experiment were performed to test the performance of 10% gelatine as a brain simulant.

1.9.2 Methods for assessing the size of temporary cavity

Fackler and Malinowski (M. L. Fackler & Malinowski, 1985) proposed a visual method for quantifying gunshot wound components. They used a 10% gelatine block, which was kept at 4 °C with the dimension of 25×25×50 cm. They present their results in the form of wound profile. They reported that the damage caused by temporary cavity is less visible in muscle compared to the gelatine. Finding the bullet fragments in radial splits is difficult. Gelatine samples are not capable of reproducing the same form of the damage caused by fragments of the bullet. X-rays of each sample were taken to find the fragments and map of the location of the fragments. The blocks of gelatine were sliced to find the radius of two largest cracks for estimating the size of temporary cavity. (M. L. Fackler & Malinowski, 1985).

Jussila (Jussila, 2005) compared three different methods of assessing the wound channel. The Fissure Surface Area (FSA), Total Crack Length Method (TCLM) (Ragsdale & Josselson, 1988) and Wound Profile Method (WPM) were compared (M. L. Fackler & Malinowski, 1985). For all the methods gelatine samples were cut into 50 mm slices. They reported that in order to have an accurate result from FSA and TCLM, blocks of the material must be cut into smaller slices, however, this is not possible due to the nature of the materials. As such they suggested that WPM is the fastest and most accurate way of assessing the wound channel.

In the study by Bolliger et al. (Bolliger et al., 2010) they used TCLM to characterize the wound channel. They cut the material into 2.5 mm slices and used CT scanning to determine the crack lengths. The advantage of using the CT scan is that it is possible to reconstruct very thin slices as it is not possible to cut the gelatine in very small slices due to its consistency. They suggested using CT-TCLM will give more accurate results and it can be stored indefinitely.

Schyma and Madea (Schyma et al., 2012) cut a block of 10% gelatine into 10 mm slices and scanned it with a 300dpi flat screen scanner. They compared all different methods available in the literature for analysing the wound characteristic such as:

1. The longest tear in each slice or maximum radius.

2. Two longest cracks (WPM).

3. The three longest cracks.

4. Sum of the length of all the cracks in each slice (TCLM).

5. Polygon fit by connecting end of the cracks (Polygon procedure).

6. The area of the polygon.

They reported that all these methods can be used to evaluate the energy transfer in to the gelatine. The gelatine samples cannot reproduce the same extension of the temporary cavity as living tissue. However, the experiment in gelatine is reproducible and energy transfer and destruction is measurable (Schyma

& Madea, 2012). As can be seen, there are variety of methods for assessing the wound track. However, from the comprehensive review by Schyma and Madea (Schyma & Madea, 2012) all the methods are accurate enough to be used for evaluation of the damage of the projectile into the gelatine samples. Of all of the above methods, maximum radius and the area of the polygon methods are the best methods to determine the wound track in brain samples as in the brain samples it is not possible to define cracks clearly. More information about the wound channel and form of the damage in the brain tissue can be found in Chapter 5.

1.10 Structure of this thesis

- Chapter two, **Equipment and Methodology**. The aim of this section is to introduce different equipment and materials used in different sets of experiments of this study. General information about different firing range used in this study will be provided. Moreover, it includes general information of properties and models of cameras, light and laser used in this study. Also mechanism of generation of the particles used for flow visualisation will be discussed. Method of preparation of different simulants used in this study is also discussed.
- Chapter three, **Development of a new brain simulant**. This chapter describes a series of experimental methods for comparison of the different simulants against ovine and bovine brains. In this study, the effect of the preservation time and temperature of ovine brain on the form of the fragmentation and kinetic energy loss by the projectile have been investigated using .22 AR. The results of this comparison shows that there are no substantial differences between chilled and fresh ovine brains. Also, different combinations of the new brain simulant have been compared with ovine brain and best materials have been chosen for further investigation with 9 mm and .22 LR. The results of development of the experimental method shows that it is desirable to use a bigger sample size for higher kinetic energy experiments. Thus bovine brain has been used instead of ovine brain in subsequent experiments performed with 9 mm and .22LR. Experiments with 9 mm .22 LR projectiles were performed to acquire data more relevant to gunshot fatalities.

- Chapter four, **Experimental investigation of the mechanical properties of brain simulants used for cranial gunshot simulation**. This chapter provides an experimental method that is used for comparison of the brain simulant with bovine brain. Expansion rate, velocity of the extruded material and repeatability of the experiments were investigated. Experiments were performed with .22 LR and .22 AR on 3, 5, with 10% gelatine and M1 and finally they were all compared with bovine brain.
- Chapter 5, **Stopping distance, form and size of the permanent cavity in simulant and bovine brain.** This chapter provides a method for comparison of the stopping distance and form of the damage in the block of the bovine brain as well as different simulants. The effect of the boundary condition on the form of the damage have been considered. Form of the damage and area of the permanent wound cavity have been compared in different Formulations of the composite materials with the bovine brain.
- Chapter 6, **Feature tracking to estimate the velocity of air ejected from the temporary cavity during gunshot wounding.** This chapter provides an experimental method for measuring the velocity of the indrawn and ejected air at the moment of the formation and collapse of the temporary cavity. Two methods for generation of the particle have been investigated. Also, a mechanism for generating a laminar flow of the fog has been designed and built. The accuracy of the velocity measurements were calculated by measuring the dimension of the particles and calculation of the Stokes number.
- Chapter seven, **Visualization of the air ejected from the temporary cavity in brain and tissue simulants during gunshot wounding.** This chapter provides a method for air flow visualisation in front of the wound cavity using laminar flow of the fog with conjunction with front and backlighting. Series of experiments were performed on 3, 5, 10%, M1, bovine and ovine heads using 9 mm projectiles.
- Chapter eight, **Conclusion and Future Work.** This chapter provides overall conclusion of all chapters of this thesis and also provides some future works.

2 Equipment and Methodology

2.1 Firing Range

2.1.1 University of Canterbury Firing Range

Testing different simulants requires a method of subjecting samples to the high strain rates, which occur in gunshot injuries. So, is impractical to use captive-bolt impact systems as it is difficult to engineer captive-bolt impact systems to achieve the required velocity. However, firearm experiments must be performed by a licensed handgun owner on a firearms range, which is expensive and very time consuming. As such a unique firing rage using a high muzzle velocity air rifle has been designed and manufactured to understand the behaviour of the materials during impact. This firing range is used to analyse the dynamic behaviour of different simulants upon impact.

The firing range and its safety mechanism are shown in Figure 2-1. Most of the materials used in the structure were medium density fibreboard (MDF), which are connected to a steel frame table. The rifle is aligned with target and is kept in a fixed position on two holders, which are made out of aluminium blocks. The holders were bolted to the structure. Each holder has two holes on the top. After placing the gun into the holder four bolts and nuts combination are used to keep the gun in fixed positions (Figure 2-1.1). The backstop is a box made of MDF with four different layers of materials, which are separated by sheets of steel (Figure 2-1.2). The first two layers are filled with paper (telephone directories) and the last two layers are filled with sand. The edge of each steel sheet has been bent to keep the projectile within the box. To avoid any accidents, two safety switches have been mounted at the front and top doors (Figure 2-1.3). Safety switches are connected to the safety lock (Figure 2-1.4), which blocks the trigger of the gun with an electromagnet. This interlocks the system and can prevent firing until the operator is at a safe distance. After each ten tests, the back stop must be checked and the paper must be replaced. Moreover, the level of the gun must be checked prior to each test.

Figure 2-1: Firing range, 1- Holder 2- Back stop 3- safety switch 4- safety lock 5- barrel holder

This firing range is designed to be modified to specific types of experiment such as air flow visualization with the laser, form of the fragmentation and stopping distance.

2.1.2 ESR Firearms Testing Laboratory (Auckland & Dunedin Pistol Clubs)

As mentioned earlier a comparison should be made on the results obtained from high velocity and low kinetic energy projectiles with high velocity and high kinetic energy projectiles. Thus, different type of experiments were performed at Otago Pistol Club as well as Firearms Testing Laboratory at Auckland. Otago Pistol Club is an open area for shooting training purposes. However, working in an open air laboratory has several disadvantage such as weather condition, safety procedure and uncontrolled lighting. The ESR Firearms Testing Laboratory is a 25 m indoor secure firing range at the ESR Mt. Albert Science Centre, which can be used for ballistic experiments. This firing range is equipped with

noise absorbing walls and also has a ballistics tank, which can be used for bullet recovery. Guns can be clamped to the bench and all the experimental setup can remain untouched for the following day. The experimental setup used in each firing range will be discussed in details for each experiment separately.

2.2 High Speed Camera and Image Processing:

It is possible to record detailed images of the very fast event in the short period of time using high-speed digital imaging (Kabaliuk, 2014) . However, it is possible to identify and measure the velocity of the object if the correct lighting set up is provided (Thoroddsen et al., 2008).

One of the simplest and most efficient methods of imaging is the backlighting. With this technique it is possible to identify and object with sufficient contrast in the image. The object blocks the light, which is coming towards the camera and creates a dark area on the recorded image (Kabaliuk, 2014). One of the advantages of using the backlighting technique is its light requirement, which is less compared to that of the usual front lighting. For two main reasons LED lights (see section 2.3) and backlighting technique were selected in this study. First, to have the best contrast of the object and second, to minimize the light sources as the light will generate heat, which can have effects on the results of the experiment.

Two Photron high speed-cameras, SA1 and SA5 (Figure 2-2) were used in this study. This gave us an opportunity to record high resolution images at high frame rate from different type of experiments performed in this research. Specification of the cameras can be found in Table 2-1.

Figure 2-2: Photron SA1 (left) and Photron SA5 (right)

Table 2-1: Specification of the high-speed cameras

Camera	Sensor	Resolution, pixels	Frame rate, fps	Exposure time µs
Photron SA1	CMOS colour	Max 1024×1024	Max 67500	From 1
Photron SA5	CMOS colour	Max 1024×1024	Max 77500	From 1

Several essential factors must be considered to capture a good quality image. The first factor is exposure time (or shutter speed), which is controlled from the operating software Photron FASTCAM Viewer (PFV). Exposure time is the time, when cameras sensor are exposed to the available light. As such it is possible to capture sharp clear images by choosing the right exposure time.

The second factor is the frame rate, which also can be controlled by PFV software. Frame rate will have major effect on the resolution of the Photron cameras. For example, by increasing the frame rate, the resolution of the image decreases (Cameras, 2014). Therefore, it is important to choose the field of view and an appropriate frame rate to obtain a better quality image. A reduction in resolution can have substantial effects on the quality of the image and it will increase the level of the noise, which will have direct influence on the error during the image processing.

The last factor is the F-number, which is the ratio of entrance pupil diameter to the focal length of the lens. Changing the aperture will change the amount of the light exposed to the camera's sensor. The smaller is the aperture the larger is F-number. So, an appropriate F-number must be selected to avoid the over exposure of the light, which depends experimental setup. Also there is a direct connection between the resolution of the image and frame rate of the camera Thus, for each specific experimental setup, different lighting and camera setup are required. The experimental set up for each set of experiments is discussed in the corresponding chapter.

2.3 LED Lights:

In order to have a uniform and high intensity light for high speed imaging a series of LED lights were designed and manufactured at the Mechanical Engineering workshop at the University of Canterbury. Eight Bridgelux BXRA-C8000 and four Bridgelux BXRA-C10000 series were mounted on a heat sink to avoid the overheat of the lights. Each LED had a medium parabolic reflector and was powered by a

Meanwell HLG series constant current power supply. The BXRA-C8000 and BXRA-C10000 were capable of generating cool white colour temperature with 7,900 and 10,000 lm respectively. Also, a sandblasted PMMA sheet was placed in front of the LED lights to produce a homogeneous distribution of the light.

Figure 2-3: LED lights 5000 lm (left) and 10000 lm (right)

2.4 Particles Generation:

In order to visualize the air motion in front of the wound cavity it is necessary to seed the air with particles. The seeding particles must be small enough to follow the air with sufficient accuracy and also they must be big enough to scatter an adequate amount of light. A fundamental discussion of the properties of the particle can be found in the work by Melling (Melling, 1997). Two methods used in this study to generate particles: first water droplets with Laskin nozzles and second propylene glycol generated by a Rave fog generator AF1214.

2.4.1 Generation of Water Particles:

Water particles with a diameter of less than one micron were generated by the Laskin process as shown in Figure 2-4. Air was injected at a gauge pressure of 800 kPa through five Laskin nozzles. To limit the size of the particles, an exit pipe with internal diameter 100 mm was installed with its intake a height of 200 mm above the water level and with a length of 500 mm. The pipe was connected to a closed PMMA box, which housed the sample to be shot. To limit the velocity of the particles, the generator

was turned off 30 seconds before the shot was fired. Particle motion was monitored on a live camera feed and the shot was fired after the particles began to move unidirectionally down, settling under gravity.

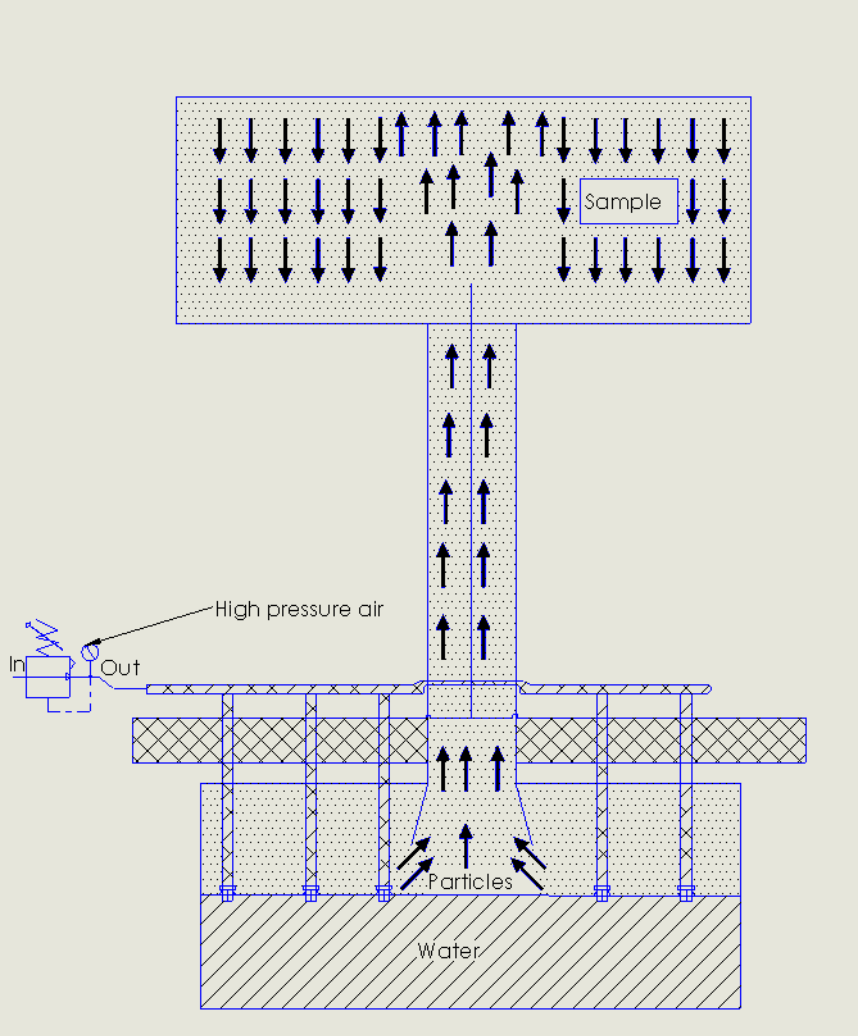

Figure 2-4: Schematic of water droplet generation

This method enabled us to generate water particles with the diameter of one micron. Procedure and measurement method of the diameter of the particle can be found in section 2.4.3. However, using one micron particles in this study was not possible as they were not bright enough, due to shortcomings with the available light source. So, it was necessary to generate bigger particles, which can scatter sufficient amount of light for high-speed imaging.

2.4.2 Generation of a Laminar Flow of Fog.

A new laminar flow generator have been design and manufacture at the Department of Mechanical Engineering of University of Canterbury in order to have a more uniform and controlled flow of particles. Figure 2-5 shows the set up used to generate a laminar flow of smoke with a constant velocity. The smoke generator was connected to a reservoir box with a heat resistant tube. A 1.5 W computer cooling fan was installed at the output of the reservoir to accelerate the particles with a velocity of ~1 m/s along the pipe to the open section. A suction nozzle was installed 200 mm from the tip of the pipe to create a narrow jet of smoke in front of the entry wound location on the sample. To return the smoke back to the reservoir a 2 W fan was installed at the end of the nozzle.

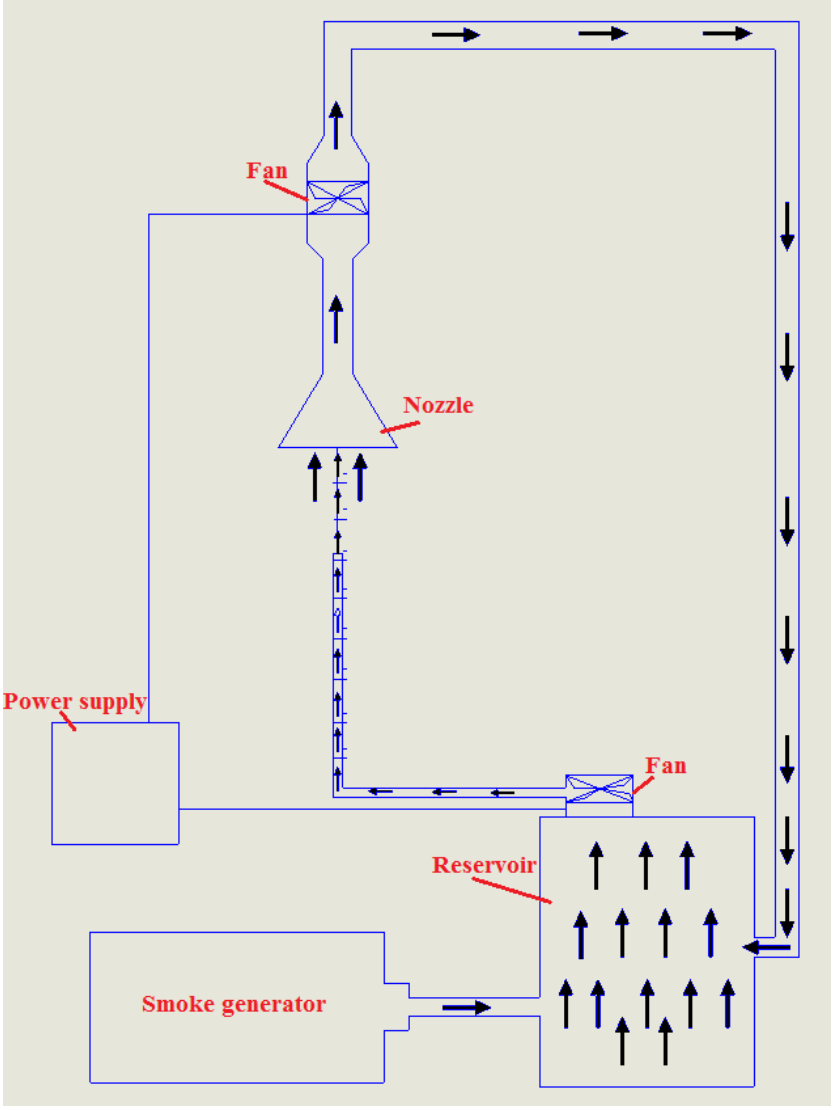

Figure 2-5: Setup for generation laminar flow of fog

2.4.3 Measurement of Properties of Propylene Glycol Particle:

It is possible assess the ability of the particle to follow the air by calculating the Stokes number (*Stk*) [59]. The Stk is a dimensionless number and is a ratio of viscous forces acting on the particle to the particles momentum. For Stk >> 1, particles will flow the path of the air in a straight line as the direction of the air changes. For accurate measurement of the flow the Stk of the particles must be less than 0.1. This indicates that ‘‘that the viscous forces on the particles dominate particle momentum and the error induced by particle inertia is less than 0.7%’’.

Dimension of the particles were measured using a DANTEC flowSense 2M PIV Camera with 50 mm lens and 300 mm of extension tube. Specification of the Particle Image Velocimetry (PIV) camera can be found in Table 2-2.

Table 2-2: PIV camera specifications

Specifications	DANTEC FlowSense 2M
Sensor type	CCD progressive scan monochrome
Sensing area (mm)	11.8 × 8.9
Cell size (µm)	7.4 × 7.4
Effective pixels	1608 × 1208
Maximum frame rate (frames/sec)	17.17

Particles were illuminated by laser 120mJ per pulse New Wave Solo120XT PIV laser. Experimental setup is shown in Figure 2-6. Laser beam was guided to the lens combination setup using DANTEC DYNAMIC laser arm. A beam stop box was installed around the working space to prevent the direct exposure of the laser beam to the laboratory. A Rave fog generator AF1214 was used to generate the propylene glycol particles.

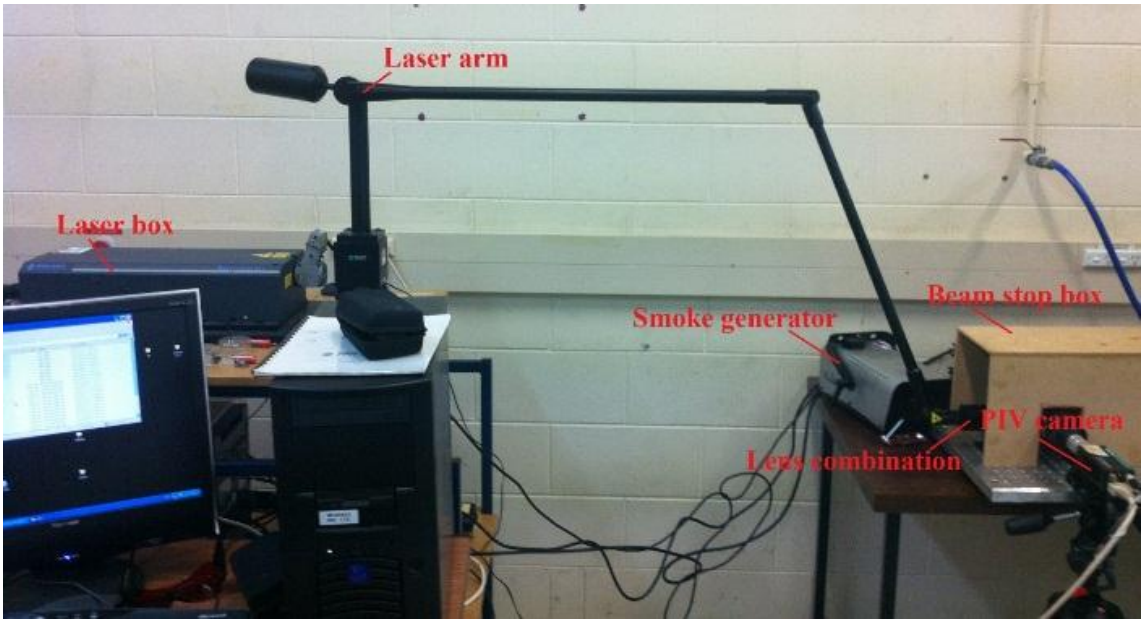

Figure 2-6: Experimental setup for measuring dimension of the particles

An image of the wire with the diameter of 0.4 mm was taken using the back lighting. The photo of the wire was used as a scale for calibration. Image was converted to grey style in MATLAB™ to decrease the uncertainty of measurement. Figure 2-7 shows the image taken for calibration. Diameter of the wire was 760 pixels measured by PFV Fastcam viewer software by counting the pixels between the two cross lines shown in Figure 2-7.

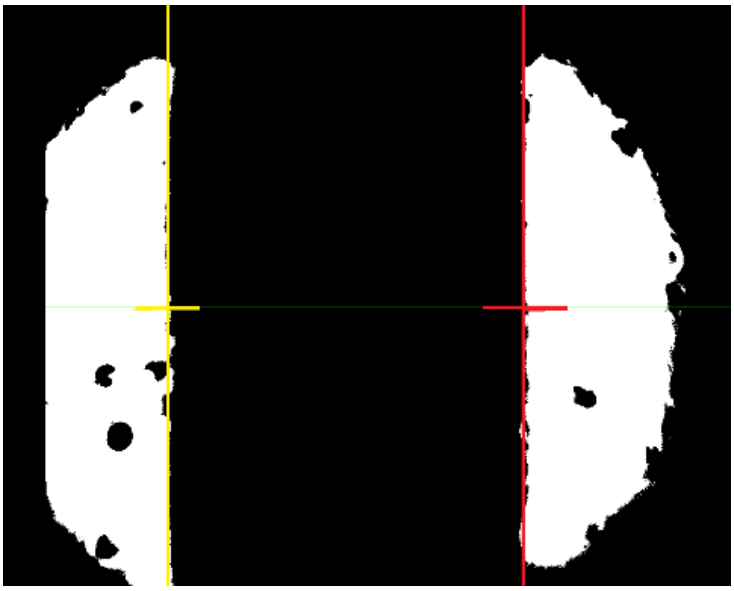

Figure 2-7: Photo of 0.4mm wire for calibration

Figure 2-8 shows the image of the smoke particles captured by PIV camera. The diameters of the particles were between one to 3 pixels. This shows the actual dimension of the particles is less than 1.6

μ. Knowing the dimension of the particles, it is possible to assess the accuracy of the velocity measurement.

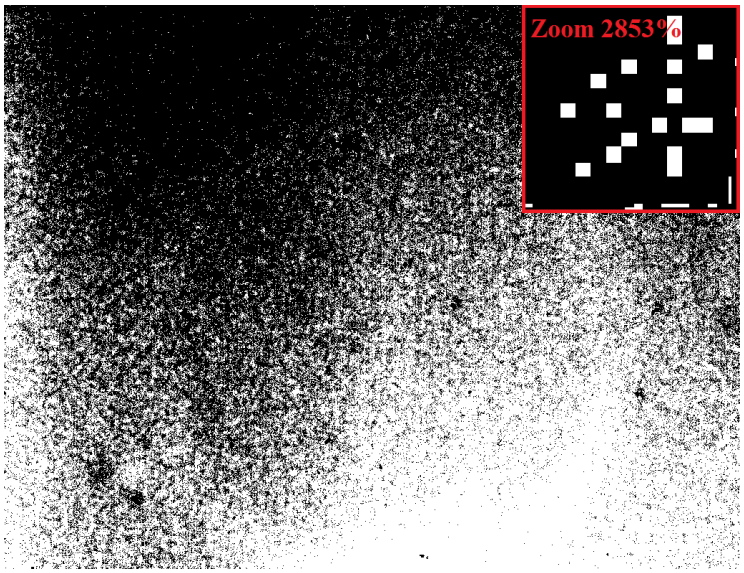

Figure 2-8: Image of the smoke particles

In order to find the accuracy of the velocity measurement, Equation 11 was used to calculate the Stk. Properties of the particles can be found in Table 2-3.

$$\mathbf{Stk} = \frac{\left(\rho_p {d_p}^2\right) U C_0}{18 \mu R} \qquad \text{Equation 11}$$

Table 2-3: Properties of the water and propylene glycol

Variables	water	Propylene glycol
$\rho_p = density\ of\ the\ particle\ kg/m^3$	999.97	1040
$\mu = dynamic\ viscosity\ kg/m.s$	18.1×10^{-6}	18.1×10^{-6}
$D_p = diamater\ of\ the\ particle\ m$	1×10^{-6}	1.6×10^{-6}
$U_0 = velocity\ of\ the\ air$ m/s	100	100
$d_0 = dimension\ of\ the\ obstacle\ m$	0.00558 - 0.009	0.00558-0.009
Stokes number	0.005 - 0.003	0.01- 0.09

The Stk for a 1.6 micron Propylene glycol particle for air rifle experiment was 0.01, and for 9 mm projectile was 0.09. Assuming that the radius of curvature in each test was the diameter of the projectile. This shows that dimension of the particles are met the criterion for effective tracking of the air motion (Dring, 1982). It must be noted that the water particles were not big enough to scatter sufficient amount of the light for high speed imaging. Thus, the Propylene glycol particles were used as a tracer particles.

2.4.4 Laser Sheet Alignment:

The accuracy of the velocity measurement in front of the wound cavity can improve compared to the backlighting, by having a high intensity light source parallel to the camera lens and perpendicular to the bullets path. With this setup it was possible to ensure that the movement of the particles are parallel to the camera. Therefore, a Coherent Innova 70 argon-ion laser with 4 W output power in multiline mode was used to generate a laser beam with a thickness of 5 mm (Figure 2-9.2). An adjustable angled mirror (Figure 2-9.3) was used to change the direction of the laser beam from horizontal to vertical. In the vertical direction, a combination of two convex lenses with the Keplerian arrangement have been used to reduce the thickness of the beam from 5 mm to 2 mm (Figure 2-9.4). A plano-concave lens was used to convert the beam into a light sheet.

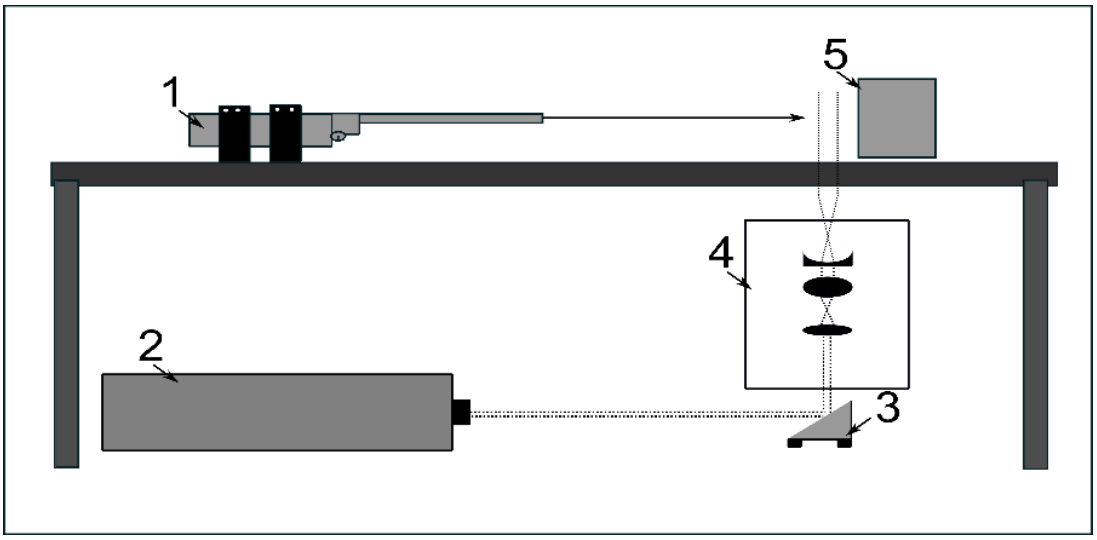

Figure 2-9: 1- Gun 2- Laser 3- Mirror 4- Lens combination 5- Sample

The above design enabled us to create a laser light sheet in front of the entrance hole of the sample. The laser light sheet then was used for illumination of the particles and feature tracking (see chapter 6). Laser related experiments were performed at the air rifle firing range at the University of Canterbury.

2.5 Guns and Projectiles

Properties of the guns and projectiles used in this study are shown in Table 2-4. In order to increase the accuracy of the experiments one type of ammunition (Webley® .22 round nose diabolo projectile) was used in all the experiments. Fifty air rifle projectiles were weighted using a Sartorius balance model ED12S with an accuracy of ± 0.1 mg to define the mean mass of the projectile. Results of the

measurements show that the mass of the projectile can be assumed to be 1g with a standard deviation of ± 0.0063g. The mass of the .22LR (solid lead projectile American Eagle) and hand gun bullet (9×19mm Parabellum American Eagle) were taken from the manufactures manual.

[64, 65]. The velocity measurement and calibration procedure are discussed for each type of experiment separately.

Table 2-4: Properties of the guns and projectile

Type of gun mode	Type of projectile	Mass of projectile	velocity
Air rifle .22 Gamo rabbit hunter	round nose diabolo	1 g	290 m/s ± 5%
Long rifle .22 semi-automatic	solid lead	2.59 g	330 m/s ± 5%
Hand gun (Glock Semi-automatic model 17)	full metal jacket	7.45g	379 m/s ± 5%

2.6 Density measurement.

As mentioned earlier one of the important parameter in validating a simulant in the literature is the density of the material. In order to analyse the effect of the density to the failure behaviour of the material upon impact it is desired to know the density of the materials. A METTLER TOLEDO density kit has been used to determine the density of the different percentage of the gelatine, bovine brain and new simulants. This kit works with the buoyancy method. The density of the material is determined using known density of the liquid, which is water (1000 kg/m^3) in this case. Materials were weighed in air and then in the water. Density ρ can be determined using two measured mass by using equation 12.

$$\boldsymbol{\rho = \frac{A}{A-B}\,(\rho_0 - \rho_L) + \rho_L} \qquad \text{Equation 9}$$

Where:

ρ = density of the sample

A= Mass of the sample

B= Mass of the sample in the liquid

ρ_0 = density of the liquid

ρ_L = density of the air (1.2 kg/m^3)

Table 2-5 shows the density of different materials. As it can be seen increasing the percentage of the gelatine did not have substantial effect on the density as all the materials have the approximately the same density as water ≈ 1000 kg/m3 except M1.

Table 2-5: Density of different materials used in this study

Material	Density (kg/m^3) $\pm 4\times10^{-6}$
3% gelatine	1009.17
5% gelatine	1015.94
10% gelatine	1027.33
M1	1204.78
Bovine brain	1040.43

2.7 Simulant preparation

In this section of the study methods of preparation of the gelatine and M1 will be discussed. Several percentage of the gelatine and new material (M1) have been used as a simulant for human brain.

2.7.1 Gelatine:

Gelatine samples were made out of GELITA export 20 grade with a bloom number of 240-260. Bloom number shows the strength of the gel. The higher the number the stiffer is the material. Gelatine with the bloom number of 250 is used for ballistic experiment. For each percentage of the gelatine exact amount of the gelatine was weighted using a commercial scale with accuracy of 1 g. Gelatine powder was mixed with the 55 ºC warm water (w/w) and stirred until all particles dissolved. The solution was kept in the refrigerator for 24 hours at the temperature of 4 ºC.

2.7.2 Preparation of the M1:

A new material M1 was developed in this research to replace the gelatine for ballistic impacts experiment. M1 is a corn based material with more viscous properties compare to gelatine. It comprised a solution of 60% glycerol, 40% W/W water, 10 g corn flour, 5 g talcum powder and 0.5 g carbon fibres cut to 0.5cm lengths to make 100 g of solution. All ingredients except the carbon fibre were mixed in a beaker. The mixture was warmed on a hot plate until the temperature reached 80 ºC, then the fibres

were added and stirred quickly for another 3 minutes. The mixture was poured into a plastic container and kept in the refrigerator for 24 hours before the experiment.

2.7.3 Casting Procedure of Bovine Brain:

In order to compare the form of the fragmentation from M1 and the bovine brain, it was necessary for the simulant to have the same approximate shape. Fresh bovine brain was cast with dentistry alginate. As the alginate has a fast setting time (less than 2 minutes) it was the best option to cast the fresh brain to produce the mould for other simulants. As the shelf life of the alginate is very short and it is fragile, using another material with a longer life shelf was essential. As shown in Figure 2-10:1 a model with the dental stone was made from the alginate mould and another cast with silicone gel were taken from the model of the brain shown in Figure 2-10 to produce more durable mould with long shelf life, which can be used for a long time. This mould was used to create a brain shape M1.

Figure 2-10: 1- Dental stone model 2- Silicone mould 3- M1 in the shape of the bovine brain

2.8 Velocity and displacement measurement techniques

Calculating the velocity of a moving objects require to measure the displacement of an object over time. In this study two techniques were used to measure the displacement and velocity of different parts of the material during an impact. First one is using the Photron FASTCAM Viewer (PFV) software and second one is a tracking code written in MATLAB™.

Photron FASTCAM Viewer is an open source software provided by Photron High Speed Camera Company. Using PFV it is possible to measure the displacement, knowing the frame rate it is possible to calculate the velocity of the moving abject. Measurement procedure can be divided in three steps. First step is to have a calibration image. Calibration image is an image of an object with the known dimension. Knowing the dimension of the object in millimetre it is possible to calculate the size of each pixel. In all of the experiments performed in this study diameter of the projectile was used for converting the pixel to millimetre in each video. The dimension of the projectile is known to be 5.58 mm. Using cross cursor mode in PFV software it is possible to count how many pixels are between two cursors. Figure 2-11 shows an example of the calibration procedure performed on .22 round nose diabolo projectile.

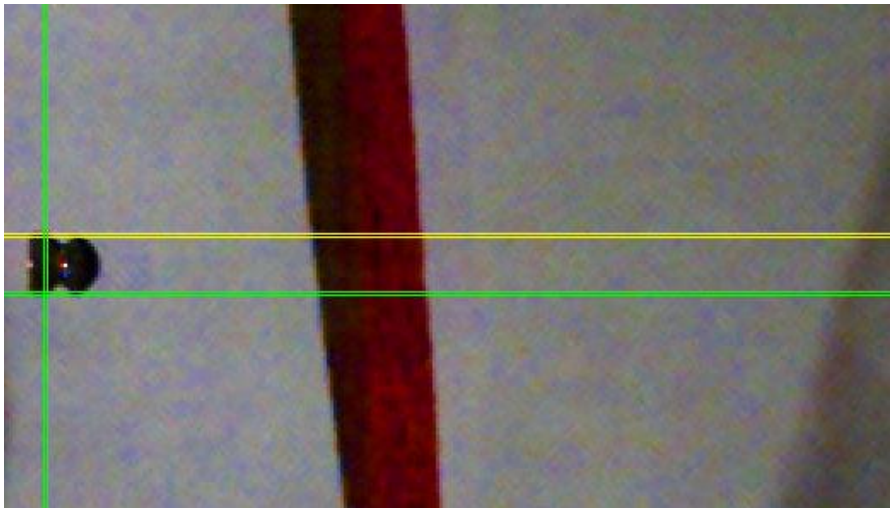

Figure 2-11: Calibration procedure

Second step is measuring the displacement of the moving object from the video. Figure 2-12 shows an example of the displacement measurement with PFV software. Projectile moves from left to right. It is possible to count the pixels between green and yellow cursor using cross cursor mode in PFV software.

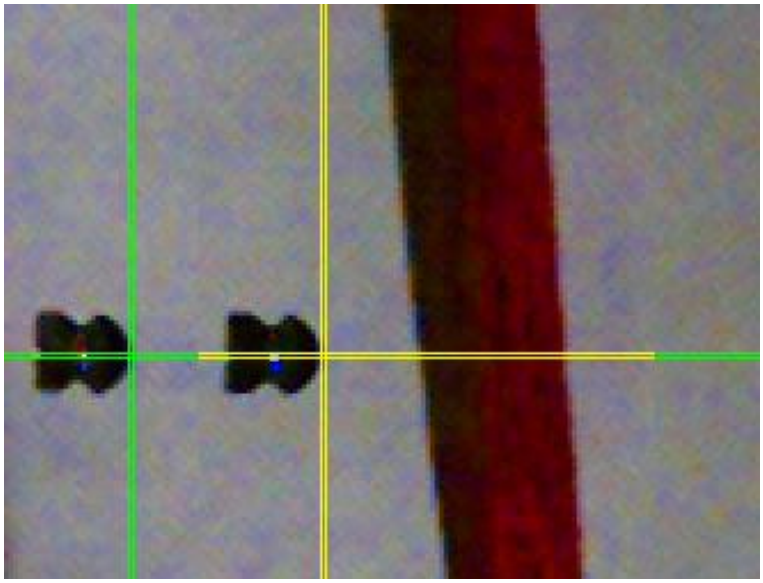

Figure 2-12: Displacement of the projectile

Third step is the velocity calculation. Knowing the frame rate of the video and displacement of the object it is possible to calculate the velocity of the moving object using equation 13.

$$\boldsymbol{v = \frac{dx}{dt}} \qquad \text{Equation 10}$$

Where:

$v = velocity$

$dx = displacement$

$dt = time = frame\ rate\ of\ the\ video$

A bullet tracking code was written in MATLAB™ (Mathworks, Natick, MA) to obtain the bullet velocity before and after impact. The bullet boundary was obtained from each image and the centroid was calculated for each boundary (Figure 2-13). The displacement of the centroid between frames was calculated and combined with the time step to determine the velocity. The same procedure can be used to calculate the velocity of different projectiles such as 9 mm, .22 LR and .22 AR.

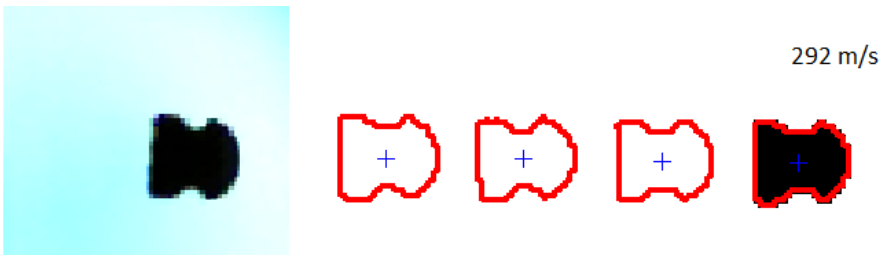

Figure 2-13: (Left) Image of a bullet during experimentation. (Right) Bullet boundary and centroid tracked between frames.

This code also can be modified to measure the displacement of different surface of the material upon impact. It must be noted that the dimension of each pixel must be entered to the code manually and also the image must be converted to grey scale image.

2.9 Cutting platform

In order to measure the dimension of the permanent wound cavity it is desire to cut the materials into a 10 mm slices. Thus, a cutting platform was design to cut the materials with the consistent thickens. Figure 2-14 shows the cutting platform and cutting blade used for slicing different materials. This cutting platform is an aluminium block with the internal dimension of 95x95x430 mm. All along the length of the block series of sluts with thickness of 2 mm and a gap of 10 mm in between has been created using milling machine. Using this platform it was possible to cut different materials with a consistent thickness.

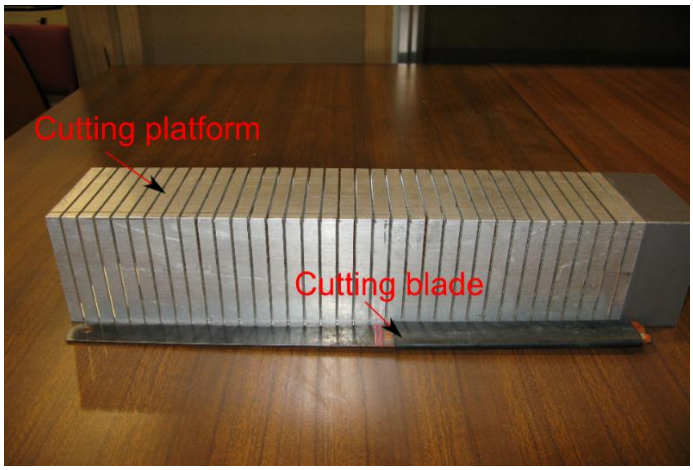

Figure 2-14: Cutting platform

3 Development of a new brain simulant

3.1 Introduction

Much current knowledge about ballistic damage and the mechanism of wounding comes from research performed with 10 or 20 % ballistic gelatine or Sylgard 527 silicone resin (Bolliger et al., 2010; M. Fackler et al., 1984; M. L. Fackler & Malinovski, 1988; Jussila, 2004; J. Jussila et al., 2005; Kneubuehl et al., 2012; Kwon et al., 2010; Rutty et al., 2008; Schyma & Madea, 2012; C. W. Schyma, 2010; Thali et al., 2002; J. Zhang et al., 2007). The effect of the different layers of the head on the generation of backspatter have not yet been studied in geometrically realistic models. Carr et al. (Carr et al., 2014) showed that in model tests, the quantity of brain simulant material in the skull has a major effect on the form of the fracture on the skull. To fully understand the formation of back spattered stains, and what they can tell us, it is necessary to understand the form of the deformation of each layer of the head and their effect on the formation of the backspatter. The focus of this study is developing a method for validating a simulant which can be used for cranial gunshot reconstruction. Experiments performed on ovine and bovine heads showed that brain would flow backward toward the firearm as a 9 mm projectile penetrates into the animal's head (the size of the entrance hole created by a projectile into the skull being approximately the same size as the projectile) (see chapter 7). As such any good brain simulant should also flow backward through the entrance hole in the skull after the intracranial pressure rises. The diameter, shape and velocity of material extruded through the entrance wounds are important factors.

This part of the study can be divided into four. First the effect of the preservation time when storing brain before an experiment on the form of the fragmentation and kinetic energy, performed using a .22 air rifle (AR). This information is important to ensure that any comparisons to the brain used have realistic in vivo characteristics. Second, development of a composite brain simulant that produces a realistic form of fragmentation from a high kinetic energy projectile is then performed. This work investigates the effect that varying the component materials has on the form of fragmentation and diameter of the entry hole created by 9 mm full metal jacket and .22 Long rifle (LR) projectiles. The third part investigates the velocity of the extruded material and kinetic energy loss and difficulties in

the quantitative measurement performed using a 9 mm hand gun to qualitatively analyse the error that can occur during experimental analysis. The aim of the fourth section of this work was to reduce the error in data analysis by having a better controlled shape of the material. The velocity of the material extruded backward and the form of the fragmentation were compared between bovine brain, a new composite material, and different concentrations of gelatine.

3.2 Effect of storage temperature on experimental results (.22 AR).

In order to validate the brain simulant and to ensure in vivo conditions are matched as closely as possible, it is necessary to have a source material for comparison which has material properties close to human brain; such as brain from other large mammals. It is convenient to chill and store brain before it is used, and several studies on the effect of the preservation time on the mechanical properties of the brain (Nicolle et al., 2005; Rashid et al., 2013; Jiangyue Zhang et al., 2011) and what changes occur. It must be noted that in the study by Rashid et al. (Rashid et al., 2013) shows that brain tissues which were preserved in ice cold temperature has the closest stiffness to in-vivo results. No study has yet addressed the effect of the length of time the brain was preserved for and the preservation temperature on the form of the fragmentation and kinetic energy loss of the projectiles.

Two sets of experiments were performed on ovine brain. The first was on fresh ovine brain with seven ovine heads collected from a local butchery. The skull was removed carefully using a chisel and hammer with the brain kept at room temperature at all times. Experiments were performed less than 5 hours after slaughter and the temperature of the brain during the experiment was 19-20±1 °C. For the second series of experiments, ovine brain was collected from the Middle Eastern Food Company (MEFCO[1]). The experiment was performed 24 hours after the animals were slaughtered. The brain was kept at 1° C, and was shot at this temperature. The brain mean mass of the 11 samples was 85 g. The kinetic energy lost by the projectile, and the form of the fragmentation, were compared.

[1] MEFCO, Acheron Drive, Christchurch, New Zealand

3.2.1 Experimental setup

3-1 shows a schematic of the experimental setup. The experiment was performed at a temperature of 18 ±1°C. Each sample was shot with a 1 ± 0.006 g, round nose diabolo projectile from a .22 air rifle, which had a velocity of 290 m/s, Repeatability and uncertainty of the velocity calculation due to the pixelation of the image and consequent uncertainty in position of the projectile gave an uncertainty in velocity of ± 5%. Experiments was performed at the University of Canterbury firing range.

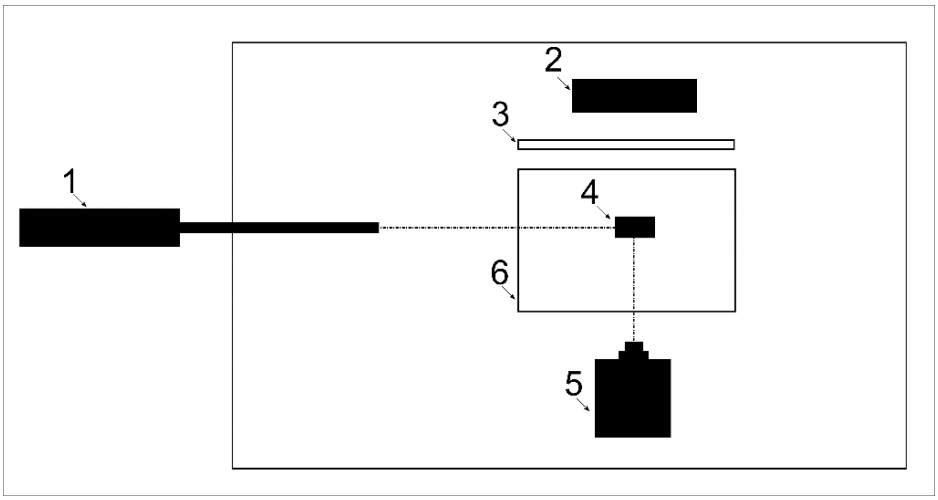

3-1: Experimental setup, 1- air rifle 2- LED 3-diffuser 4-sample 5-camera 6-containment box

Each sample was placed into a sample holder (Figure 3-2.1) with the internal dimensions of 70×50×40 mm. In order to save time for cleaning and replacing the sample, a frame box was designed. The sample holder was slid into the frame box, and replaced by the new sample after each test (Figure 3-2.3). The frame box was connected to an adjustable stand. The stand was designed so that the centre of the sample could be aligned with the path of the bullet (Figure 3-2.2). This entire mechanism was installed in a Perspex box for cleaning proposes (Figure 3-2.1). To prevent air ejected from the barrel affecting the fragmentation, the entrance section of the Perspex box was covered with a sheet of cellophane.

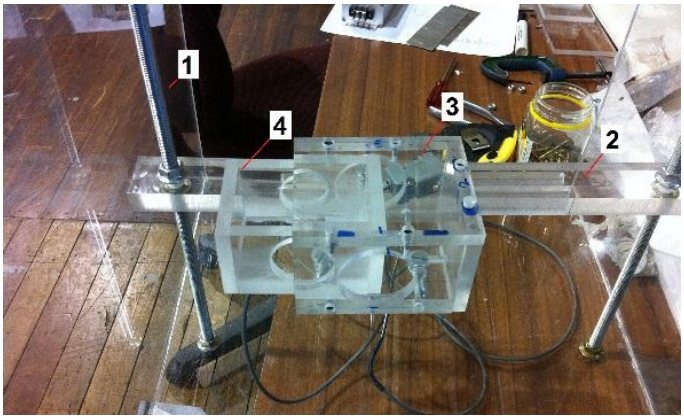

Figure 3-2: 1-protection box 2- stand 3- sample holder frame 4-sample holder

3.2.2 Results and conclusions

Figure 3-3 shows the kinetic energy loss from bullets passing through both types of brain. Bullets lose more energy passing through the colder samples. Cooling down the material increases the stiffness, may change the ultimate strength and may reduce either the elastic or plastic work done by the bullet. Zhang et al. (Jiangyue Zhang et al., 2011) they reported that at higher temperatures (37° C) porcine brain have a stiffer response. The effect of preservation of porcine brain was tested by Nicolle (Nicolle et al., 2005) using a custom-designed oscillatory shear device, they reported that there is no significant differences between data obtained in the interval of 24 hours at 6 ° C, it must be noted in their experiment the temperature was kept constant and the time was the only variable whereas in the present results, the temperature at the time of the test differed. Rashid et al. (Rashid et al., 2013) studied the effect of preservation temperature on the mechanical properties of the brain tissue at three different temperature (ice cold, 22° C and 37 ° C). They reported that by increasing the temperature, the stiffness of the material decreased. They suggested that the brain tissue must be kept at ice cold temperatures to minimize differences between in vitro and in vivo results (Rashid et al., 2013). The results of this current study conform with those of Rashid et al. (Rashid et al., 2013).

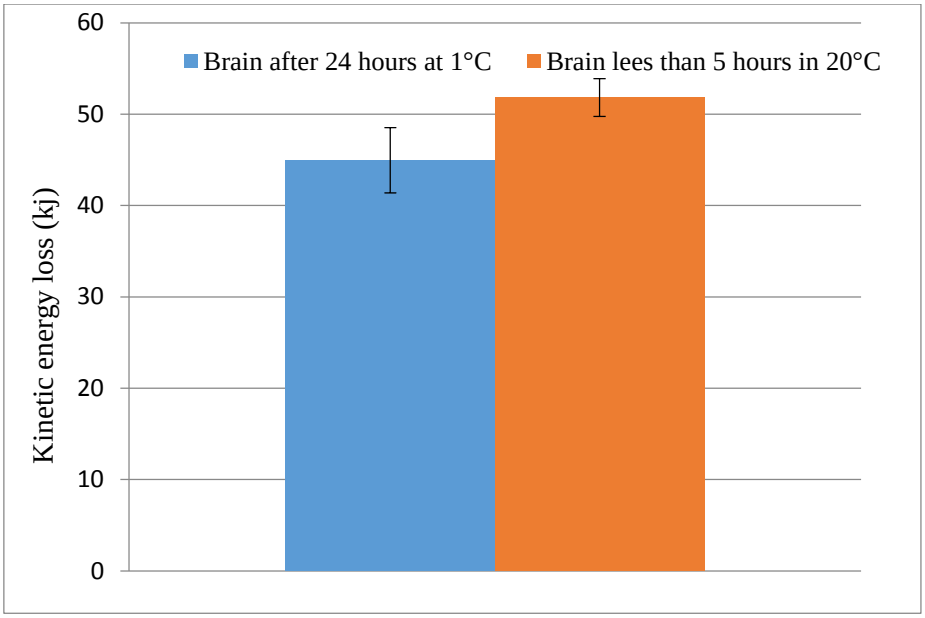

Figure 3-3: Kinetic energy losses by preserved and fresh brain

The differences in kinetic energy losses between the fresh ovine brain and preserved brain are very small. Kinetic energy loss was calculated by measuring the velocity of the projectile before and after impact using PFV Fastcam Viewer software. More detail of the velocity calculation can be found in chapter 2.8. The next step is to analyse the effect of the preservation on the form of the fragmentation. Figure 3-4 shows the form of fragmentation from ovine brain. Figure 3-4.A is the fresh ovine brain and Figure 3-4.B is the brain after 24 hour at 1° C. There are not substantial differences between two sets of experiments. The fragments around the projectile (red box) have the same approximate shape. All samples produced a small extrusion of the fragmented material around the projectile. Also backspatter formed as small lines with fragments around the line.

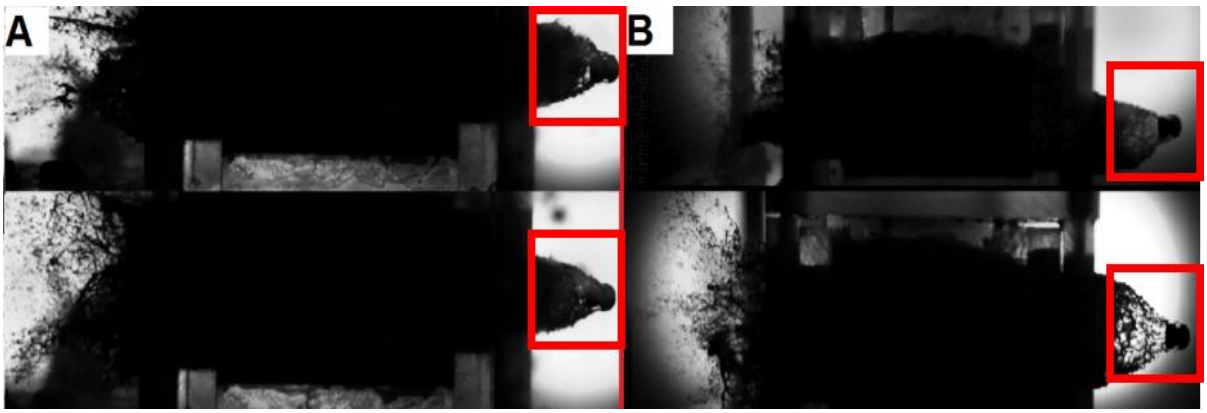

Figure 3-4: A-form of fragment fresh brain B- form of the fragments after 24 hours storage

However, the differences in the mechanical properties of the animal brain vary in the literature (M. Hrapko et al., 2006; Miller & Chinzei, 2002; Nicolle et al., 2005; Pervin & Chen, 2009, 2011; Rashid et al., 2012; Samuel et al., 2004; Tamura et al., 2008). The variety of the mechanical properties of the brain mostly depends on the measurement technique and the strain level applied. As the brain is a viscoelastic material it is expected to have different results for different strain rates. With reference to dynamic behaviour of the brain and generation of the backspatter, for validating a new material both fresh and chilled brain can be used.

3.3 Comparison of the form of fragmentation of ovine brain and simulant with different compositions.

Due to ethical and hygiene considerations there is a need for an inert simulant for experimentation on cranial backspatter. In order to compare the results of this experiment with ovine brain, the experimental setup remained the same as the one used for comparison of the fresh and chilled ovine brain (see chapter 3.2). This section compares the form of fragmentation and kinetic energy loss of a projectile impacting on ovine brain with a newly developed composite material which contains carbon fibre, water and glycerol (see chapter 2.7.2). The effect of the water glycerol ratio and carbon fibre length is also investigated. Several preliminary trials were performed with different ratios of water and glycerol, this was reduced down to samples that used a glycerol and water content between 30 to 60 g. Table 3-1 shows the different mixtures of composite material used for the present experiments. By increasing the water content to more than 40 g, the material loses its shape and increasing the percentage of glycerol causes the material to become very adhesive. By increasing the carbon fibre content it is possible to change the form of the fragmentation and also control the kinetic energy loss. Talcum powder was used to reduce the adhesiveness of the mixture and corn flour is the base material for polymerisation of the mixture. It must be noted that in this section of the study one sample of each material was tested to find the best material.

Table 3-1: Simulant with different composition

Simulant	Water (g)	Glycerol (g)	Corn flour (g)	Talcum powder (g)	fibre	Kinetic energy loss ±5 (%)
1	30	60	10	0	0.5 g (carbon) 100 mm	49
2	40	60	10	5	0.5g (Nylon) 80 mm	64
3	40	60	10	5	0.5 g (carbon) 5 mm	50
4	40	60	9	0	0.2 g (carbon) 5 mm	44
5	30	50	10	5	0.3 g (carbon) 5 mm	49
Ovine brain	NA					51

Figure 3-5 provides a visual comparison of the different simulants which absorbed similar kinetic energy with the ovine brain. Simulant number one in Figure 3-5 is a composite material without talcum powder and with 0.5 g of 100 mm length carbon fibre. It can be seen that the material did not produce the same form of fragmentation as the brain. This simulant creates a uniform bulging of the material with a very small tail around the projectile. The kinetic energy loss in simulant number one was 49%. Simulant number two is a composite of the base material with 5 g of talcum powder and 0.5 g of nylon fibre with the length of 80 mm. The energy loss by this simulant was 64 %. The main reason of the change in energy loss was due to the use of the nylon fibre, which is stiffer than carbon fibre. The composite with the nylon was chosen to elucidate the effect of the fibre material on the energy losses of the projectile. The form of the fragmentation can be described as several tails around the bullet with the degree of bulging of the material smaller compared to simulant number one. The reason behind the narrow bulging of the material is the length of the fibre. Thus in simulant number three, 0.5 g of carbon fibre with the length of 5 mm was used. As can be seen, simulant number three has more brain like deformation and energy absorption characteristics with 50% kinetic energy loss, which is close to that of ovine brain. Simulant number four has the same combination of the base material with 1 g less corn flour and zero talcum powder with 0.2 g of carbon fibre with length 5 mm. As can be seen from Figure 3-5 simulant number four has a narrower bulging behind the projectile compared to simulant number one. This indicates the effect of the amount of carbon fibre and talcum powder to the form of the fragmentation. Decreasing the quantity of the carbon fibre and talcum powder material will not reproduce the same form of fragmentation as brain. Also Figure 3-5 shows four example of the ovine

brain experiments. It can be seen that there is a small variety in the form of the fragments around the projectile. However the overall form of the fragmentation are similar. Of all materials tested in this section, simulant number three has been chosen for further investigation and will be referred to as M1.

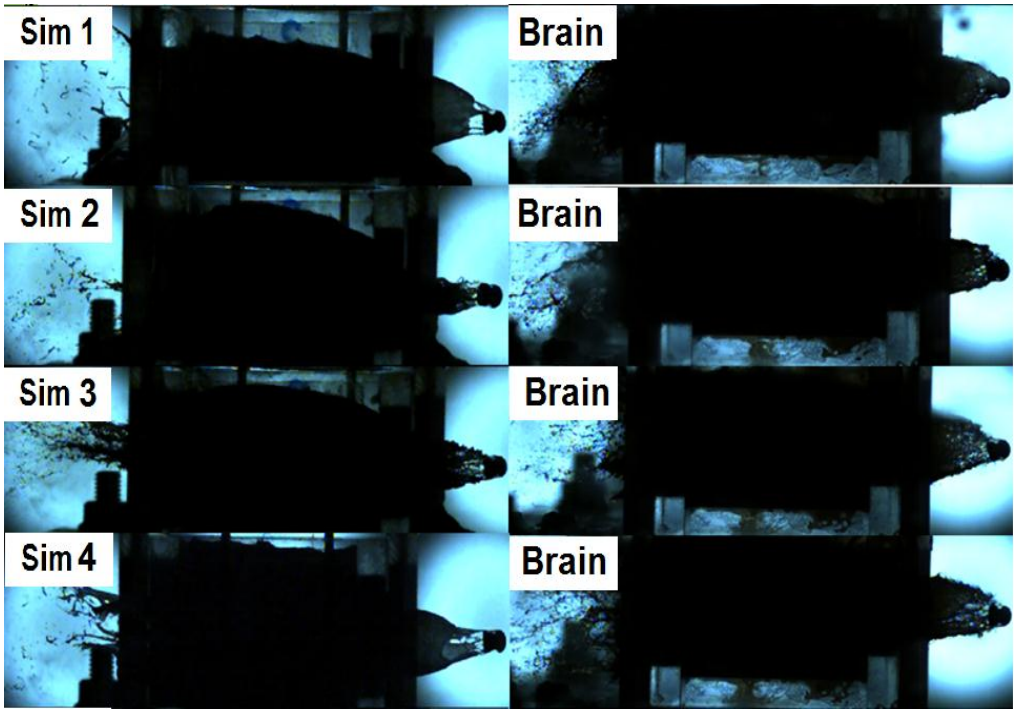

Figure 3-5: Ovine's brain and different simulant

3.4 Effect of the fibre length on the form of fragmentation

The results of visual comparison and kinetic energy loss suggest that M1 is the most realistic brain simulant of all composite materials tested. M1 can reproduce a similar form of fragmentation and absorb similar kinetic energy from a projectile, as ovine brain. As can be seen in Figure 3-5 the fibre length has an important effect on the form of the fragmentation and kinetic energy absorption. According to Table 3-1 simulant number two with 80 mm nylon fibre absorbed more energy compared to the rest of the materials tested in this experiment. Thus, a set of experiments was performed on the M1 simulant with different fibre lengths. In order to perform the experiment with higher kinetic energy projectiles such as 9 mm and .22 LR it was necessary to use larger sample pieces. Small samples will disintegrate faster upon impact and extracting data from video requires a higher frame rate and a more intense light source. As mentioned earlier according to the study by Pervin and Chen (Pervin & Chen, 2011) there

are no significant differences between gender and species of mammal brain on the dynamic behaviour of the brain. Therefore, in this section bovine brain was used for comparison with the M1.

3.4.1 Experimental setup:

The experimental set up is shown in Figure 3-6. Experiments were performed on the bovine brain at the Otago Pistol Club[2] and were compared to M1 with different fibre length at an ambient temperature of 20±1 º C. Experimental data was recorded using a Photron SA1 and SA5 high speed camera (key parameters shown in Table 3-2). Each sample was shot with a 7.45g 9×19 mm full metal jacket (American Eagle Manufacture), which had a muzzle velocity of 379 m/s and .22 LR with mean velocity of 350 m/s. A Glock model 17 semi-automatic hand gun for 9 mm projectiles and a .22 rifle for .22 LR projectiles were clamped to a firing bench was used in this experiment. Eight fresh bovine brains[3] were used for comparison with the brain simulants. The time from slaughter to removal of the brain was 30 minutes and all brains were stored at 1° C for less than 24 hours. In order to have the same approximate position of the brain in the holder, one and a half bovine brains were placed into the plastic container which had dimensions of 150×120×90 mm with an open entry and exit hole with diameter of 35 mm. It must be noted that due to the cost and availability of the equipment's each material was tested minimum two times. Thus performing the statistical analyse are not possible on the available data. Repeatability and uncertainty in the velocity calculation due to the pixelation of the image and consequent uncertainty in position of the projectile gave a maximum uncertainty in velocity of ± 5%. The SA1 camera was used to make sure that the projectile hits the target at the entrance hole.

Table 3-2: Camera and illumination parameters

Camera	SA1	SA5
Frame rate	30000	30000
Shutter speed (sec)	1/338000	1/500000
Type of lens	55 mm Nikor	90 mm Tamron
Aperture	2.8	2.8

[2] Otago Pistol Club, Green Island, Otago (New Zealand)

[3] Provided by Silver Fern Farms company (Dunedin, New Zealand)

Light	8×8000 lumens (LED)	8×8000 lumens (LED)
Resolution (pixel)	448×384	896×176

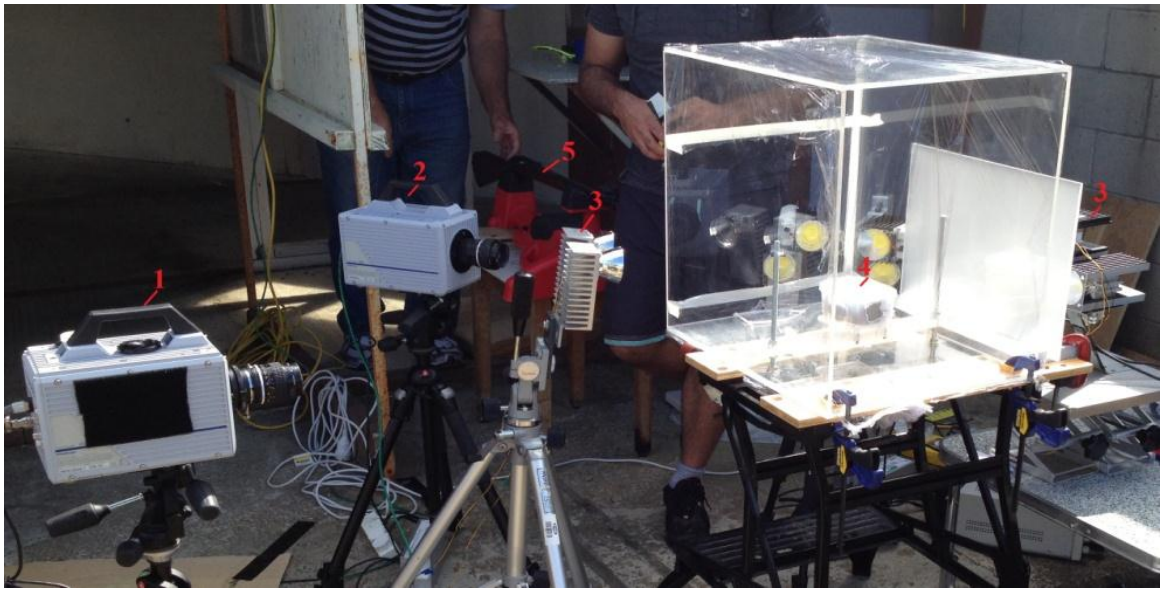

Figure 3-6: Experimental setup; 1- SA5, 2- SA1 3- LED lights 4- samples 5- gun

3.4.2 **Methodology**

In order to compare the form of the fragmentation from simulant and the bovine brain, it was necessary for the simulant to have the same approximate shape. A mould of a fresh bovine brain was made. The moulding and casting procedure can be found in section 2.7.3. This mould was used to create a brain shape in M1. A sheet of cling film, coated with petroleum jelly was placed in to the mould and the M1 material was poured in to the mould. After one hour, samples were wrapped in Glad Wrap and removed from the mould and were kept in the refrigerator at a temperature of 4 °C for 24 hours. With this procedure it is possible to create a simulant with the same shape as the bovine brain. The diameter of the extrusion of the material at the bullet entrance point and the energy absorption were compared between different materials. It must be noted that the SA1 camera was used to make sure that the bullet hit the target exactly at the entrance section of the box.

Figure 3-7: 1- dental stone model 2- Silicone mould 3- M1 in the shape of the bovine brain

3.4.3 **Results and discussion**

PFV FASTCAM viewer software was used to measure the diameter of the entry hole as the bullet hit the target and passed through the material. An example of the measurement of the entry hole is shown in Figure 3-8. Frame one is the bullet before impact and frame two shows the moment of the impact. Measurements were performed after the first complete appearance of the extrusion (Figure 3-8.3). As can be seen from frames three and four, the diameter of the entry hole increased as the bullet penetrated. All the error bars are 5% fixed error which might occur during the image processing due to pixelation.

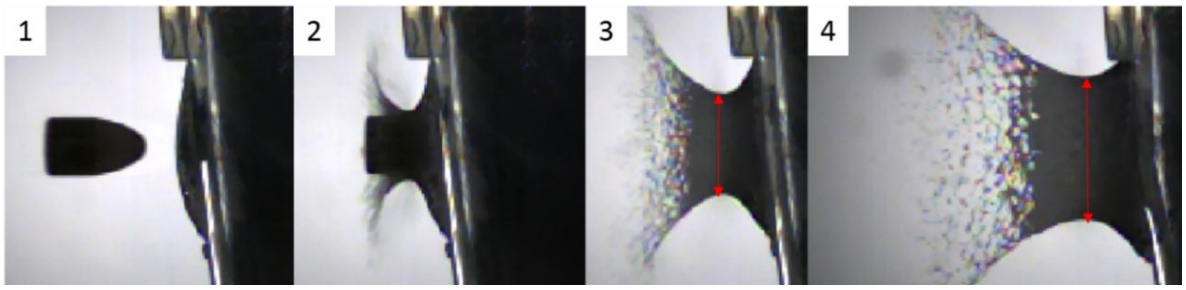

Figure 3-8: Measurement of the diameter of the entry hole

Figure 3-9 shows the diameter of the entry extrusion of the materials at the entry hole as the bullet passes through the samples. It can be seen that by increasing the length of the fibre, it is possible to change the diameter of the extrusion of the material. M1 with 5 mm fibre length can reproduce the extrusion of the bovine brain under impact from a 9 mm bullet.

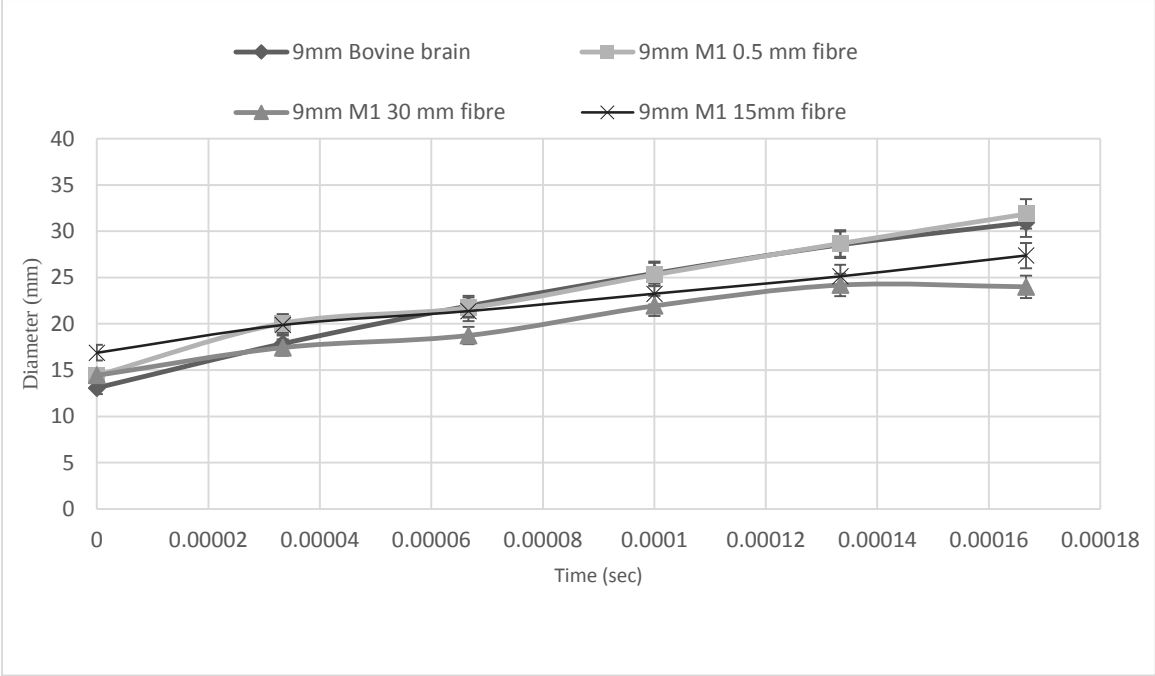

Figure 3-9: Diameter of entry hole from 9 mm projectile

The energy loss from the 9 mm bullet passing through different materials is shown in Figure 3-10. Kinetic energy loss of the projectile was measured using PFV Fastcam viewer, by measuring the velocity of the projectile before and after impact. The procedure for the measurement of the kinetic energy can be found in chapter 2.8 . Results show that there is no major effect on the energy absorption from the sample with the fibre length of 5 to 15 mm. However, by increasing the size of the fibre from 15 to 30 mm, the energy absorption increased. The error bar in Figure 3-10 is the ±5% fixed error which accrued during the image processing.

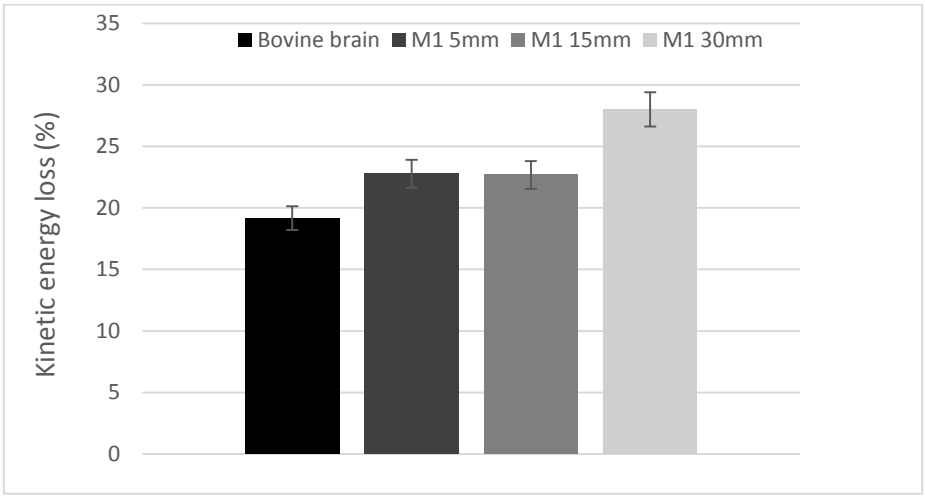

Figure 3-10: Kinetic energy loss by 9 mm in different materials

Figure 3-11 shows the diameter of the extruded material created from .22 LR as the projectile passes through the material. The diameter of the extruded material in bovine brain was bigger than any other material. There was no substantial differences in the diameter of the extruded material in M1 samples with different fibre length. However the diameter of the extrusion of the M1 material well matched for the experiment with 9 mm projectiles but not for .22 LR.

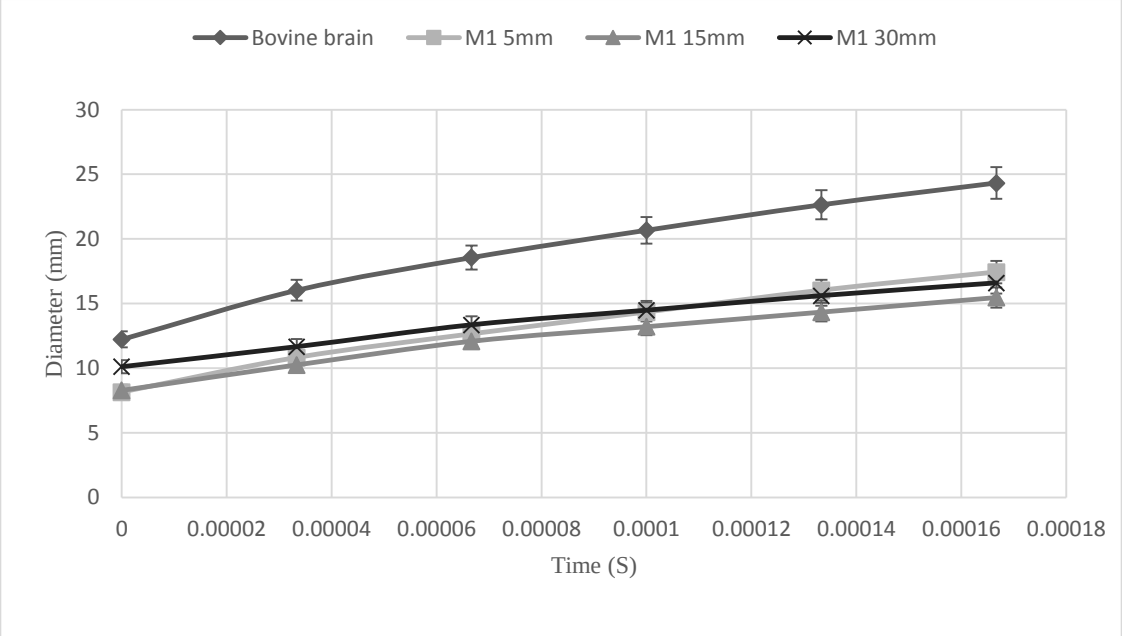

Figure 3-11: Diameter of entry hole from .22 projectile LR

In order to measure the kinetic energy absorption from the videos, it was necessary to measure the velocity of the moving object with high accuracy. Accurate measurement of the energy absorption by the material from .22 LR was not possible in this experimental setup. The projectile rotated on different axis in each set of experiments, thus it was impossible to be sure that the path of the bullet was parallel to the field of view of the camera. An example of the rotation of the .22 LR projectile as it exited the material shown in Figure 3-12.

The results of this section indicate that M1 with 5 mm fibre length is the best available material for the experiment performed by 9 mm projectile and it is not worse than the other simulant for .22 LR as it has the similar energy absorption and reproduced similar form of fragmentation. The next section of this study shows the limitation and common errors which might accrue in quantitative data analysis in ballistic experiments.

Figure 3-12: Example of the tumbling effect on .22 LR projectile

3.4.4 Velocity of the extruded material backward

Figure 3-13 shows an example of the image obtained from the high speed camera. The velocity of the extrusion of the material was calculated using PFV Fastcam viewer software. The velocity measurement was performed by measuring the displacement of the material 0.00016 sec after the bullet hit the target. The red arrow in Figure 3-13 shows the displacement of the material backward. The green line in Figure 3-13 shows the position of the surface before impact and the yellow line shows the position which material travelled in 0.00016 sec.

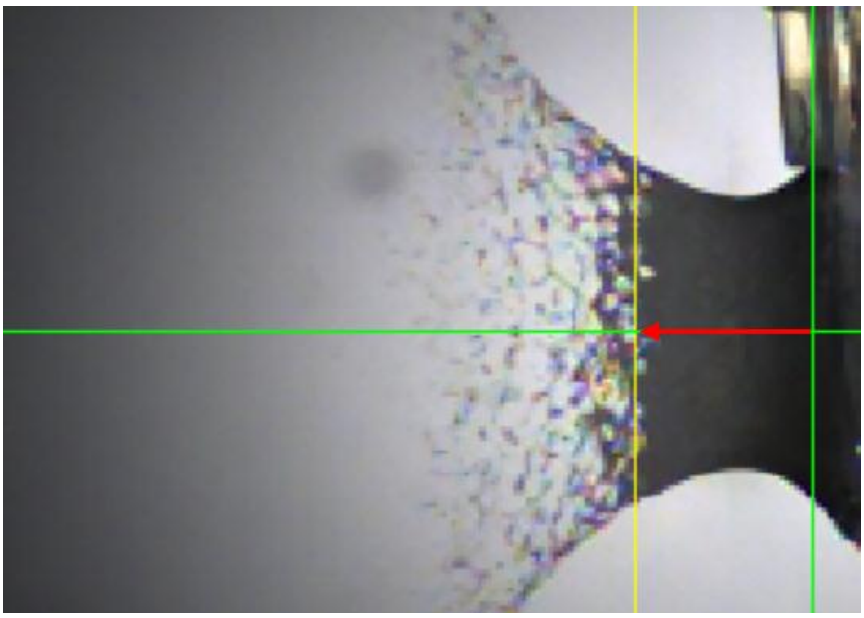

Figure 3-13: Velocity of the extrusion of the martial backward

Figure 3-14 shows the velocity of the extrusion of different materials which were shot with a 9×19 mm full metal jacket projectile. As can be seen, the bovine brain moved backward with an mean velocity of 83 m/s. M1, with 5, 15, 30 mm fibre length had the mean velocity of 75, 76, 58 m/s respectively. As can be seen from Figure 3-14, results obtained for M1, with 5 and 15 mm fibre length are within the limit of each other within the error bars. M1 with the 30 mm fibre length had the lowest velocity, 58 m/s.

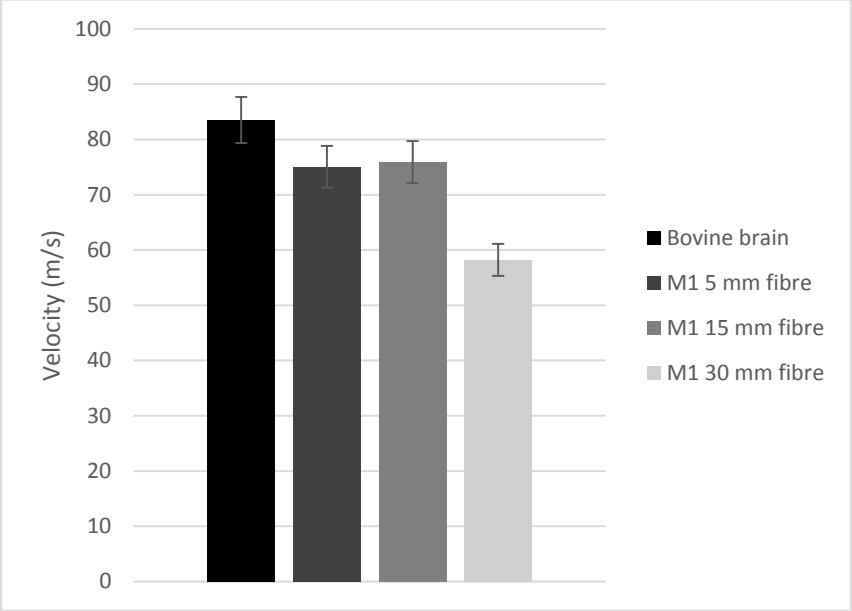

Figure 3-14: Velocity of the extrusion of the materials backward

Figure 3-15 shows images of the experiments with four different materials. The top left corner in Figure 3-15 is the bovine brain, and top right is the M1 with 15 mm carbon fibre. Bottom right is the M1 with 5 mm carbon fibre and bottom left is M1 with 30 mm carbon fibre. It can be seen clearly that the M1 with 5 mm carbon fibre is producing the fragmentation pattern closest to the bovine brain. By changing the length of the carbon fibre it is possible to change the angle of the throat of the extruded material. A change in the angle and throat diameter can have severe effect on the quantity of the material which is able to move backward from the wound channel.

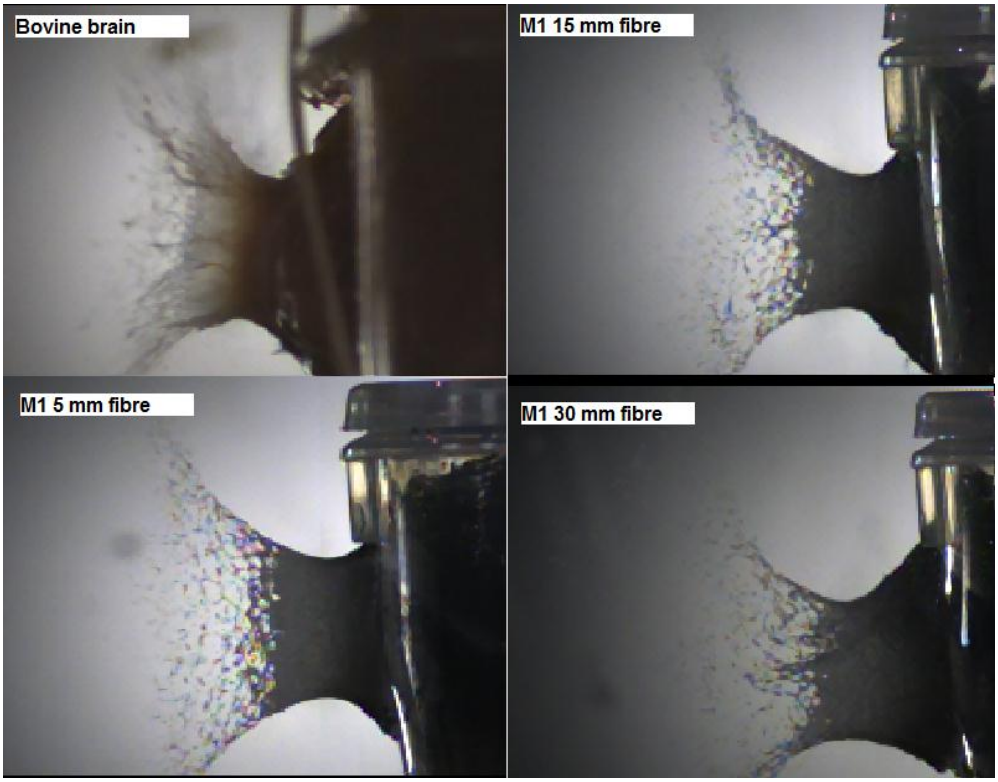

Figure 3-15: Top left corner is the bovine brain, and top right is the M1 15 mm Carbon fibre. Bottom right M1 5 mm carbon fibre and bottom left M1 30 mm carbon fibre

It is difficult to achieve repeatability in quantitative measurement of ballistic impact effects as it is difficult to hit the target at the exact same position. This section aims to show the difficulties in the measurement and find the sources of error during the image processing and experimental setup. It must be noted that the ammunition, light and camera setup were the same at all times. Figure 3-16 shows combined images taken from two sets of experiment performed on the bovine brain. Two images were combined using a Matlab code to identify the differences between them. The function ‘’imshowpair’’ with ('falsecolor') option was used in the main code. This function combines two images and shows the difference using different colour bands. The grey section in the composite image shows locations with the same intensity. The green and magenta regions are the places in the image with different intensities. This analysis led to the question of repeatability of the experiment. It can be clearly seen from Figure 3-16 that measuring the velocity of the extrusion of the material can be affected by the repeatability of the experiment. Preferably, these two images would have the same exact form of fragmentation and tail splash.

Figure 3-16: Two combined images from the experiment performed on bovine brain

3.4.5 Conclusion

Using high speed cameras it was possible to develop a new method for quantitative and qualitative comparison of different material upon impact. The results of this work show that the differences between the fresh ovine brain and preserved ovine brain are negligible for proposes of this study. The effect of the fresh, refrigerated and frozen then refrigerated of porcine muscle studied by Breeze et al (Breeze et al., 2015) shows that there are no differences in the depth of penetration in this three groups of the tested material, which is confirms the findings of this study. However fresh ovine brain absorbed more energy compared to the one preserved at the temperature of 1°C for 24 hours. It is possible to change the components in the composite material to produce a simulant that matches the velocity and diameter of the extrusion of the material with the brain tissues. The results clearly show that M1 with 5 mm carbon fibre produced more brain like form of the fragmentation for 9 mm experiments and it is the best material available for experiment performed with .22 LR. However even by moulding the material in the bovine shape it was not possible to have the same external shape, as the variety exist in each brain sample. The form of the fragmentation depends on different variables such as rotation of the bullet, angle of the first impact and recording time of the impact. In order to reduce the error in image processing, effort must be made to keep the experimental setup constant. However obtaining the same form of fragmentation from the same material in different test is not possible, as a very small changes in the angle of the gun or sample will lead to different forms of fragmentation and will cause error in the quantitative data, but it will not change the overall mean result. Thus this study suggests that qualitative analysis parallel to quantitative measurements are required for analysing the mechanism of formation of the backspatter and fragmentation generated from soft tissues. Results of the experiments suggested that a more brain like material such as M1 compared to gelatine must be used as a brain

simulant for ballistic study of the human head particularly if the aim is to generate the same form of the backspatter and fragmentation.

4 Experimental investigation of the mechanical properties of brain simulants used for cranial gunshot simulation

4.1 Introduction

As previously mentioned measurements of physical properties at ballistic strain rates are extremely difficult. Instead, in this study, the mechanical response of samples is studied during projectile penetration by analysis of high speed video images. The response of the sample is studied quantitatively, with greater thoroughness than in previous studies, by considering both the kinetic energy absorption and the motion of the sample. A quantitative comparison of the simulants and animal tissue is then possible. As mentioned before in chapter three it is not possible to have the same exact external shape for brain samples. External shape can have direct effect on the form of the fragmentation. Thus in the section of the study series of experiments were performed on samples of material cut into cuboids to obtain better results. For the study of the dynamic behaviour of the brain upon impact and the effect of the behaviour of the material to the generation of the back-spatter three factors have been considered. The expansion rate, velocity of the extrusion of the material backward, and overall form of deformation of the material. In order to compare the form of fragmentation of the brain with simulants, a series of experiments were performed with .22 LR and .22 AR projectiles. 10 % gelatine as a standard material were tested along with M1 and 3, 5 % gelatine and were compared with the bovine brain.

4.2 Experimental Methodology

A schematic of the experimental set up is shown in Figure 4-1. The experiment was performed with the sample material at the laboratory temperature of 18±1 ºC and recorded using a Photron SA1 high speed camera (key parameters shown in Table 4-1: Camera and illumination parameters). Each sample was shot with a 1 ± 0.006 g, round nose diabolo projectile from a .22 air rifle which had a velocity of 290 m/s, and a solid lead projectile with 2.59 g 0.22 LR and a velocity of 330 m/s (measured from the video). Temperature of the samples at the moment of the experiments were 4°C. Repeatability and uncertainty of the velocity calculation due to the pixelation of the image and consequent uncertainty in position of the projectile gave an uncertainty in velocity of ± 5%.

Table 4-1: Camera and illumination parameters

Frame rate	Shutter speed	Type of lens	Aperture	Light
24000	1/684000 s	55 mm Nikor	2.8	4×8000 lumens (LED)

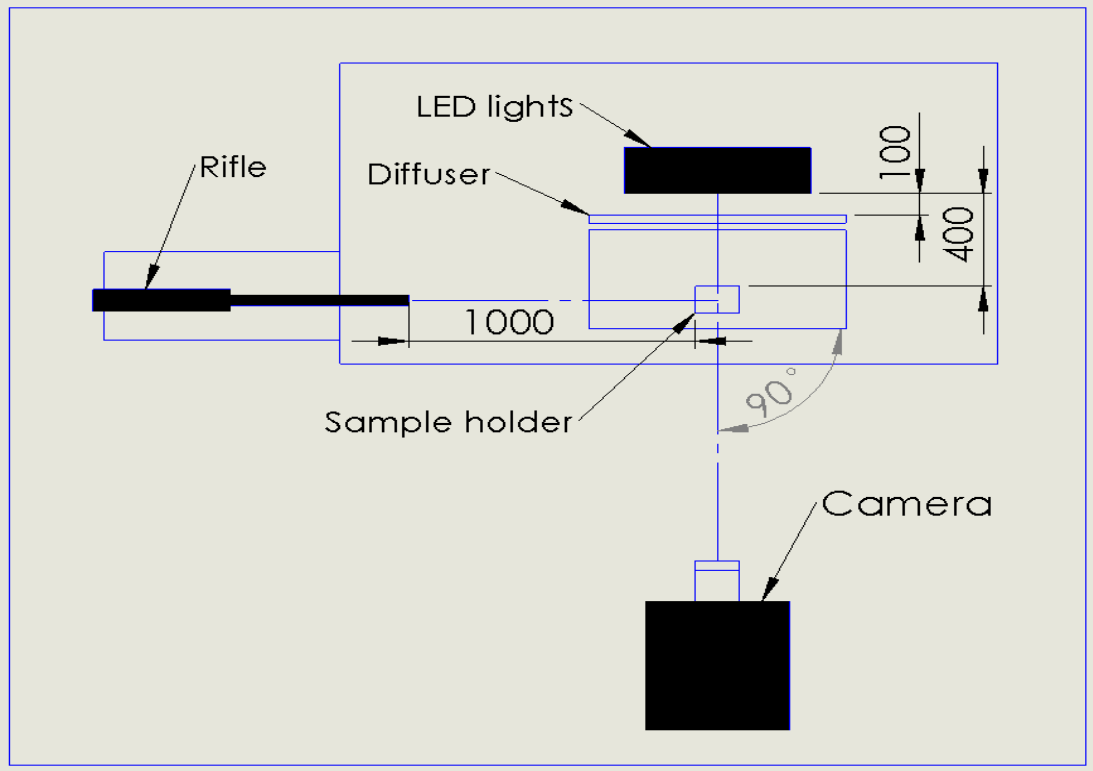

Figure 4-1: Experimental setup

Ten fresh bovine brains[4] were used for comparison with the brain simulants. The time from slaughter to removal of the brain was 30 minutes and all brains were stored at 1 °C. Three samples with dimensions of 52×29×37 mm were cut from one hemisphere of the brain and placed in a Perspex box (Figure 4-2). The box had internal dimensions of 2 mm less than the brain sample in order to avoid any gaps between material and wall of the box. The diameters of the predrilled entry and exit holes in the box wall were 22 mm. The thickness of the wall of the box was 12 mm to limit the expansion of the simulant and brain to one direction (vertically upwards). The procedure for the preparation of the gelatine and M1 can be found in chapter section 2.7. The material was poured into a plastic container and kept in the refrigerator for 24 hours before testing. The gelatine and M1 samples were cut before

[4] Provided by Silver Fern Farms company (Dunedin, New Zealand)

testing to the same dimension as the bovine brain samples. All samples were shot less than three minutes after the material was taken out of the fridge.

Figure 4-2: Bovine brain (a), Gelatine (b) holder for samples(c)

4.3 Data analysis

Figure 4-3 shows an example of the high speed video images obtained used in this study. The expansion of the material over each frame of the video was measured using PFV Fastcam software by tracking a specific point (the red line in each frame in Figure 4-3) on the surface of the material. Each pixel has a dimension of 0.31 × 0.31 mm and the time between frames was 41.7 µs. Knowing the dimensions of each pixel and time between frames it was possible to calculate the displacement of the material. The surface of the material was tracked by averaging the displacement over 10 frames. Uncertainty in the displacement measurement due to the pixelation of the image was ± 0.31 mm.

Figure 4-3: Example of data processing using Fastcam viewer and Matlab

A bullet tracking code was written in Matlab™ (Mathworks, Natick, MA) to obtain the bullet velocity before and after impact. Detailed procedure of the velocity and displacement calculation can be found in chapter two section 2.8.

4.4 Results

Figure 4-4 shows a comparison of the expansion of each simulant material compared to a bovine brain sample, after impact from the AR (Figure 4-4 a) and LR (Figure 4-4 b) bullets over time. After an initial expansion, the gelatine samples recoiled elastically into the sample holder. The final datum point for each of the gelatine samples represents the time this elastic recoil started to occur, after which no further expansion was observed. The bovine brain and M1 exhibited no such recoil. The final data points for the bovine and M1 samples are the times where the sample surface exited the field of view and no more data could be obtained.

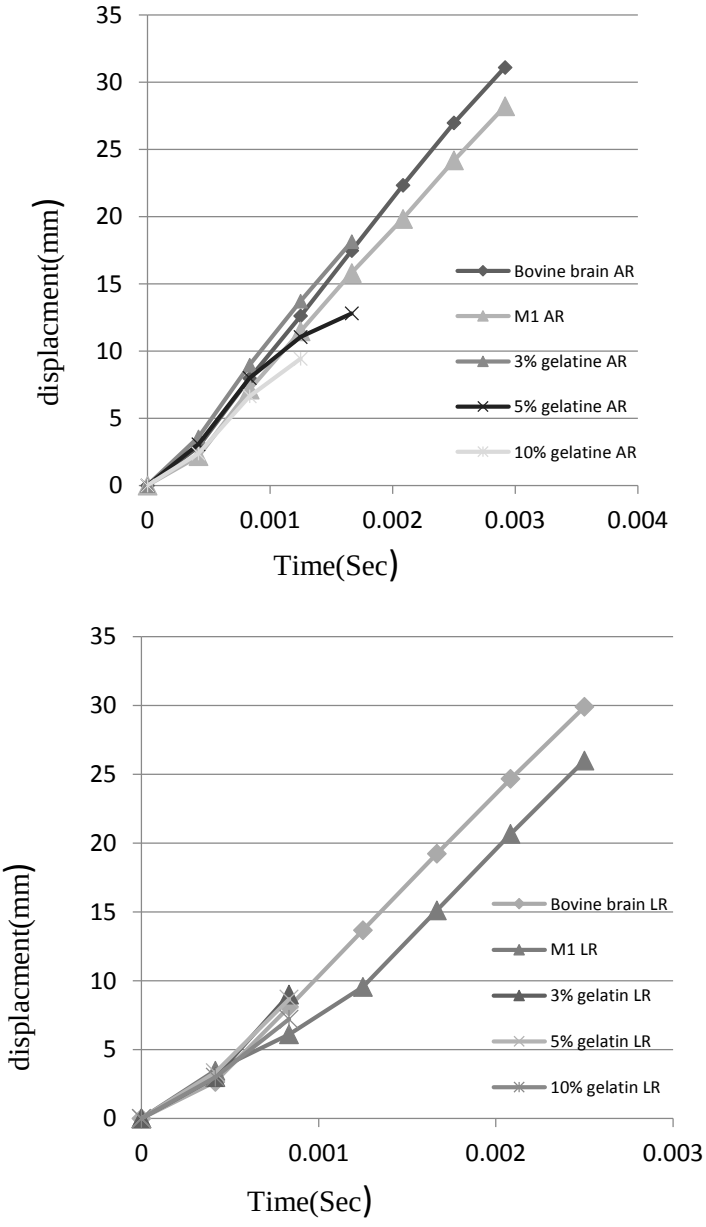

Figure 4-4: Comparison of the displacement of the upper surface of the samples after impact from the (a) AR and (b) LR

Figure 4-4 shows that the bovine brain experiences plastic deformation as the material tears apart after impact whereas the gelatine solution exhibits elastic recoil, reverting to the original shape. The brain sample and M1 material have similar displacement histories. For the AR impacts it can be seen that the rates of expansion of the 5% and 10% gelatine differ markedly from that of bovine brain. It can be seen that the 10% gelatine sample has the lowest expansion rate and due to the elastic deformation it experienced it starts to return to its original shape faster than the other materials. The 5% and 3% gelatine samples stopped expanding at the same time. The 3% gelatine sample initially has a similar expansion rate to the bovine sample before elastic recoil occurred. The 5% gelatine sample expanded at a lower rate than brain in the latter stages of its expansion period, and then experienced elastic recoil. Figure 4-5 shows the final deformation of the different materials. The permanent wound track in the gelatine is accentuated when the concentration of gelatine is reduced. The gelatine samples recoil back to their original external dimensions after the projectile passes through. Apart from the narrow permanent wound track, gelatine does not present the same permanent plastic deformation as the bovine brain and M1 material. In the latter two materials, after impact the upper section above the path of the bullet separates from the lower section and exits the box in a highly viscous flow. The lower section remains in the box.

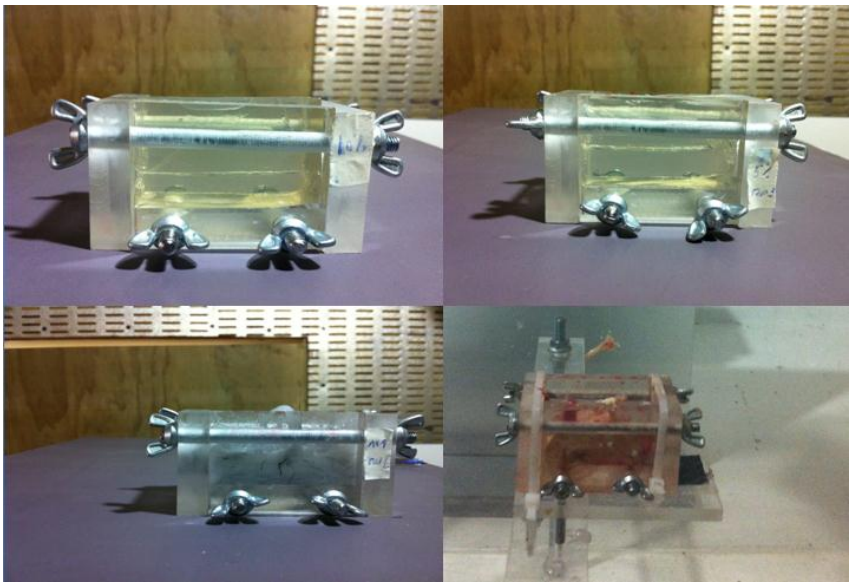

Figure 4-5: Final deformation in different materials: clockwise from top left: 10% gelatine, 5% gelatine, bovine brain, M1

The results with the .22LR show the same behaviour as the AR tests, but over a shorter time period. All the gelatine samples (at all concentrations) showed an initial rate of expansion similar to brain, but again elastic recoil occurred, that was not observed in the bovine sample. Kinetic energy of the projectile was calculated using Equation 8.

The kinetic energy of the projectile before impact was 42 ± 1.32 J for the AR and 141 ± 3.7 J for the .22 LR (uncertainty figures are standard deviations calculated on 13 and 12 shots respectively). The projectile did not deform or fragment after impact and therefore the mass of the projectile did not change. As shown in Figure 4-6 all the materials absorb a similar fraction of E_k (46 - 58% for the AR and 15-29% for .22 LR) compared to the bovine sample (50% for AR and 27% for LR) , any differences being less than the measurement uncertainty. This absorption equates to 0.88 - 1.11% of E_k per mm of material for the AR and 0.28 - 0.55% per mm for the .22LR.

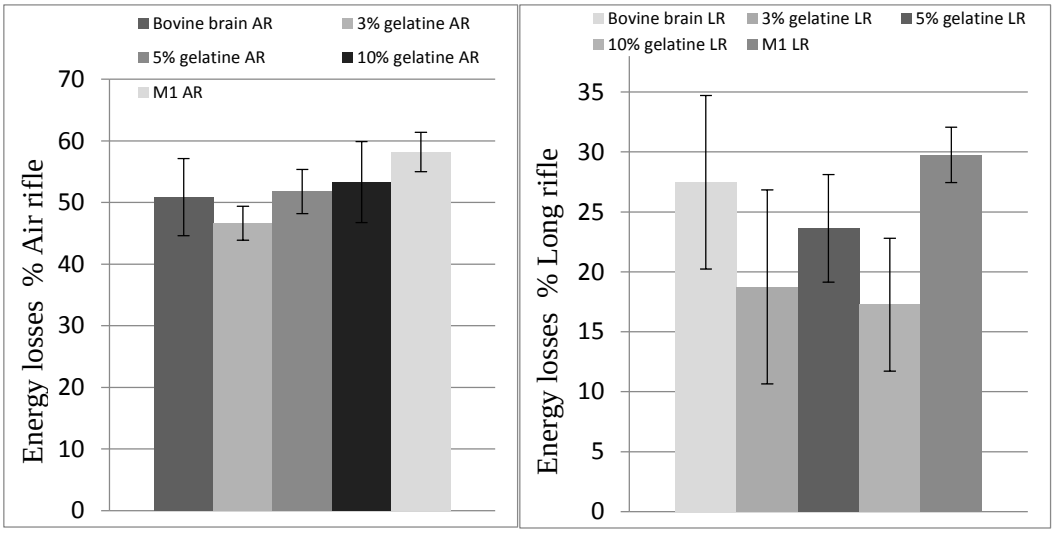

Figure 4-6: Energy absorption by different material from AR and LR projectiles

Figure 4-7 shows an example of the image obtained from high speed camera. The velocity of the extrusion of the material was calculated using PFV Fastcam viewer. Velocity measurement performed by measuring the displacement of the material in 0.00029 sec after the bullet hit the target. The red arrow in the Figure 4-7 shows the displacement of the material backward. The green line in Figure 4-7 shows the materials position before impact and yellow line shows the position which material travelled in 0.00029 sec.

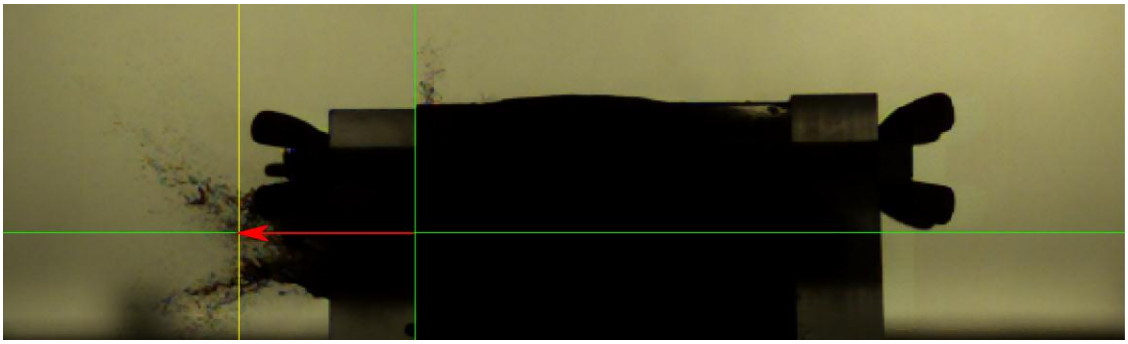

Figure 4-7: Velocity of the extrusion of the martial backward

Figure 4-8 shows the velocity of the extrusion of different materials. As can be seen the bovine brain moved backward with an mean velocity of 134 m/s. M1, 3%, 5% had the velocity of 121, 120, 114 m/s respectively. As it can be seen from Figure 4-8 results obtained for M1, 3% and 5% gelatine are within the limit of each other within the error bars. 10% gelatine had the lowest velocity 70 m/s.

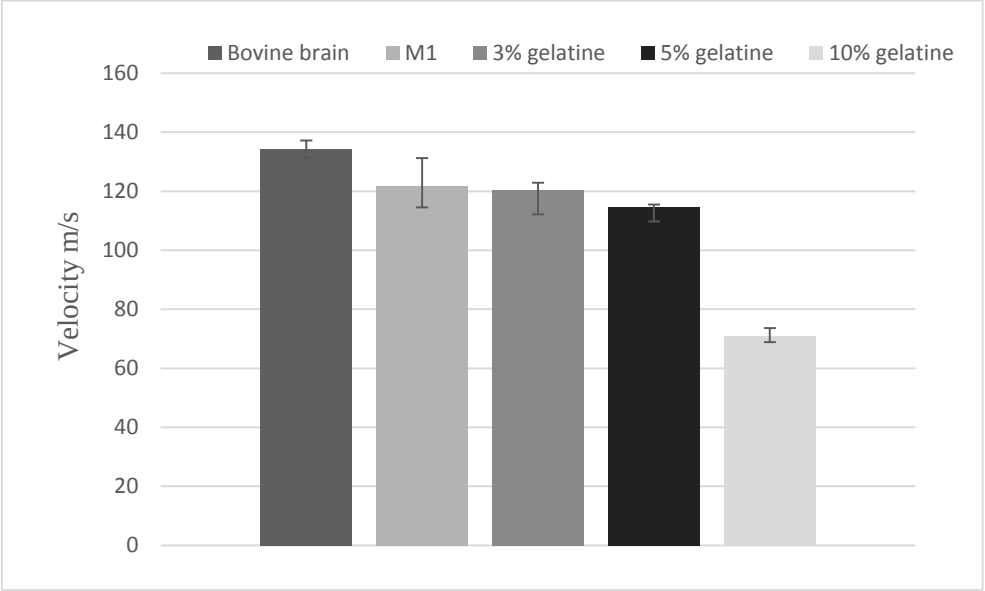

Figure 4-8: Velocity of the extrusion of the materials backward

Figure 4-9 shows combined images taken from two sets of experiment performed on the bovine brain. Two images were combined using a Matlab code to identify the differences between two images. Two images were combine with the same procedure as Figure 3-16 and shows the difference using different colour bands. The grey section in the composite image shows the places with the same intensity. Green and magenta are the places in the image with different intensity. This analysis lead to the question of repeatability of the experiment. It can be clearly seen from Figure 4-9 that measuring the mean velocity of the extrusion of the material can be affected by the repeatability of the experiment. This comparison

indicates that even by creating the same exact external shape it is not possible to have identical results between two experiments on the same material. Some of this difference will be due to small differences in projectile impact point.

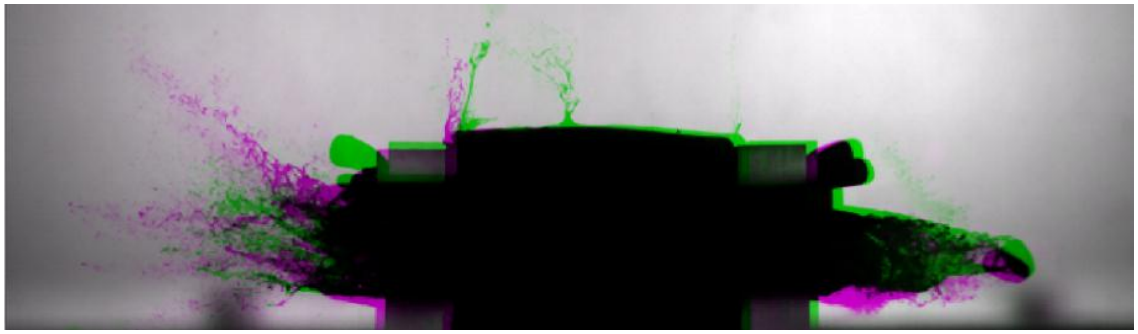

Figure 4-9: Two combined images from the experiment performed on bovine brain

Figure 4-10 shows three set of experiments for four different materials. Figure 4-10 the top left corner is the bovine brain, and top right is the M1. Bottom right is the 10 % gelatine and bottom left is 3 % gelatine samples. It can be seen clearly that the M1 is producing fragmentation closest to the bovine brain. Gelatine sample with 10% concentration is not capable of producing fragments, it can be seen that there is very small tail splash in 10% gelatine. By reducing the percentage of the gelatine from 10 to 3% it is possible to generate more tail splash, however it is far less comparable to the bovine brain samples. The form of the forward spatter in the gelatine samples is quite different to the bovine brain samples. It can be seen clearly that gelatine forms as a narrow channel which has a uniform shape around the projectile. By reducing the percentage of the gelatine the diameter of the forward spatter will increase. By reducing the percentage of the gelatine, the material becomes less elastic and it can flow around the bullet, however this form of deformation is not even close to the one observed from bovine brain.

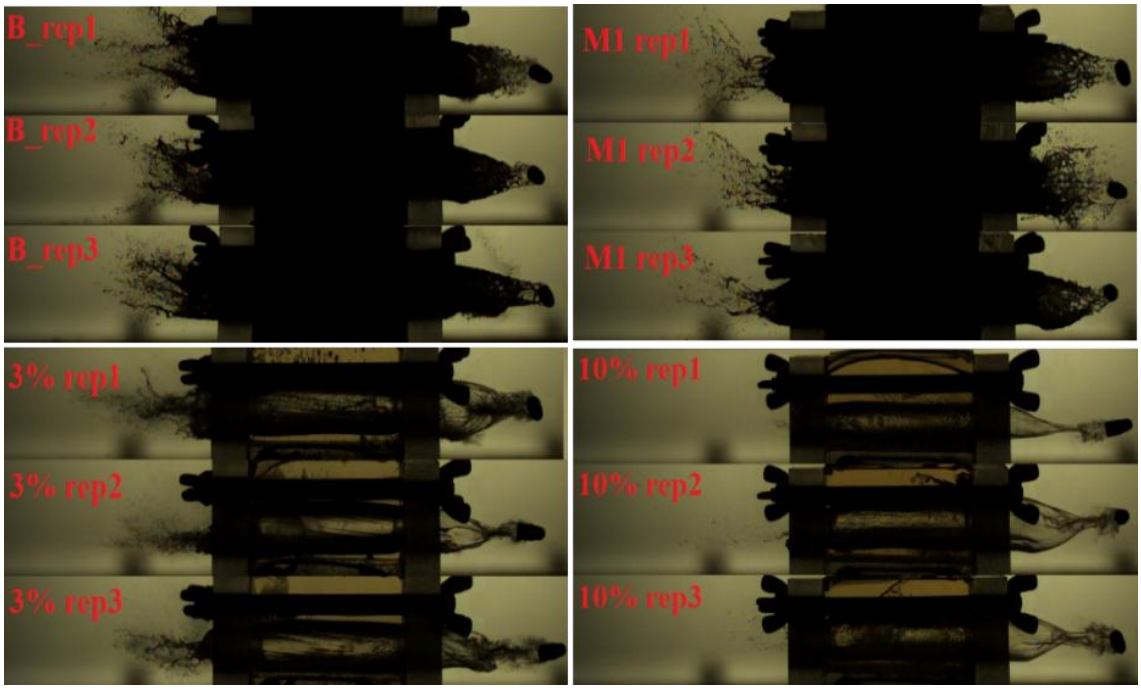

Figure 4-10. Top left corner is the bovine brain, and top right is the M1. Bottom right is the 10 % gelatine and bottom left is 3 % gelatine samples

4.5 Discussion

The displacement measurements suggest that gelatine underperforms as a brain simulant during ballistic impacts. The 10% concentration of gelatine commonly used in the literature would not replicate the deformation of brain tissue realistically under high velocity impact. Gelatine recoils elastically back into the sample holder in a way which brain does not. Further, the brain is seen to deform like a highly viscous flowing fluid as it leaves the box, which the gelatine does not. The recoil becomes more pronounced as the concentration of gelatine is increased. Recoil was least at the smallest gelatine concentration tested here (3% w/w). Besides its elastic and viscous properties, the M1 material is shown to expand at a rate much closer to brain, producing a more realistic deformation than gelatine in this ballistic range of impacts.

The energy absorption of all materials is similar, despite apparently quite different elastic and viscous properties. It may be that the energy absorption is principally due to the inertial force $\frac{1}{2}A\rho v^2$, where A is the cross sectional area of the bullet, ρ the density of the brain (or simulant) and v the velocity of the bullet. It is known in hydrodynamics that the inertial force becomes greater than the viscous force as the speed is increased above a certain value. The densities of brain tissue and all simulants (except M1)

are similar, all being close to the density of water ≈ 1000 kgm^{-3}, so if the inertial force is dominant in kinetic energy absorption, all samples would be expected to show the same absorption, as it was observed in this study. The velocity of the extruded materials were 130, 121, 120, 114, 70 m/s from bovine brain, New material M, 3%, 5% and 10% gelatine respectively. The form of the fragmentation generated from M1 material was the closest to the one observed from the bovine brain.

Much of the literature describing the temporary cavity is based on studies using gelatine. The data presented here, showing that gelatine responds with stronger elastic recoil than brain, invites a re-examination of the detail of gelatine-based studies. Evidence for the temporary cavity is however not restricted to gelatine studies, cavities of greater than the bullet diameter being seen for example in studies with glycerine soap (Frank et al., 2012; Kneubuehl et al., 2012; Thali et al., 2001), which has almost no elastic recoil at all.

A notable advantage of gelatine is that it is transparent, and the dynamics of the internal cavities can be seen clearly. The M1 simulant used in this study is opaque, and this suggests a direction for further development. Also, the tests described here are far from exhaustive and further testing with larger calibre firearms, other measurements of displacement and fragmentation, and adjustments to the formulation of the simulant and should be carried out to test the response of the material stringently. The cuboid, open-topped sample box used in the present study is a convenient method to isolate the response of the brain or simulant.

4.6 Conclusions

The dynamic response of bovine brain, gelatine in three concentrations (3%, 5% and 10% w/w) and a new simulant based on glycerol, water, starch and fibre has been investigated. All gelatine samples showed an initial expansion followed by elastic recoil. Neither the brain, nor the new simulant showed this elastic recoil. The expansion rate of the new simulant, the viscous flow when extruding from the sample box, and the form of the permanent damage, all resembled closely those of the brain sample. Kinetic energy absorption was similar for all materials, gelatine included. The form of the fragmentation

from M1 was the closest to the one observed from bovine brain. The response of the M1 material is much closer to the bovine brain over the time period observed in this work.

5 Stopping distance, form and size of the permanent cavity in simulant and bovine brain

5.1 Introduction

Ballistic gelatine has been used in the past several decades as a simulant for soft tissues in ballistic experiments (Carr et al., 2014; M. Fackler et al., 1984; M. L. Fackler & Malinowski, 1985; Jussila, 2004, 2005; Kneubuehl et al., 2003; Knudsen et al., 1995; Korac, 2001; Rutty et al., 2008; Jiangyue Zhang et al., 2005; J. Zhang et al., 2007). It has been validated against porcine muscle by measuring the stopping distance in samples (Jussila, 2005). 10 and 20 % gelatine are also used as a brain simulants (Carr et al., 2014; 2002; Jiangyue Zhang et al., 2005). However, there is minimal validation of such material as a suitable brain simulant. In the chapter 4.4 which is also published by Lazarjan et al. (Lazarjan et al., 2014) It can be seen that that bovine brain has a higher expansion rate compared to 3,5 and 10 % gelatine. As such series of experiments were performed on 5, 10% (W/W) gelatine, new simulant (M1) were compared with bovine brain. There are several methods in the literature which describes the measurement technique of the kinetic energy dissipation of the bullet into the material, such as longest tear in each slice by Schyma and Madea (Schyma & Madea, 2012), two longest tears Fackler and Malinowski (M. L. Fackler & Malinowski, 1985) and total crack length by Ragsdale and Josselson (Ragsdale & Josselson, 1988). However, implementing these methods to assess the kinetic energy dissipation in the brain tissue is not possible. Due to the opaque nature of the brain tissue it is not possible to identify the start and end points of the cracks in the brain tissues. Thus, in this study ellipse and polygon fits were used to measure the area of the permanent wound track. Also the stopping distance and from of the damage created by a .22 air rifle in 5, 10% gelatine and M1 were compared with the bovine brain. Finally, the effect of the boundary condition on the form of the damage in different material has been investigated.

5.2 Experimental method:

The stopping distance of the impact of a 1±0.006 g, round nose diabolo projectile from a .22 calibre air rifle, which had a velocity of 290±2 m/s was compared between bovine's brain, 10%, 5% w/w gelatine and M1. The experimental setup is shown in Figure 5-1. The distance between muzzle and samples was 410 mm and the test samples dimensions were a 95×95×430 mm^3. The method of preparation of gelatine and M1 can be found in chapter 2.7.1 and 2.7.2. Bovine brain was defrosted overnight in saline solution

and had a temperature of 4°C prior to the experiment. All gelatine and M1 were kept at the temperature of 4°C 24 hours before the experiment. The brain samples were made of 6 to 7 individual bovine brains which, were placed side by side each other to have the length of 430 mm. All the samples were shot in two different boundary conditions, constrained (Figure 5-1) in an aluminium case with the open entrance and exit, and with no external boundary.

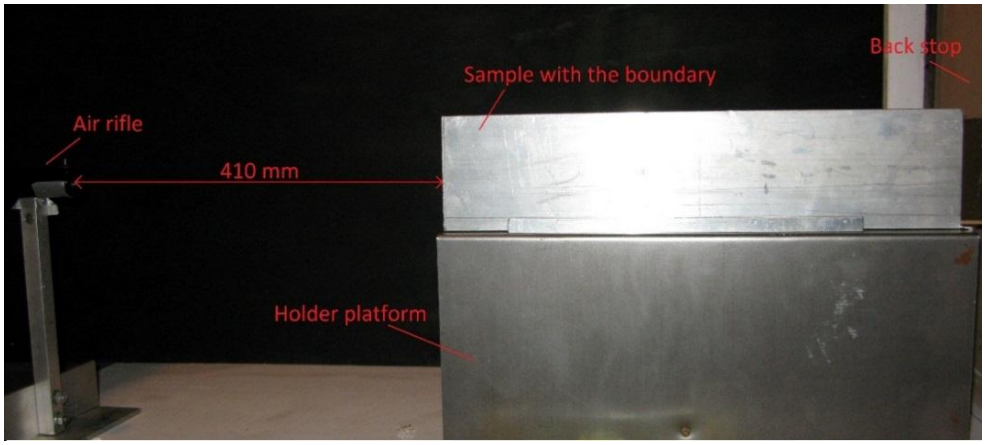

Figure 5-1: Experimental set up

5.3 Results and discussions

Figure 5-2 shows the stopping distance of the projectile in different materials. As can be seen the stopping distance increased by decreasing the percentage of the gelatine from 10% to 5% in which the stopping distances was 269 mm±10 mm and 402 mm±10 mm respectively. For the M1 material the bullet passed through the entire sample (430 mm) and exited out the other side, this indicated that the M1 material underperforms as simulant for measuring the stopping distance in the brain tissue. Thus, the M1 material was not included in the results section. The projectile stopped at a depth of 390 mm±10 mm in the bovine brain sample. Measurements were taken of the permanent wound track in the transparent gelatine. For the brain samples measurements were taken by cutting the brain samples into 10 mm slices. Therefore, 10 mm uncertainty in measurement might occur during the cutting procedure of the brain samples. The error bars in Figure 5-2 are ±10 mm.

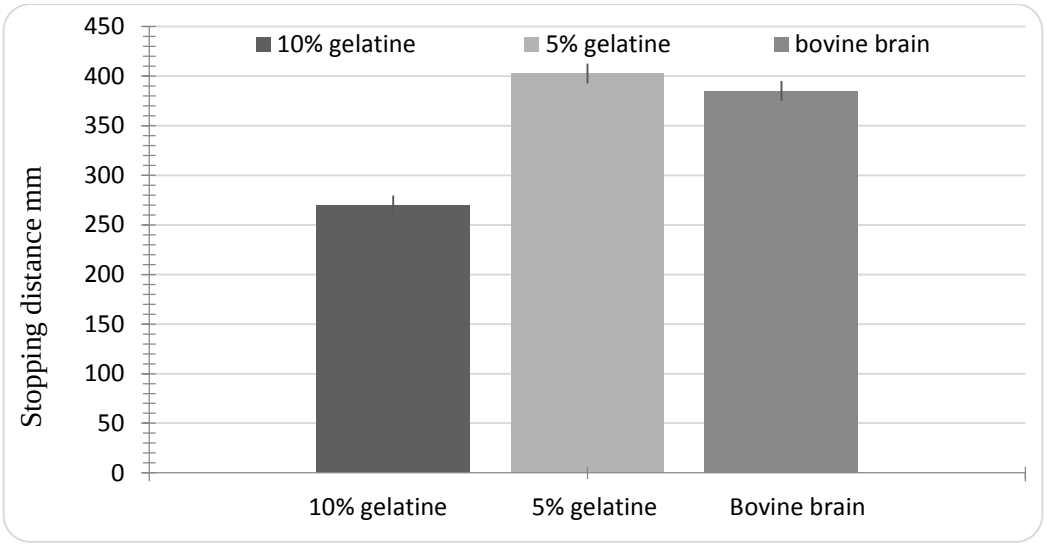

Figure 5-2: Stopping distance of the projectile in different materials

The effect of the boundary condition (Confined with open entry and exit and unconfined) on the depth of penetration was compared in different materials. Figure 5-3 shows stopping distance of the projectile in 10% gelatine with and without boundary. Depth of penetration reduced by about 14 mm in the samples with the rigid boundary for 10% gelatine. However, the effect of the boundary was not substantial in the 5% gelatine. It must be noted that the experiment with the boundary for bovine brain was not successful. Containing bovine brain in the aluminium block is difficult as one brain is not big enough to fill the block. So it is necessary to use several bovine brains on top of each other, and as the sample cannot then be homogeneous, it is difficult to fit the boundary around the sample.

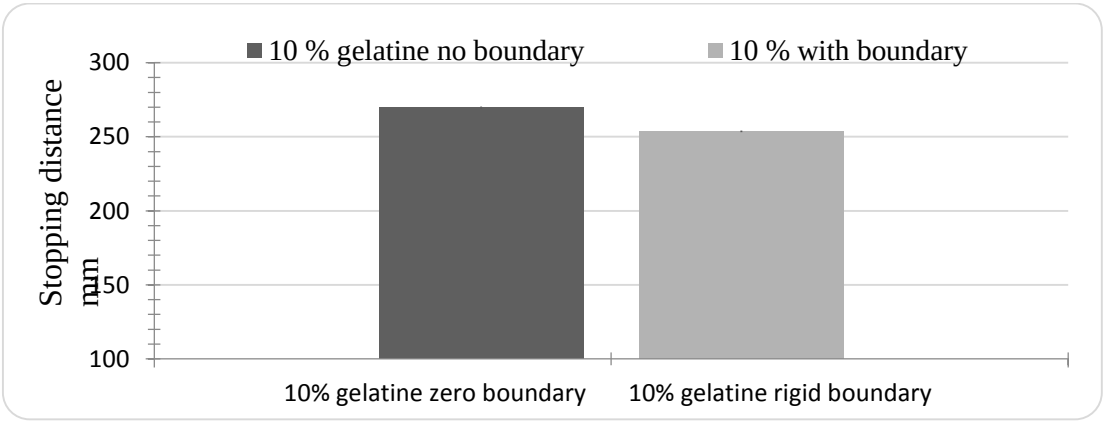

Figure 5-3: 10% gelatine without and with boundary

5.4 Form of the damage in different material

In order to have a constant thickness of the material slices a cutting platform was used. In order to create a uniform cut the brain samples were kept in the freezer after the experiment for 30 minutes at a

temperature of -20°C. Each block of the material was placed into the cutting platform and was cut using a blade. An example of the boundary condition, cutting platform and gelatine mould is shown in Figure 5-4.

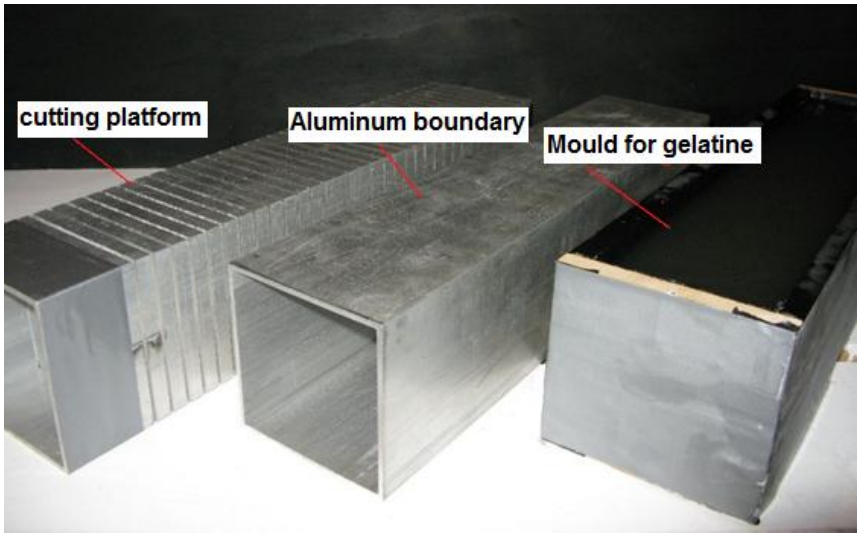

Figure 5-4: Photo of mould for gelatine, aluminium boundary and cutting platform

An image of each slice was taken using a Nikon D600 camera with the 130 mm macro lens. Each image had a dimension of 4000×3000 pixels. Two LED light with 20000 lm was used for illumination. Each sample was sprayed with flawfinder penetrant spray (Rocol) to visualize the cracks in the samples. The crack detection liquid was cleaned from the surface as the remaining paint in the crack gave a good contrast for visualization of the form of the damage. Figure 5-5 shows an example of the form of damage in the wound channel in 10% gelatine with a confined boundary condition. As can be seen, the energy of the bullet dissipates in the material in the form of a large crack in one side. The crack rotates in a clockwise direction, which is the direction of the rotation of the bullet due to the rifling in the barrel.

Figure 5-5: Form of the damage in 10% gelatine with the rigid boundary

Figure 5-6 shows an example of the form of damage on the wound channel in 10% gelatine unconfined. It is clear the energy dissipation in to the material is more uniform all around the wound track compared to Figure 5-5. Moreover, in the study by Jussila (Jussila, 2005) they noted that the longest crack tends

to be in the direction of the supporting platform. Thus, a conclusion can be drawn that if the material is confined the longest crack will rotate around the wound channel as the bullet penetrates.

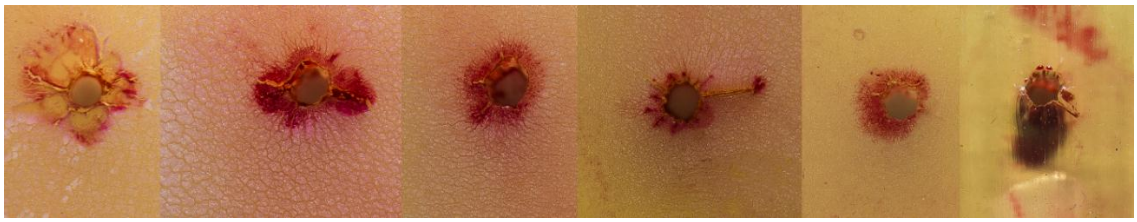

Figure 5-6: Form of the damage in 10% gelatine without boundary

The form of the deformation of the permanent wound channel was different for 10% gelatine compared to 5%. The scenario of one big crack in one side was observed in the experiment with the boundary. The form of the damage in the 5% gelatine without boundary is different from 10% gelatine. In 5% gelatine three large cracks can be seen throughout all the wound track. However, in 10 % gelatine several small cracks can be found around the central hole. Figure 5-7 presents the differences in the 5% gelatine samples in two different conditions, confined and unconfined.

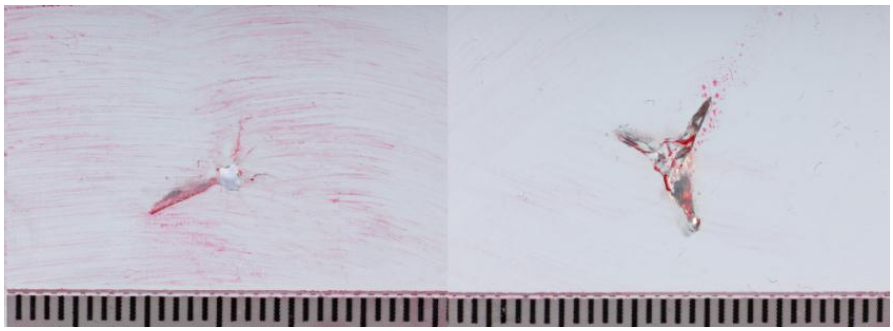

Figure 5-7: 5% confined gelatin (left) and right 5% unconfined gelatine (right)

Figure 5-8 shows the rotation of the bullet, black arrow shows the direction of the projectile traveling from right to the left. As previously noted in Figure 5-5 the rotation of the bullet has a substantial effect on the form of the damage. Therefore, it is possible to observe the twisting motion of the bullet in the gelatine in Figure 5-8.

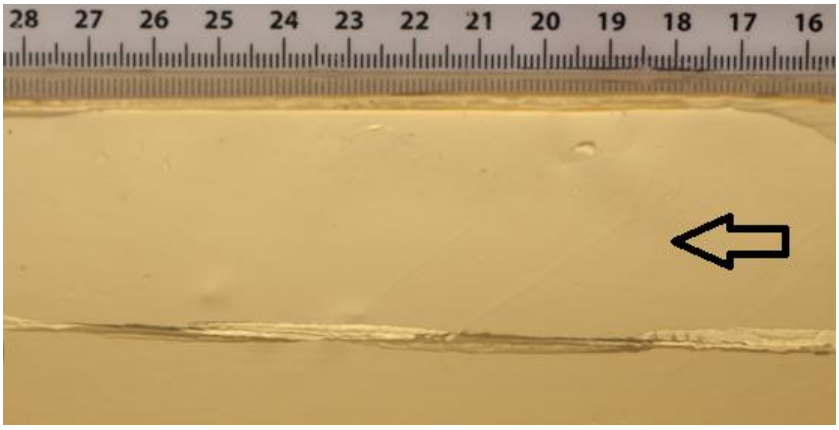

Figure 5-8: Rotation of the bullet and form of the damage

Figure 5-9 shows the form of the deformation of the permanent wound channel from the first impact in 5, 10% gelatine and bovine brain. Scales in each image shows 1 mm increments. As can be seen neither of the simulants mimic the same form of the damage as observed in the bovine brain. The central hole in the gelatine samples has the shape of a circle and in the bovine samples it is a more elliptical shape.

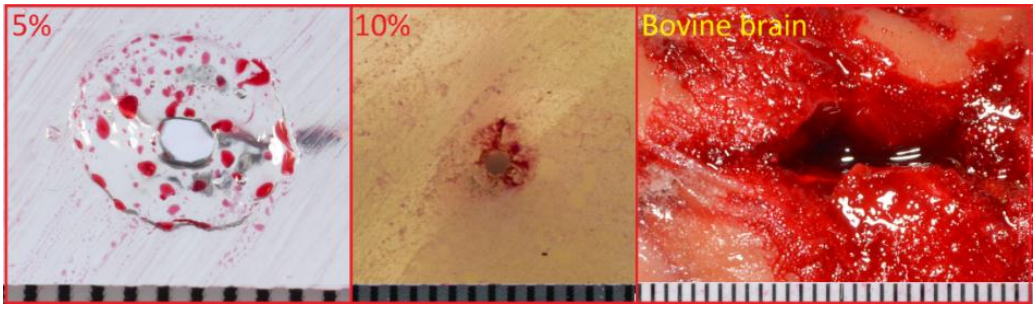

Figure 5-9: Form of the permanent cavity at the surface 5% gelatine, 10% gelatine and bovine brain

Figure 5-10 shows the mean age diameter of the permanent cavity in 5, 10% gelatine and bovine brain. To reduce the error in image processing. In order to reduce the error in image processing a ruler was placed at the top surface of each slice and each image was calibrated separately. Measurements were taken using ImageJ open source software by fitting an ellipse in the central wound track. All the measurements are mean of two to three repeated values for each material. The results are the mean of the major radius of the fitted ellipse through all the length of the permanent cavity. The error bars in Figure 5-10 are ±5%, which might occur due to pixilation in image processing. The mean diameter of the permanent wound track in bovine brain was 4.35 mm and for 5 and 10% gelatine was 1.91 mm and 1.32 mm respectively.

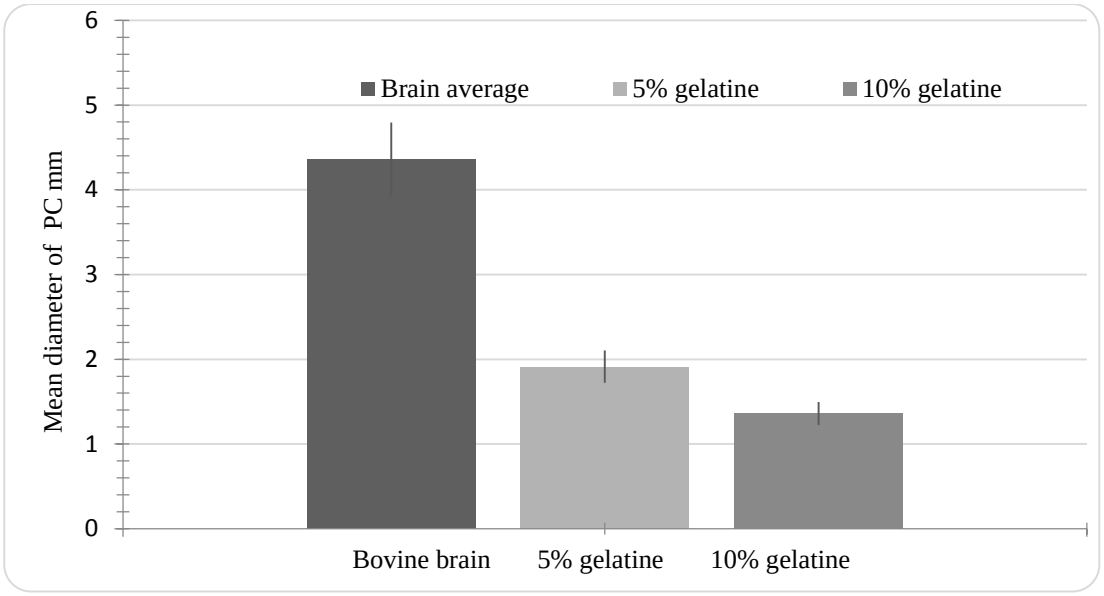

Figure 5-10: Ellipse fit to the wound track

The diameter in the permanent wound track of the 10% gelatine with the boundary and without the boundary condition changed. The boundary condition have substantial effect on the form and size of the wound track. 10% gelatine with boundary condition and without, had a mean diameter of 1.02 mm and 1.36 mm respectively.

In order to increase accuracy of the measurement of the permanent wound track, the polygon fit option in ImageJ was used to measure the area of the permanent wound track. An example of these measurements shown in Figure 5-11.

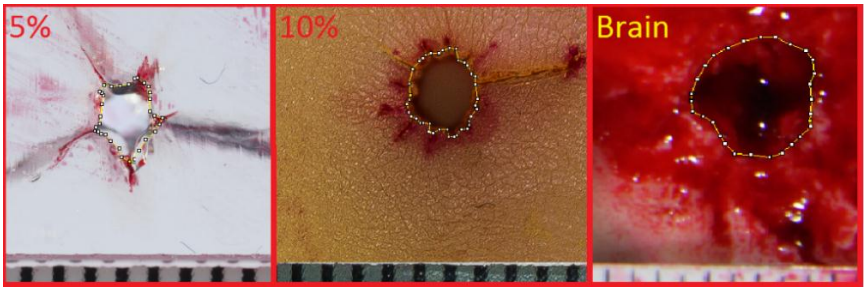

Figure 5-11: An example of polygon fit into the permanent cavity in different materials

Figure 5-12 shows the area of the permanent wound track in 5, 10% and bovine brain in the first 200 mm of the material. The area of the permanent wound track in the bovine brain is approximately three times larger than 10% gelatine. Moreover, this shows that the 10% gelatine with boundary has a smaller area compared to the 10% gelatine without boundary. The results of the polygon fit and ellipse fit are

comparable, which indicates that for preliminary tests it is possible to use ellipse fit as it is less time consuming and it gives the overall results as polygon fit.

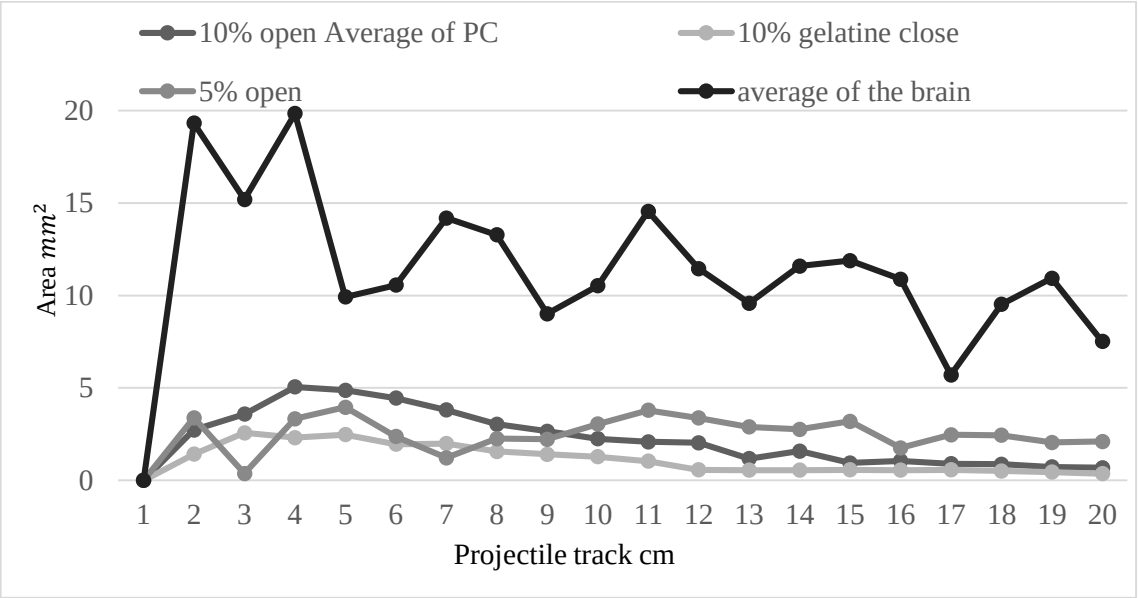

Figure 5-12. Area of permeant wound track

5.5 Modification of Composite material

In chapter 4.4 the M1 material was proposed as a material which shows a similar form of fragmentation and expansion rate compared to bovine brain. However, this study shows that the form of the damage and the stopping distance in M1 was not the same as the bovine brain. This finding suggested that the original M1 formulae is not suitable for comparison of the form of the damage. Thus, a series of experiments were performed on the different formulations of the composite to investigate the effect of the corn flour and talcum powder to the area of the permanent wound channel. The procedure for the preparation of the M1 can be found in chapter 2.7.2.

In this section the effect of the corn flour and talcum powder on the size of the permanent wound channel will be investigated. It must be noted that the main differences corn flour and talcum powder ids that corn flour crosslink and talcum powder will bind moisture and prevent adhesion. Table 5-1 shows different combinations of the M1 used in this study. In first section change has been made in the quantity of the talcum powder and second section quantity of the corn flour has been changed. In order to have more realistic comparison between simulant and bovine brain all the materials were casted into the

bovine brain shape mould to have the same external shape as the bovine brain. An example of the material in the shape of the bovine brain is shown in Figure 5-13.

Figure 5-13. An example of the casted materials

Table 5-1: Different combination of the M1

Simulant	Glycerol (g)	Water (g)	carbon fibre (g)	Corn flour(g)	talcum(g)
	Change in talcum				
M1	60	40	0.5	10	5
M2 bp2	60	40	0.5	10	20
M2 bp3	60	40	0.5	10	40
Simulant	Change in Corn flour				
M3cr2	60	40	0.5	30	5
M3 cr3	60	40	0.5	60	5

The mean area of the permanent wound whole length track in different material is shown in Figure 5-14. As it can be seen from Figure 5-14, the mean area of the permanent wound track in original M1 is three times bigger than bovine brain. As such increasing both corn flour and talcum powder will decrease the size of the permanent wound cavity. So, by increasing the percentage of the talcum powder it is possible to reduce the mean area of the permanent cavity. However, percentage of the corn flour has more effect on the size of the permanent cavity compared to the talcum powder.

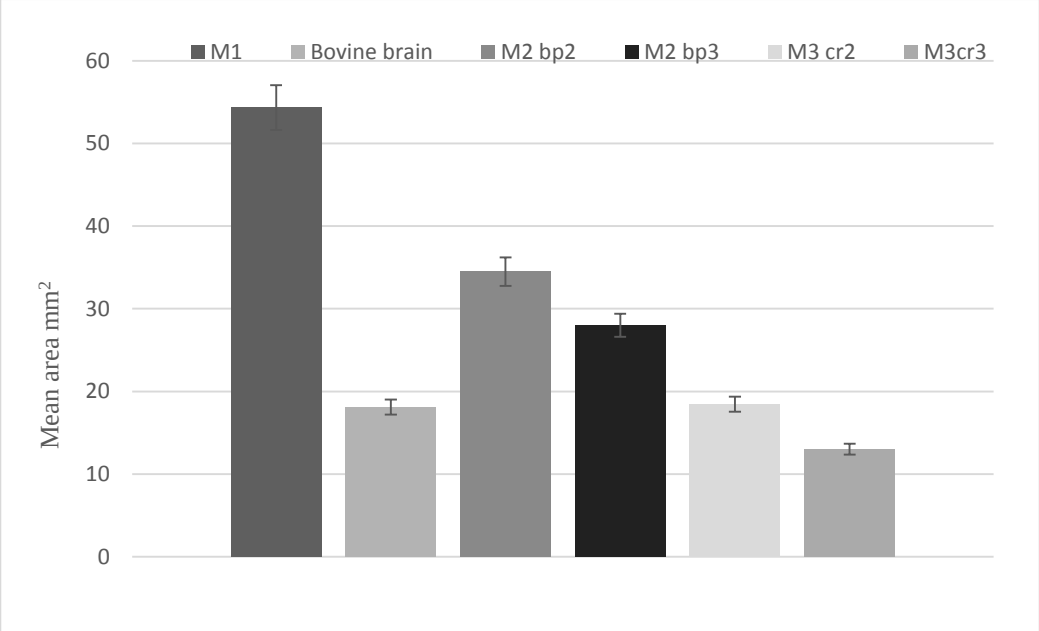

Figure 5-14: Mean area of the permeant wound cavity in different materials

Figure 5-15 shows the form of the permanent wound cavity in different materials. It is obvious that by changing the percentage of the corn flour and talcum powder it is possible to change the size and form of the permanent wound cavity. However, none of the composite materials were able to create a similar form of the damage as that of the bovine brain. Form of the damage in the brain can be described as central polygon with several inhomogeneous cracks. Form of the crakes in the brain tissue are different from the composite materials. It can be seen from Figure 5-15 that there are several distinguishable cracks at the left side of the wound channel in the brain tissue. The form of the damage in the composite materials are mostly elliptical with some smooth tearing all around the wound channel. Nature and form of the damage in the composite materials, Figure 5-15, vary from each other due to differences in their brittleness. Together, they are less brittle than brain and as a result have the tendency to shear under tension whilst brain tissue has more tendency to tear under tension.

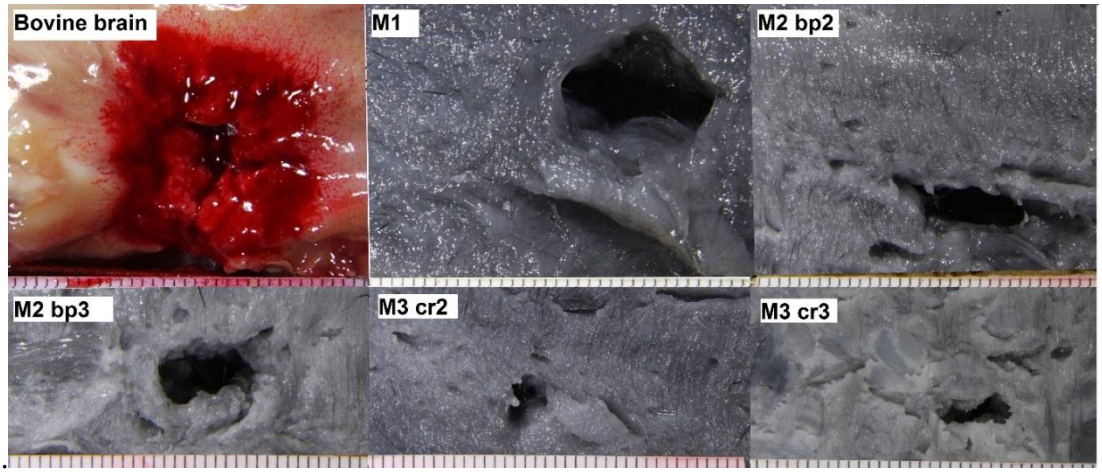

Figure 5-15: Form of the permanent cavity in different material

5.6 Conclusion

The results of this study show that stopping distance of a projectile in 10% gelatine is 120±10 mm less than that observed in the block of bovine brain. Reduction of the percentage of gelatine will increase the stopping distance. However, it does not have a large impact on the cross section area of the permanent wound track. A rigid boundary around the material will reduce the depth of penetration and also it will reduce the mean area of the permanent wound track. The form of the damage in the 5 and 10% gelatine samples are different. However, none of the percentage of the gelatine used in this study was even close to the stopping distance and mean area of the permanent wound cavity, which was observed in the brain tissues. M1 exhibited a stopping distance more than 430 mm. Moreover, the size of the permanent wound track in the M1 material was three times higher than the one in the bovine brain. Experiments on different combinations of the components of M1 showed that it is possible to control the size of the permanent cavity. However, none of the formulations of the composite material was able to create a similar form of the damage compared to the bovine brain. The results of this study suggests that a more fundamental study is required in order to create a simulant for a brain tissue for purposes of studying the damage caused by high velocity impact. Also, this study strongly suggests that gelatine samples are not suitable materials for ballistic experiments of a brain simulant. The brain is a very complex tissue, as such it is currently necessary to have different simulants for different types of the experiment as one material can reproduce the same form of the fragmentation but it might not be

able to create the same size of the permeant wound cavity. The effect of deforming and fragmenting bullets have not been studied in this research and it should be considered in future research.

6 Feature tracking to estimate the velocity of air ejected from the temporary cavity during gunshot wounding

6.1 Introduction

Much of the present knowledge of wound damage dynamics and the mechanical response of tissue comes from experiments performed on gelatine. Ballistic gelatine with 10 to 20% concentration is widely used as a standard simulant for human soft tissues (Carr et al., 2014; M. Fackler et al., 1984; M. L. Fackler & Malinowski, 1985; Jussila, 2004, 2005; Kneubuehl & Thali, 2003; Knudsen et al., 1995; Korac, 2001; Rutty et al., 2008; Jiangyue Zhang et al., 2005; J. Zhang et al., 2007), as it has a stopping distance and density close to mammalian muscle tissues. The effect of wound contamination was studied by Von See et al. (Constantin von See et al., 2012), who placed barium particles in the gun chamber and tracked the particles after the bullet penetrated the target using CT scan. The results show that there is a significant difference in wound characteristics between gelatine and porcine hind limb. The diameter of the permanent cavity in porcine hind leg was significantly smaller and the mean diameter of the temporary cavity was larger in the porcine hind leg. It was also reported that the gelatine block had more contamination compared to the porcine hind leg.

Three mechanisms are assumed to cause back-spatter: the interaction of blood with muzzle gases; a momentum effect known as tail-splash, and collapse of the temporary cavity. The temporary cavity, shown in Figure 6-1is the result of the compression of tissue adjacent to the wound channel in a direction perpendicular to the bullet path (Kneubuehl et al., 2012). Kinetic energy of the bullet is converted to elastic energy, heat and plastic work (Kneubuehl et al., 2012). The cavity subsequently fills with air, blood and tissue after the bullet has passed through. The size of the cavity depends on the elastic and viscous properties of the material. However, there is a lack of information in the literature about the temporal evolution of the cavity and the ejection of the material (to form backspatter) as it collapses.

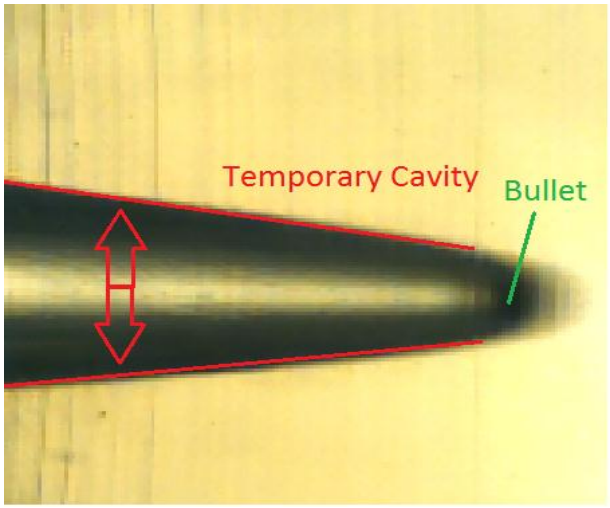

Figure 6-1: Temporary cavity. The bullet is moving from left to right.

Open questions include: what the air pressure is inside the temporary cavity, and whether this slows the collapse, also whether there is entrainment of blood and tissue fragments in air entering or leaving the cavity. It has been hypothesized that the ejection of the air backward through the wound channel entraining blood droplets and tissue fragments is an important factors in the generation of back-spattered blood stains (Davidson et al., 2012). Ballistic gelatine is the most commonly used simulant material for gunshot wounding experiments as it has a similar density to muscle and stops bullets in the same distance as porcine soft tissue (Frank et al., 2012; Kneubuehl et al., 2012; Thali et al., 2001). Ballistic gelatine experiments show that, when shot with typical handgun ammunition (e.g. 9mm Parabellum or .38 Special) the temporary cavity collapses completely in 4 to 7 cycles of contraction and expansion with the amplitude decreasing each cycle. However the number of contraction and expansion cycles in human brain and muscle tissue is unknown. Air motion into the cavity was studied by (Hinz et al., 2012) with a view to understanding wound contamination. 10.5 % gelatine was used as a simulant for tissue. Their results clearly show the suction effected at the moment of the formation of the temporary cavity. This chapter describes an experiment which aims to measure the velocity of the air motion at the mouth of the cavity in four different materials such as 3% to 10 % gelatine, bovine brain and a new simulant (termed ‘M1’), and to measure the velocity of the air ejected from the wound channel. This information will assist in elucidating the mechanism linking the formation of the cavity to ejected material and subsequent deposition of bloodstains. The outcome of this research may also assist trauma surgeons to determine the likelihood of the air drawing bacteria and debris in to the wound channel.

Questions addressed directly by this experiment are:

Is air ejected from the wound channel as a result of the collapse of the temporary cavity?

What is the velocity of the ejected air?

What is the effect of the elasticity of the material on the velocity of the ejected air?

6.2 Experimental setup: tracer particle trials:

This section describes the trials with one micron diameter water droplets and their shortcomings with the available light source. Water particles with a diameter of less than one micron were generated by the Laskin process (see chapter 2.4.1) as shown in Figure 6-2. Air was injected at a gauge pressure of 800 kPa through five Laskin nozzles. To limit the size of the particles, an exit pipe with internal diameter 100 mm was installed with its intake a height of 200 mm above the water level and with a length of 500 mm. The pipe was connected to a closed PMMA box which housed the sample to be shot. To limit the velocity of the particles, the generator was turned off 30 seconds before the shot was fired. Particle motion was monitored on a live camera feed and the shot was fired after the particles began to move unidirectionally downwards, settling under gravity.

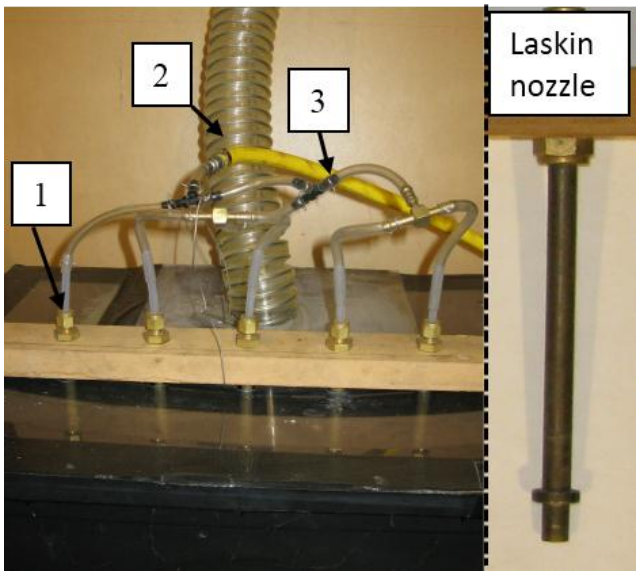

Figure 6-2: Image of water droplet generator 1- Laskin nozzle 2-exit pipe 3- high pressure air

By illuminating the particle cloud with a laser sheet it was possible to observe the motion of the air from the wound channel. The relaxation time of the particles and their Stokes number were calculated to assess the accuracy of the velocity measurement. The Stokes number of a one micron water droplet

in this experiment for the air flow with the velocity of 100 m/s is 0.005, assuming a streamline radius of curvature of 5.58 mm, meeting the criterion for effective tracking of the air motion (Dring, 1982). Smaller particles may follow the air motion, especially the high accelerations expected, better, but would not scatter enough light to form acceptable images given the necessarily short exposure time. The available light sources were insufficient to image individual particles above the noise level, so PIV was not possible. An example of the water particle visualization is shown in Figure 6-3 (B). In order to obtain better illumination with the available light source, the water droplets were replaced with 1.6 micron propylene glycol fog. The Stokes number for a 1.6 micron particle of propylene glycol in this experiment for 100 m/s air flow is 0.01 which meets the requirement for accurate measurement of the velocity. An example of the 1.6 micron propylene glycol fog is shown in Figure 6-3(A).

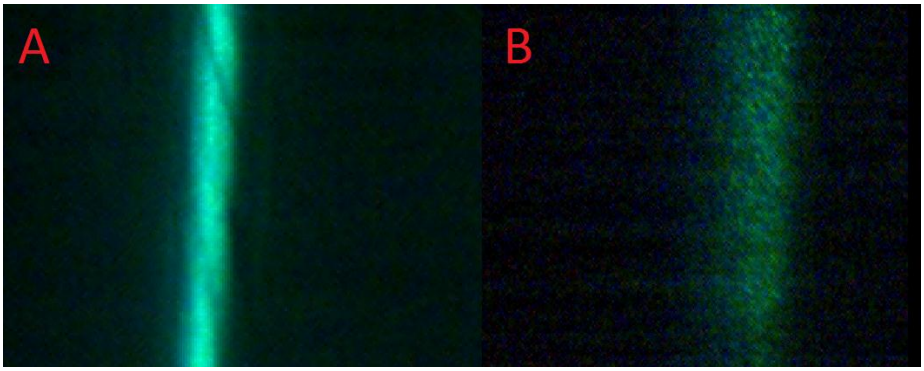

Figure 6-3: Propylene glycol fog (A) & water fog (B) illuminated by the laser

6.3 Generation of a laminar flow of fog.

It is desired to observe the air motion near the entrance wound, and to view the evolution of the temporary cavity inside the target sample simultaneously. The air motion requires highly localized, intense sheet illumination, whereas the cavity is best viewed with diffuse backlighting of lower intensity. Obtaining good quality images simultaneously on a single camera is challenging, requiring similar intensities from the two regions to best utilize the dynamic range of the camera. A new set of experiments were performed with LED backlighting of the gelatine and laser sheet illumination of the fog. To maintain a high concentration of the fog particles, and hence high scattered intensity, efforts were made to collimate the fog in a laminar stream. Figure 6-4 shows the set up used to generate a laminar flow of smoke with a constant velocity. The smoke generator was connected to a reservoir box with a heat resistant tube. A 1.5 W computer cooling fan was installed at the output of the reservoir to

accelerate the particles with a velocity of ~1 m/s along the pipe to the open section. A suction nozzle was installed 200 mm from the tip of the pipe to create a narrow jet of smoke in front of the entry wound location on the sample. To return the smoke back to the reservoir a 2 W fan was installed at the end of the nozzle.

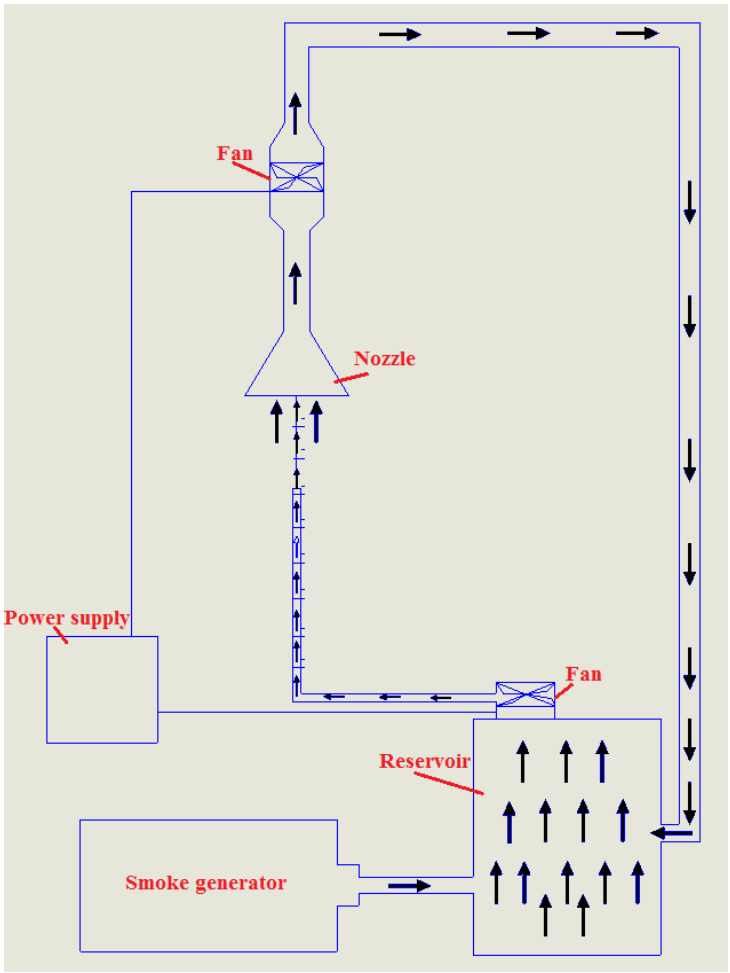

Figure 6-4: Setup for generation laminar flow of fog

6.4 Flow visualization using simultaneous LED and laser illumination, and a laminar flow of fog

A schematic image of the experimental set up is shown in Figure 6-5. The experiment was performed with 3, 5, 10% w/w Glita bovine gelatine (bloom 240-260), bovine brain[1] and new material M1 as a brain simulant. The method of preparation of gelatine and M1 can be found in in chapter 2.7 which is also published in Lazarjan et al. (Lazarjan et al., 2014). Experiments were performed at 20ºC and recorded using a Photron SA1 high speed camera (key parameters shown in Table 6-1. Each sample was cut and placed in a PMMA box with internal dimensions of 52×29×37 mm, and a wall thickness

of 12 mm. The samples were shot with a 1.000±0.006 gram, round nose diabolo projectile from a .22 calibre air rifle, which had a velocity of 290±2 m/s. This projectile has a lower kinetic energy, but nearly the same muzzle velocity, as a .22LR rifle round or a 9mm pistol round. It is more important to match the muzzle velocity, as the elastic and viscous properties of the target depend on the strain rate. A Coherent Innova 70 argon-ion laser with 4 W output power in multiline mode was used to generate a light sheet with a thickness of 2 mm perpendicular to the path of the projectile, in order to illuminate a fog of propylene glycol with particle diameter of ~1.6 micron generated by the fog generator. The projectile passes through a laminar flow of fog which is placed with its center 30 mm in front of the target. The velocity of the air was measured using PFV software (Photron Inc.) by tracking the low particle concentration mixing features.

Table 6-1: Camera and illumination parameters

Frame rate	Shutter speed	Type of lens	F-number	Light
30000	1/56000 s	50mm	1.2	4W CW Argon ion laser 20000 lm LED light

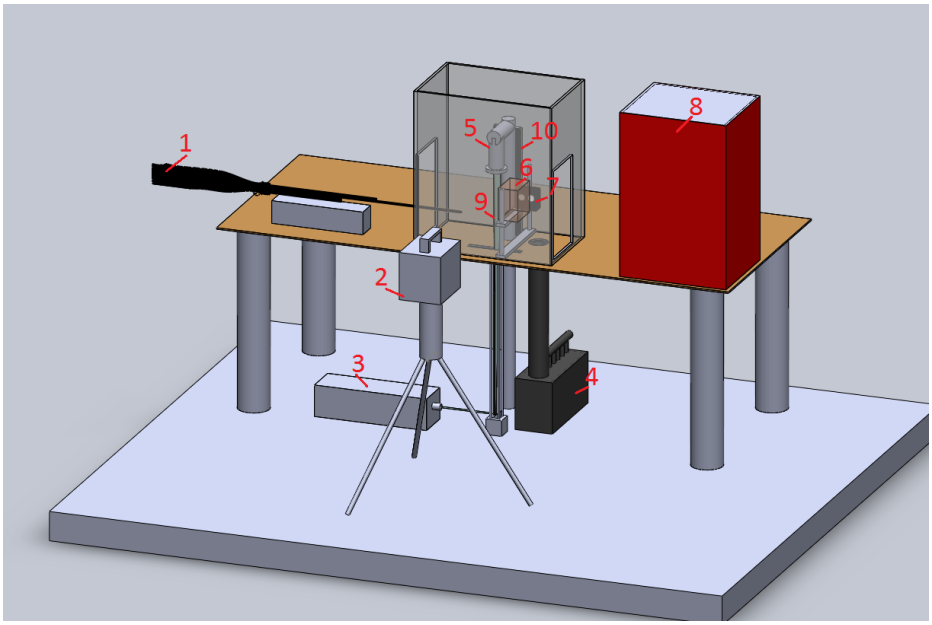

Figure 6-5: Experimental set up; 1-Air rifle 2- Camera 3- Laser source 4- Fog reservoir 5- Suction nozzle 6-Sample 7-LED light 8- Back stop 9- Laser sheet 10-Black background

Results and discussion

Figure 6-6 shows a sequence of frames from one of the experiments. The projectile is moving from left to right. The first frame on the left shows a moment before the projectile reaches the laser sheet.

Undisturbed particles can be seen in this frame. Frame two shows the moment when projectile passes through the laser sheet (the red rectangle in the first two frames marks the position of the projectile). The target sample is on the right of each frame, with its surface approximately 30 mm from the centre of the laser sheet. Frame three shows the moment of the formation of the temporary cavity. It must be noted that the goal in this experimental set up was to measure the velocity of ejection of air. The low-intensity feature caused by mixing of fresh air into the fog, used for velocity estimation, can be seen in frames 4 to 6 within the red rectangle.

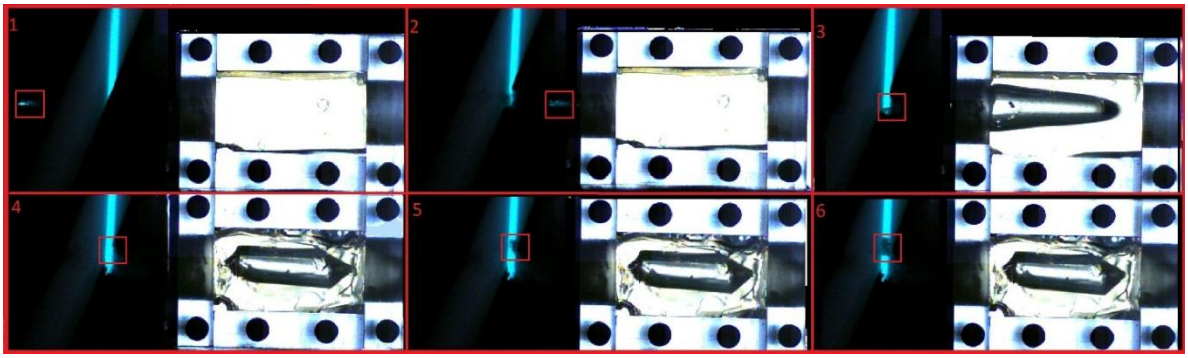

Figure 6-6: Sequence of frames from one of the experiments

The velocity of the air ejected by the collapse of the temporary cavity from 10 % and 5 % gelatine was 105 ±5% m/s and 70 m/s ±5%. Air ejection was observed from 3% gelatine but the motion of the particles was not measurable as they were too slow and motion of the flow was not uniform. Ejection of air was not observed from bovine brain or M1 samples, in any of the three repeat experiments. The mean velocity of the collapse of temporary cavity in 5 ,10 % gelatine were measured using PFV Fastcam viewer software by measuring displacement of maximum of diameter of the temporary cavity as it forms until it collapses. Velocity of the collapse of the cavity in 5, 10% gelatine were 4.16 and 3.40 m/s respectively. A temporary cavity if exists, is not visible in brain and M1 due to the opacity of the material. These results may be interpreted to show that the velocity of the ejected air is correlated to the elastic response of the material. Reducing the concentration of gelatine reduces the shear elastic moduli, but only minimally affects the density. The density of the materials was measured using a MT density measurement machine with an uncertainty of ±0.01 gcm^{-3}. The relation between gelatine concentration and its density is shown in Table 6-2. The relation between concentration of the gelatine and shear elastic moduli of the gelatine solution studied by Amador et al. (Amador et al., 2011) shows that shear

elastic modulus increases from 1.61, 3.57 and 5.37 kPa respectively for 7, 10, and 15% w/w gelatine.

Table 6-2: Density of different materials used in this experiment at 20° C

Material	10% gelatine	5% gelatine	3% gelatine	Bovine brain	water
Density(gcm^{-3})	1.027	1.018	1.009	1.040	0.998

By reducing the percentage of the gelatine, the velocity of the air ejection will be decreased. The absence of air ejection from the bovine brain indicates that gelatine has different temporary cavity dynamics compared to brain, and that gelatine does not replicate all aspects of gunshot wounding in brain tissue. M1 like brain, shows no detectable ejection of air. The differences in density between these materials is negligible. M1 and brain, unless confined, noticeably sag under their own weight, and have lower Young's modulus than 5% gelatine, at least at low strain rates. The difference in behavior may be due to Young's modulus, or to visco-elastic parameters (elastic response being characterized by the storage modulus, and viscous response by the loss modulus), the exact value of which depends on the strain rate which is difficult to measure at ballistic strain rates. Moreover in the chapter four of this study which is also published in (Lazarjan et al., 2014) the expansion rate of different percentages of gelatine were compared with bovine brain and M1 samples. The results shows that gelatine samples recoil to their original shape but bovine brain and M1 samples experience permanent plastic deformation.

Conclusions

For the first time it was possible to visualise the motion and measure velocity of the ejected air caused by the contraction of the temporary cavity in 10%, 5% and 3% w/w ballistic gelatine, bovine brain and M1. The results of this experiment showed that air was ejected from the cavity in 10, 5 % gelatine. The ejection of the air was not measurable from 3% gelatine as the movement of the particles were not uniform and very slow. There was no detectable air motion from either the bovine or M1 samples. The absence of the ejection of the air from the bovine brain and M1 can be explained, knowing that they have greater plastic deformation compared to the gelatine samples. The measured air velocity was approximately one third or less of the projectile velocity in the gelatine samples. The passing of the projectile draws air from 15-20 mm from the entry wound towards the surface of the target. It is

postulated that with air velocities of order 100 m/s there will be sufficient shear to entrain blood droplets and tissue fragments and carry them out of the wound. The bovine brain does not have the same elastic response as the gelatine because gelatine recoils to its original shape, whereas the brain will deform and some of the energy of the bullet will be converted to plastic work. This study suggests that ejection of the air from the collapse of the temporary cavity in the brain, if such exists, is not solely determined by the recoil of the material under elastic stresses. However pressure inside the cranium raises as the bullet penetrates the cranium, and this pressure has the potential to eject the brain and blood backward.

7 Visualization of the air ejected from the temporary cavity in brain and tissue simulants during gunshot wounding

7.1 Introduction

This part of the study consists of three sections. First the visualization of the air motion in front of the entry hole of the bullet to measure the velocity of the suction and ejection of the air at the moment of expansion and contraction of the temporary cavity. This is performed on gelatine samples of 3, 5 and 10 % concentration. In the second section the experiment is repeated with bovine and ovine heads. In the third section, the minimum pressure required to eject brain tissue from the cranium of the bovine and ovine heads, at the velocities observed in the second section, is estimated.

7.2 Experimental setup:

The setup for high speed imaging is shown in Figure 7-1. The experiments were recorded using a Photron SA1.1 (resolution 384×432 pixels) and a Photron SA5 (resolution 640×376 pixels) camera (key parameters shown in Table 7-1). The samples were shot with 7.45g 9x19 mm full metal jacket bullets (American Eagle). The distance from the muzzle to the samples was one metre. A Glock model 17 semi-automatic hand gun clamped to a firing bench was used in this experiment. Bullet velocity was calculated by tracking the bullet displacement between individual images. Uncertainty in velocity due to the pixelation of the bullet and consequent uncertainty in position of the projectile gave a maximum uncertainty in velocity of ± 5%. The velocity when the bullet first enters the image frame is 350 m/s. Four LED lights were used for the front lighting and two Kaiser video lamps were used for backlighting.

Table 7-1: Camera and illumination parameters

Frame rate	Shutter speed	Type of lens	F-number	Light
30000	1/220000 s	90 mm Tamron	2.8	4 LED lights (total 3200 lm) 1 Kaiser video lamps (2000 W)
30000	1/220000 s	50 mm Nikkor	2.8	

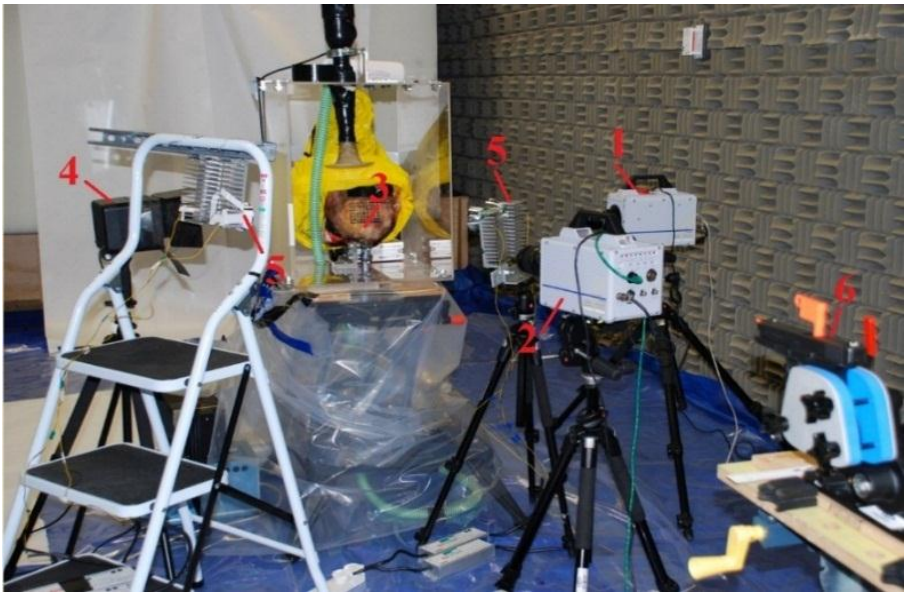

Figure 7-1: Experimental set up; 1- SA5 2- SA1 3- Sample holder 4- Kaiser Video lamp 5- LED lights 6- Gun

In order to visualize the air motion in front of the wound cavity a laminar sheet of smoke was arranged in front of the samples perpendicular to the path of the bullet. More detailed information on the generation of the laminar flow of the fog can be found in 6.3.

The experiment was performed on blocks of 10, 5 and 3% w/w gelatine, on bovine heads and on sheep heads. Gelatine samples were prepared using 55ºC warm water agitated until all the gelatine particles dissolved. The gelatine was poured into plastic containers with dimensions of 125 × 90 × 65 mm, a wall thickness of 1 mm, and with open entrance and exit holes with diameters of 22 mm. These samples were then kept in a refrigerator at 4 ºC for 24 hours. Simulants were removed from the refrigerator 1-2 minutes before the test.

The animal heads were collected from Auckland Meat Processors Ltd. Animals were electronically stunned before their neck arteries were severed. The heads were removed from the body 10 to 15 minutes after death. The heads were shaved on the frontal section where bullet impact would occur. All heads were kept at room temperature (18-22 ºC). The distance between the entry hole and smoke line varied (10 to 25 mm) in each set of experiments due to the difference in anatomy of the animal heads. The distance from the gun to the samples was 1 m. To prevent the forward-travelling muzzle gases from affecting the air motion near the sample, a 0.5 mm thick sheet of plastic was installed between the gun and samples.

7.3 Results

Figure 7-2 shows the sequence of frames from one of the 10% gelatine samples. The first frame shows the bullet before entering the smoke sheet. The second frame shows the moment the bullet exits the smoke. Frames 3 to 5 shows the smoke traversing laterally towards the bullet entry point and the evolution of the entry wound. From frames 6 to 10 the displacement of the smoke was measured by tracking contrast features through consecutive frames. The same procedure was applied to all the videos. Details of the tracking procedure can be found in chapter 3.

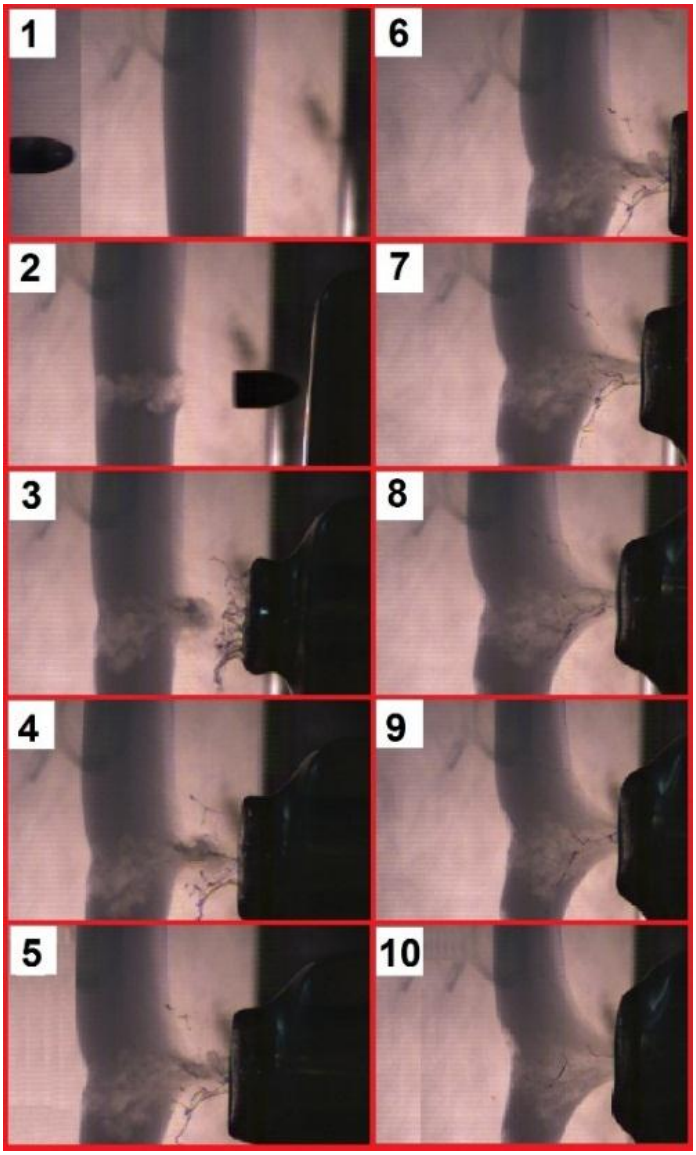

Figure 7-2: Example of the air motion visualization from 10 % gelatine.

The relaxation time and Stokes number of the smoke particles were calculated to determine whether the smoke would follow the air as it moves. The dimensions of the particles were measured by imaging

them at high magnification using a Dantec 2 megapixel camera with 50 mm lens and 300 mm of extension tube. Particles were illuminated by a New Wave Solo120XT pulsed frequency-doubled Nd:YAG laser. Images were calibrated by imaging a fixed wire with a diameter of 0.4 mm in the laser path to obtain the pixel to mm scale of the image. Knowing the dimensions of each pixel it was possible to calculate the dimensions of the particles. The Stokes number equation 1 should be < 0.1 to follow the flow faithfully. Detailed method for measuring the particle dimension can be found in section 2.4.3.

Knowing the dimension of the particles it was possible to use equation 14 to calculate the Stokes number. Thus for the 1.6 micron diameter droplets of propylene glycol used in this experiment, at 100 m/s air speed, the Stokes number is 0.09. The maximum velocity of the air observed in this experiment was 76 m/s. This makes the maximum error in velocity calculation less than 6% (Dring, 1982). However, the Stokes number for tracking the air velocity of the 350 m/s (velocity of the bullet) is 0.31 which does not meet the criteria: the particles will lag behind the air.

Figure 7-3 shows the velocity of the air as it enters the entry wound and as it is ejected from it in the gelatine samples. It was observed that the air moved into the entry wound at the moment of the formation of the temporary cavity with a mean velocity of 64.8 m/s from 10% gelatine, 75.6 m/s from 5% gelatine and 81m/s from 3% gelatine. The mean velocity of the air ejected from the entry wound was 72 m/s for 10% gelatine and 43m/s for 5 % gelatine. For 3 % gelatine, air ejection from the entry wound was not observed. Error bars in Figure 7-3 and Figure 7-5 show +/- the difference between the mean and the extreme values. All results are presented in this chapter are the mean of 3 repeats for each material.

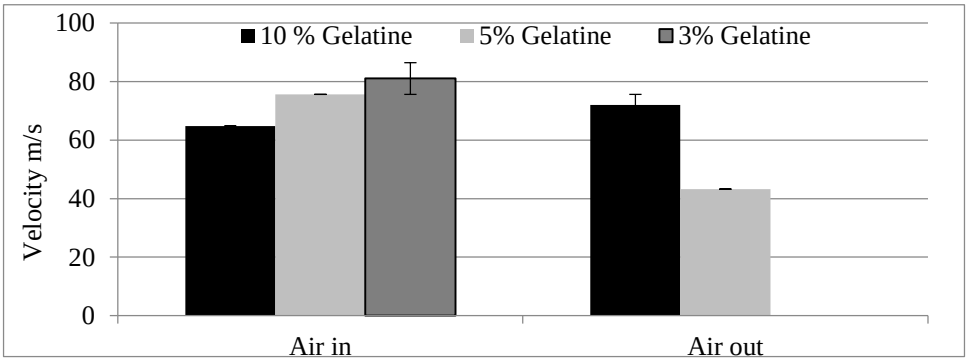

Figure 7-3: Velocity of the air motion as a result of formation and collapse of the temporary cavity in gelatine

Figure 7-5 shows the velocity of the expansion of the temporary cavity in the 0.0003 s immediately after the first contact of the bullet. The measurement performed on PFV viewer software (Ver. 351) by measuring the diameter of the temporary cavity as it forms in the gelatine. Figure 7-4 shows the schematic procedure for measuring the diameter of the temporary cavity.

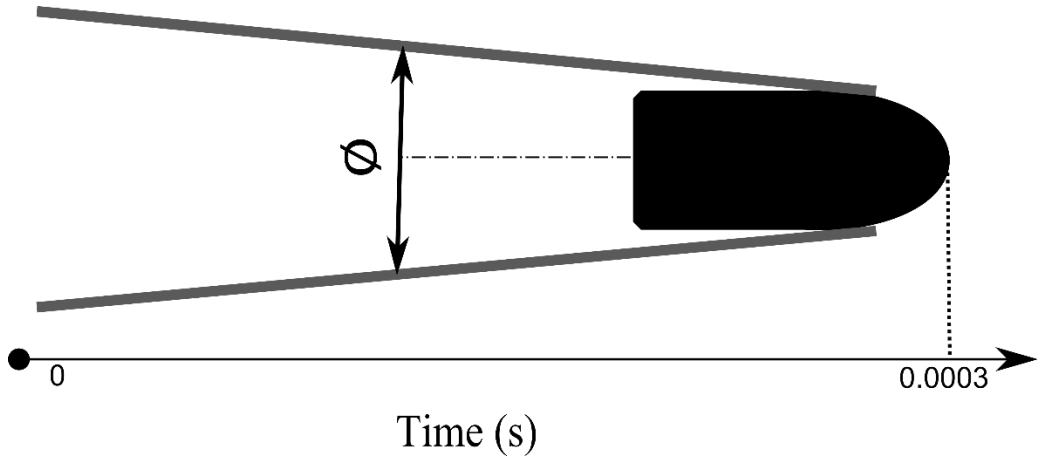

Figure 7-4: schematic procedure for measuring diameter of the temporary cavity

Velocities of the expansion of different percentage of the gelatine as a result of the formation of the temporary cavity were 63.6, 69 and 77.4 m/s respectively for 10 5 and 3% gelatine.

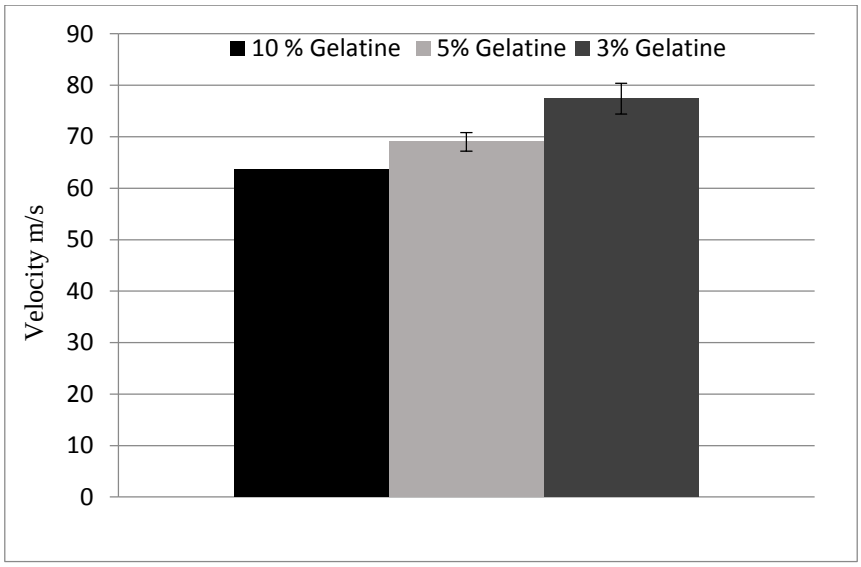

Figure 7-5: velocity of the expansion of the temporary cavity

Figure 7-6 shows a sequence of frames from the bovine head experiment. Frame one shows the bullet before entering the smoke sheet. Frame two shows the bullet after passing through the smoke sheet and

frame 3 shows the smoke after the bullet enters the sample, the edge of which can be seen on the extreme right of each frame. A very slow motion of the air was observed in the animal head experiments, which may be caused by the bullet motion and tail splash. However air motion as a result of formation and collapse of the cavity, if such exist in the cranium, was not observed in the experiment.

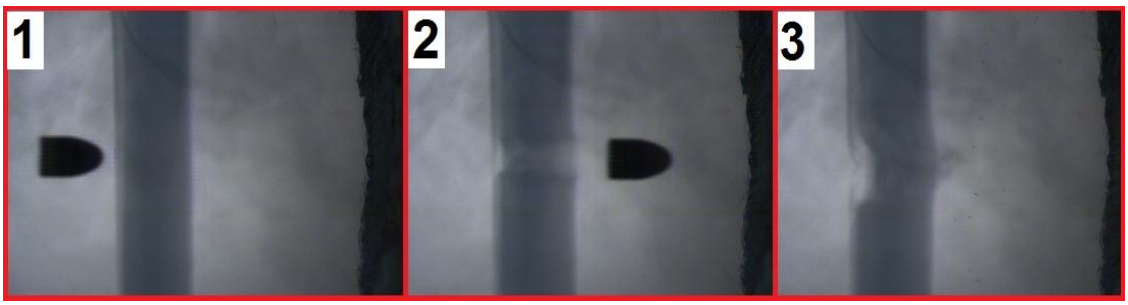

Figure 7-6: Early phases of the bovine head experiment

During the experiment it was observed that brain tissue was ejected with a mean velocity of 37±6 m/s from sheep's head 0.0011s after penetration. Figure 7-7 shows a sequence of frames from the sheep head experiment. Frame one shows the bullet before impact, frame two shows the extrusion of the skin after impact, frame three shows the skin returning to its original shape and frame four shows brain tissue emerging from the entry hole. Visual observation after the experiment confirmed that the ejected tissue was brain.

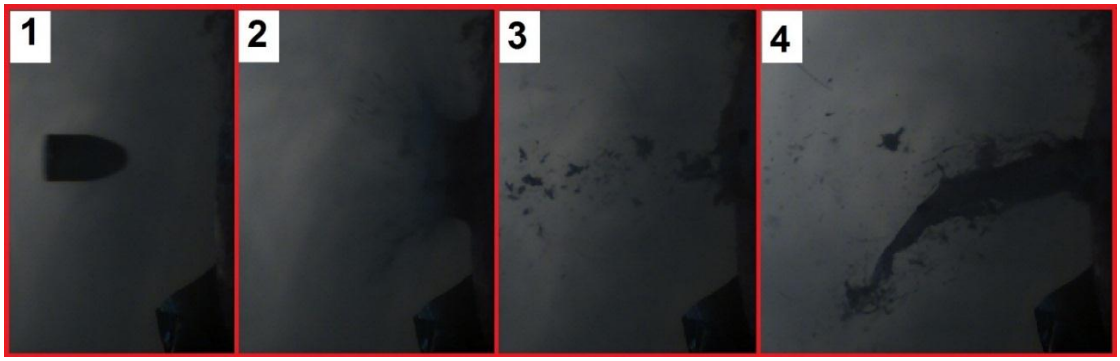

Figure 7-7: Sheep's head experiment: 1- Bullet before impact 2- Extrusion of the skin 3- Skin back to the original shape 4- Ejection of the brain

Another experiment was performed on the bovine head. The frontal section of the bovine head was shot three times with 9 mm bullets. Figure 7-8 shows the position of the entry of the bullet on the bovine head. After the third shot, brain tissue ejected from the second wound channel with a mean velocity of 30 m/s (shown in Figure 7-9 with the yellow cursor) after 0.0007s of the bullet impact. The second

ejection started from the first wound channel (shown in Figure 7-9 with the green cursor) with a time delay of 0.00123s from the first ejection. The velocity, averaged over time, of the ejected brain from the first channel was 21 m/s.

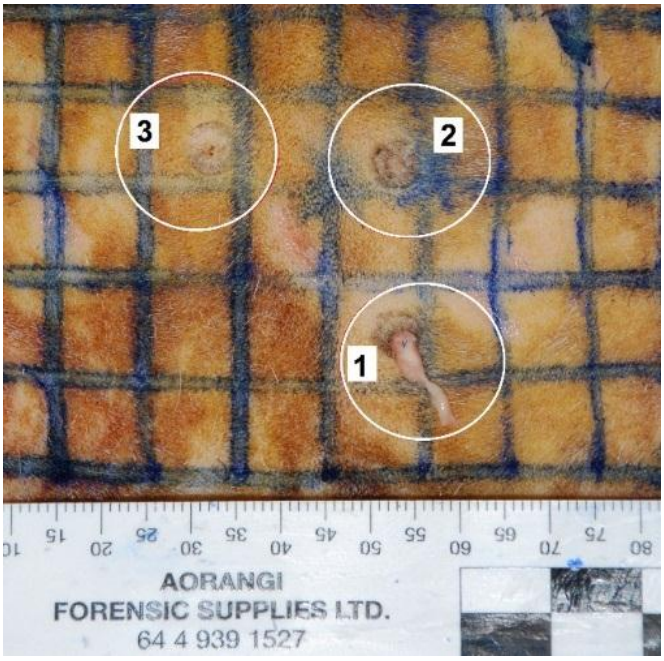

Figure 7-8: Position of the wound channel

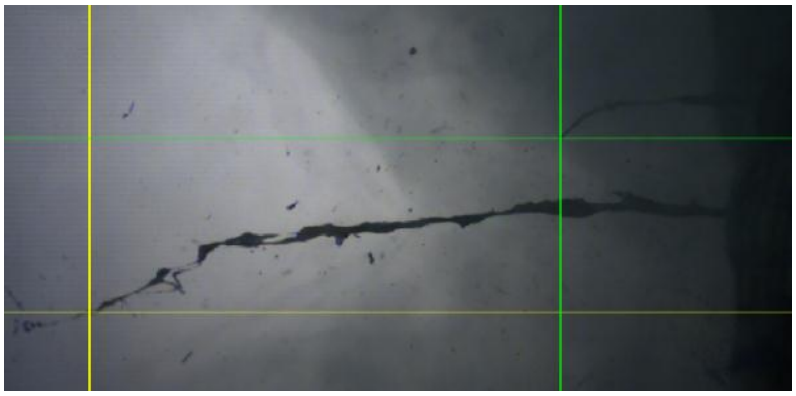

Figure 7-9: Yellow cursor shows the first ejection and green cursor the second ejection from the bovine head

The velocities of the ejected brain from both experiments was calculated by tracking the position of the ejected material in each frame. Knowing the velocity it was possible to use the dynamic pressure equation (Equation 7) to calculate the minimum internal pressure required to drive the brain outside the cranium from the wound channel, assuming no viscous pressure loss at the entry hole. p is the pressure in the cranium, ρ is the density of the brain (1040 kg/m3) and v is the velocity of the ejected brain.

Table 7-2: velocity of the ejected brain and relevant dynamic pressure

Experiment	Velocity of the ejected brain(m/s)	Dynamic Pressure (kPa)
Sheep head	37	712
Bovine head first ejection	30	468
Bovine head second ejection	21	229

7.4 Discussion

A temporary cavity is known to form in gelatine when penetrated by 9 mm bullets (Jiangyue Zhang et al., 2005; J. Zhang et al., 2007). The temporary cavity has been hypothesised to explain the zone of stretched material surrounding the permanent wound track in muscle and brain (Thali et al., 2002; Jiangyue Zhang et al., 2005; J. Zhang et al., 2007). However the temporary cavity has not been directly observed in brain tissue, due to the opacity of the tissue. If a temporary cavity is formed in brain, its size may not match that seen in gelatine due to a difference in material properties. This may explain the lack of observed air motion into and out of the entrance wound in the head samples.

The degree of inwards and outwards air motion observed with gelatine samples as a result of expansion and contraction of the cavity depends on the elastic response of the material. As shown in Figure 7-3 and Figure 7-5 there is a clear correlation between the elastic response of the material and the velocity of the ejected air and velocity of the expansion of the temporary cavity. Moreover, material with lower elastic modulus has a higher cavity expansion rate. As shown in Figure 7-3, as the gelatine concentration is reduced from 10 to 5 to 3%, reducing the elastic modulus, the velocity of inflow of air is increased. The opposite trend is seen in the contraction of the material, where a lower elastic modulus causes a slower recoil (Figure 4). The velocity of the ejected air is thus reduced by reducing the percentage of the gelatine from 10% to 5%. For 3% gelatine, ejection of the air was not observed. By decreasing the elasticity of the material the elastic response of the material may not be sufficient to move the air inside and outside the cavity. The animal heads did not show ejection of air, suggesting the elastic modulus of mammalian brain tissue at ballistic strain rates is lower than that of 10 or 5% gelatine. In chapter 4 of this study which is also published by Lazarjan et al. (Lazarjan et al., 2014) the expansion rate of samples in open-topped containers, the elastic response of the brain was shown to be lower than that of 10 or 5% gelatine which may explain the lack of air motion from the animals head.

The velocities of ejected brain tissue, and a simple calculation assuming no viscous losses, suggest that the minimum pressure required for driving brain tissue from the sheep and bovine heads are respectively 712 and 468 kPa. For comparison, the peak pressures measured in previous work using a block of Sylgard 527 silicone as a brain simulant which was shot with 9 mm bullet were 55 to 242 kPa (Jiangyue Zhang et al., 2005), lower but of the same order of magnitude. Another set of experiments were performed on spherical shape models made from Sylgard 527 and 10% gelatine in (J. Zhang et al., 2007), where the results suggested that the pressure peak has a range between -92.8 to 644.6 kPa, the upper figure lying close to the pressures calculated in the present work. The peak pressure is likely to depend on the volume and shape of the cavity.

In this work, brain was seen to eject from entry wounds in the bovine head on the third shot. One hypothesis is that after the second shot, the brain had suffered sufficient permanent damage to compromise its structural strength, and subsequently flows as a high viscosity fluid. This was not observed in the gelatine samples, as the gelatine recoils to its original shape, leaving a narrow channel of permanent damage. In the experiment with the sheep and bovine head it was shown that the brain started to eject outside the head at 0.0011s after bullet impact from the sheep head and after 0.0007s for the bovine brain. The time required to raise the internal pressure of the head is thus short, as expected from the known behaviour of near-incompressible materials inside closed cavities.

7.5 Conclusion

Using high speed camera imaging and a fog of small liquid droplets it was possible to visualise the air motion in front of the entry wound in samples of ballistic gelatine and animal heads shot with standard 9x19 mm pistol ammunition. The velocity of air motion into and out of blocks of 3, 5 and 10% gelatine was correlated to the concentration of gelatine, and hence to the elastic modulus. Higher concentrations of gelatine led to slower inflow of air, and faster outflow. Air motion was not observed into or out of the animal heads. This may be explained if the elastic modulus of mammalian brain, at ballistic strain rates, is less than that of 10 or 5% gelatine. The collapse of the temporary cavity may not therefore be as substantial contributor to back-spattering of blood in cranial gunshot injuries as previously thought. The results of this experiment may help to develop a better model of ballistic impact to the head, whether

laboratory models or finite element computational models. New materials with lower elasticity and some viscous flow properties should be explored as brain simulants for high velocity impact experiments.

8 Conclusion and Future Work

8.1 Experimental Method for Validation of the Simulant

In this study it was possible to develop a new method for quantitative and qualitative comparison of different material upon impact using high speed cameras. The form of the fragmentation and kinetic energy absorption by ovine brain in both preserved and fresh samples were compared. The results of this study show that the differences between the fresh ovine brain and preserved ovine brains are negligible for proposes of this study.

The dynamic response of the bovine brain was compared with different concentrations of gelatine and a new composite material (M1). All gelatine samples experienced an initial expansion, followed by elastic recoil to the original shape. Neither the bovine brain nor the M1 showed this elastic recoil (see appendix A). Results of the experiments on the bovine head shows that one of the important factor in the brain simulant for generating the backspatter is that, the material must be able to flow backward towards the firearm from the permanent wound cavity that is created in the skull (see appendix A Figure 9-2). Thus, the expansion rate, velocity of the extrusion of the material and form of the fragmentation must be considered as important factors for validation of the simulant for cranial gunshot. The expansion rate of the bovine brain was close to the M1 material. The results indicate that M1 material with 5 mm carbon fibre is capable of producing a more brain-like form of fragmentation, expansion rate and velocity of the extruded material for 9 mm experiments. M1 is the best material available for the experiments performed with .22 AR and .22 LR. However, the results of the stopping distance and form of the damage in different materials showed that M1 material is not capable of creating the same form of the damage and stopping distance as the one observed in the bovine brain. These findings indicate that for each specific type of experiment a unique simulant must be used. One simulant might be able to produce the same form of the fragmentation and kinetic energy absorption, but not the form of the damage and stopping distance. Gelatine samples of 10% concentration should not be used as a brain simulant. Gelatine samples were not capable of reproducing neither form of the fragmentation nor expansion rate even close to the bovine brain tissues. Overall, the results of this study suggested that in order to increase the repeatability of the experiments, it is better to cut samples in a cuboid shape. However, producing the same exact form of the fragmentation is not possible due to

rotation of the bullet as well as small changes in the angle of impact and also limitations from the frame rate of the high speed cameras used. As such qualitative analysis in conjunction with quantitative measurements are required to obtain the best outcome.

The methodology used in this study is not limited to measuring mechanical properties, rather it is a holistic approach which makes it possible to examine the effects which are influenced by all the important mechanical properties, rendering it a more stringent test than measuring individual mechanical properties such as shear modulus.

8.2 Experimental Method for Flow Visualisation

A novel method for flow visualisation in front of the wound cavity has been developed. Air flow in front of the wound cavity in 3, 5, 10% gelatine, M1, Bovine brain and bovine head have been investigated. The results show that suction and ejection of the air from the wound cavity depend on the elastic response of the material. Samples with higher concentration of the gelatine had slower inflow of the air and faster outflow. Ejection of the air can be measured from 5, 10 % gelatine samples. However, it was not possible to measure the velocity of the ejected air from 3% gelatine samples due to not uniform and very slow movement of the particles. The air motion was not detectable for neither the bovine brain, nor the M1. The lack of the ejection of the air from the bovine brain and M1 can be explained by knowing that they have larger plastic deformation compared to the gelatine samples. Air motion was not observed into or out of the animal heads. This clearly shows that elastic response of the mammalian brain tissue is less than 5 and 10% gelatine. Thus, formation and collapse of the temporary cavity may not therefore have important effects of the generation of the backspatter as previously thought. However, results of the study on the animal heads shows that intracranial presser rises as the bullet penetrates the head. This pressure has potential for the ejecting the biological material in the form of the backspatter and blood stain pattern.

In summary, the results of this study suggests that a more brain like material must be used as brain simulant in order to create more realistic 3D model of the human head. The boundary condition around the samples has strong effect on the form of the damage created by the

projectile. This was mentioned in the study by Jussila (Jussila, 2005) the direction of the biggest crack around the wound cavity is towards the supporting platform. This indicates the importance of the boundary layer of the tested material to the form of the damage. Also, the results of the current study shows that in the material with the rigid (aluminium) boundary the longest crack will rotate around the wound channel as the projectile penetrates 10% gelatine. Moreover, in the study by Fackler and Malinowski (1985) they clearly showed the effect of the bullet construction to the form of the damage in the tissue. However, the effect of the fragmenting and deforming projectile to the form of the damage should be addressed in future studies.

8.3 Future Work

Work presented in this study has provided new techniques for experimental investigation of the formation of the backspatter and a method for comparing the properties of different materials in a ballistic penetration test. However, further investigation must be performed to produce a material that can fit all criteria such as stopping distance, nature of fragmentation and form of the permanent damage. The simple blocks used in this study allow tests of material property effects as distinct from geometric effects, thus more experiments on different types of the simulant must be conducted. Materials such as alginate and agar mixed with glycerol and other composite materials must be tested to find more realistic simulant for the brain. Further work should include realistic skin-skull-brain geometries. Also each layer of the 3D model of the human head can be pressurised with a blood simulant, so it can reproduce more realistic backspatter. However, more study should be done on materials such as M1 to optimise their performance. New composite materials such as glycerol agar, alginate glycerol and glycerol gelatine have promising properties and should be investigated with the methodology proposed in this study.

9 Appendix A- Bovine Brain VS Simulants

This appendix presents some additional images to elucidate the form of the damage in different simulants and bovine brain.

Figure 9-1 shows the form of the deformation of the brain tissue, different percentage of gelatine and M1 shot with .22 AR. As it can be seen, the bovine brain and M1 material experience totally plastic deformation around the path of the projectile while plastic deformation was not observed in any of the gelatine samples, at any concentration.

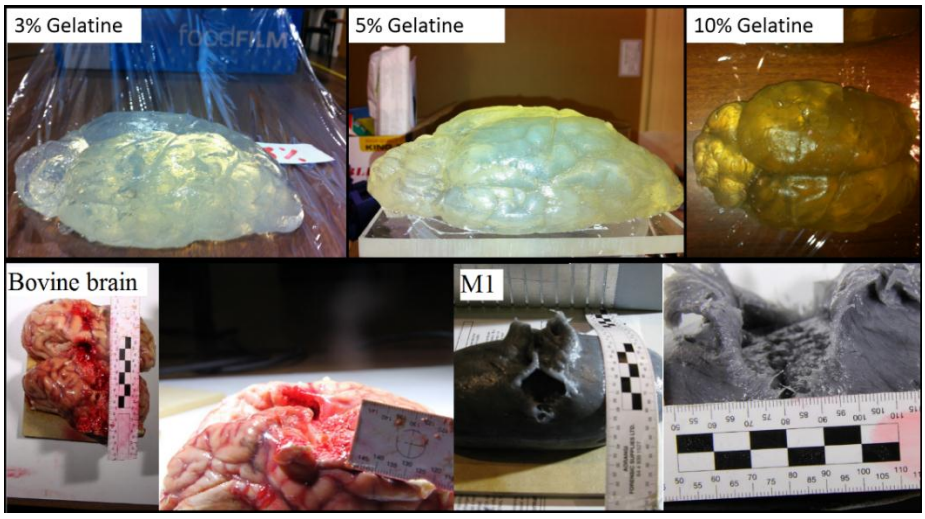

Figure 9-1: Form of the deformation in bovine brain, different percentage of gelatine and M1

Figure 9-2 shows the diameter of the permanent wound cavity in the bovine brain. The diameter of the permanent wound cavity in the bovine head was approximately the same size as the diameter of the projectile.

Figure 9-2: Diameter of the permanent wound cavity in bovine head

Figure 9-3 shows the fragments of the bovine brain tissue shot by a .22 air rifle. It must be noted that in the experiment performed with 9 mm calibre on the unconfined bovine brain, all the brain tissues were disintegrated due to high kinetic energy of the projectile therefore most of the experiments performed with .22 LR and .22 AR.

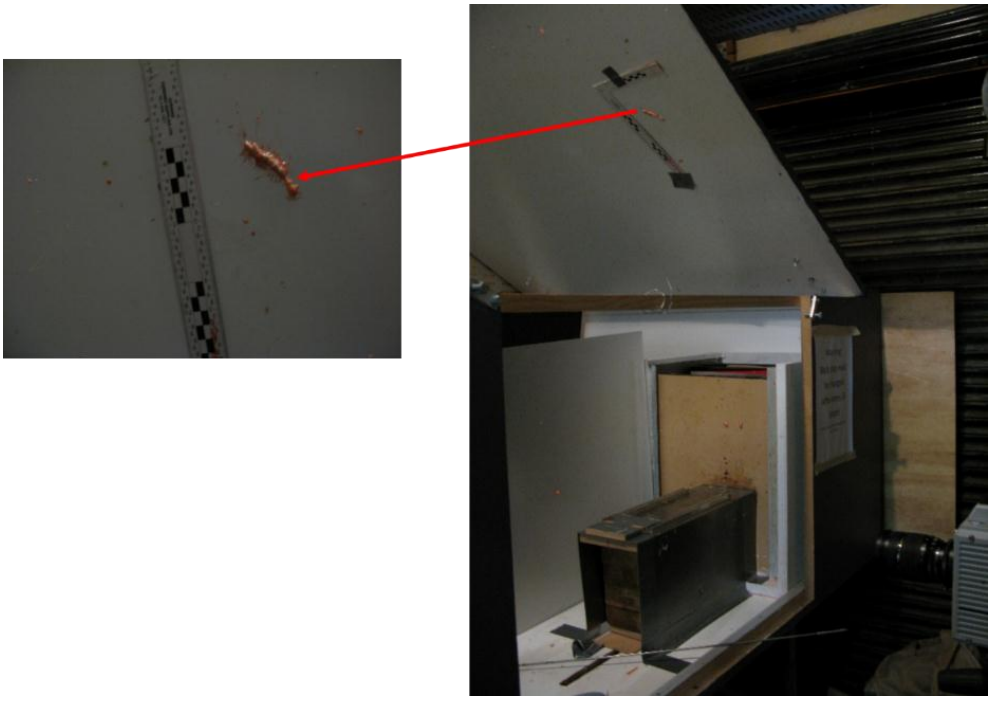

Figure 9-3: Fragments of the bovine brain tissue

Figure 9-4 shows the bovine brain and M1 material after being shot by .22 AR. As it can be seen material has been separated from the path of the bullet. Material hits the top of the box and falls on the floor.

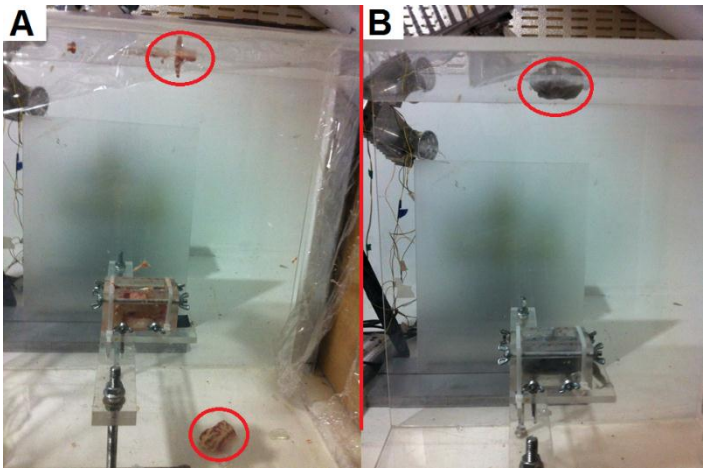

Figure 9-4: A-Bovine brain B- M1 after shot

Figure 9-5 shows 3, 5, 10% of gelatine and bovine brain. The brain tissue experienced a plastic deformation and it has to be cut from the path of the projectile. However, gelatine samples had very small plastic deformation and the diameter of the permanent cavity was smaller than diameter of the projectile.

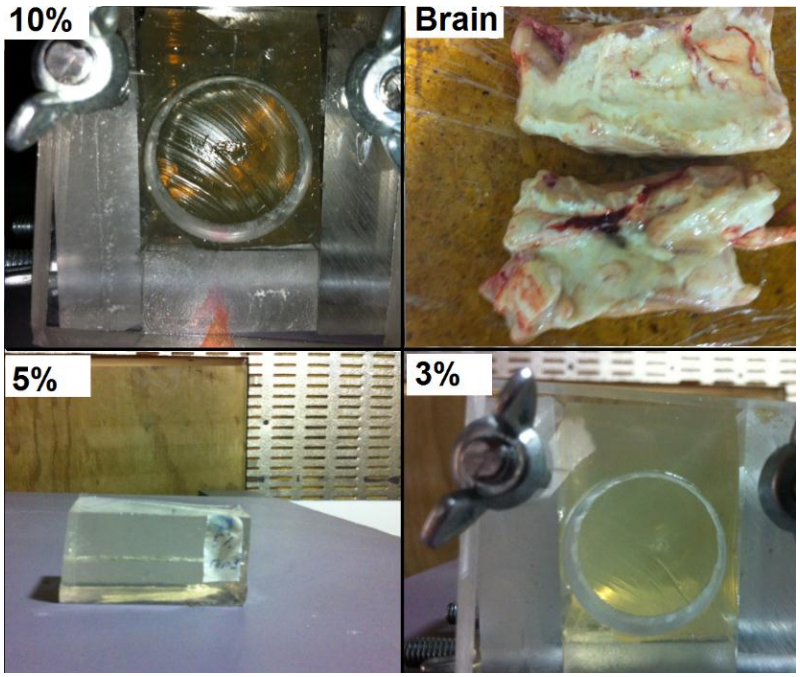

Figure 9-5: 3, 5, 10% gelatine and brain after shot with .22 AR

10 References

Aarabi, B., Tofighi, B., Kufera, J. A., Hadley, J., Ahn, E. S., Cooper, C., . . . Uscinski, R. H. Predictors of outcome in civilian gunshot wounds to the head. *Journal of Neurosurgery, 0*(0), 1-9. doi: doi:10.3171/2014.1.JNS131869

Almansa, E. M., & Cánovas, M. F. (1999). Behaviour of normal and steel fiber-reinforced concrete under impact of small projectiles. *Cement and Concrete Research, 29*(11), 1807-1814. doi: 10.1016/s0008-8846(99)00174-x

Amador, C., Urban, M. W., Shigao, C., Qingshan, C., Kai-Nan, A., & Greenleaf, J. F. (2011). Shear Elastic Modulus Estimation From Indentation and SDUV on Gelatin Phantoms. *Biomedical Engineering, IEEE Transactions on, 58*(6), 1706-1714. doi: 10.1109/TBME.2011.2111419

Bellamy, R. F., Zajtchuk, R., & Buescher, T. M. (1991). *Conventional warfare: ballistic, blast, and burn injuries* (Vol. 5): Walter Reed Army Institute of Research, Walter Reed Army Medical Center.

Berlin, R. H., Janzon, B., Rybeck, B., Sandega˚rd, J., & Seeman, T. (1983). Local effects of assault rifle bullets in live tissues. Part II. Further studies in live tissues and relations to some simulant media. *National Defence Research Institute, Tumba and the Department of Surgery II, University of Goteborg, Goteborg,*

Sweden, 1983.

Bevel, T., & Gardner, R. M. (2012). Bloodstain pattern analysis with an introduction to crime scene reconstruction. Book CRC Press

Bolliger, S., Thali, M., Bolliger, M., & Kneubuehl, B. (2010). Gunshot energy transfer profile in ballistic gelatine, determined with computed tomography using the total crack length method. *International Journal of Legal Medicine, 124*(6), 613-616. doi: 10.1007/s00414-010-0503-z

Bowyer, G. W., J., C. G., & P., R. (1996). Small fragment wounds: biophysics and pathophysiology. *J Trauma, 40(Suppl.3):S159—64.*

Bradshaw, D. R. S., Ivarsson, J., Morfey, C. L., & Viano, D. C. (2001). Simulation of acute subdural hematoma and diffuse axonal injury in coronal head impact. *J Biomech, 34*(1), 85-94. doi: 10.1016/s0021-9290(00)00135-4

Breeze, J., Carr, D. J., Mabbott, A., Beckett, S., & Clasper, J. C. (2015). Refrigeration and freezing of porcine tissue does not affect the retardation of fragment simulating projectiles. *Journal of Forensic and Legal Medicine, 32*(0), 77-83. doi: http://dx.doi.org/10.1016/j.jflm.2015.03.003

Cameras, P. H. S. (2014). from http://www.photron.com/

Carr, D., Lindstrom, A.-C., Jareborg, A., Champion, S., Waddell, N., Miller, D., . . . Kieser, J. (2014). Development of a skull/brain model for military wound ballistics studies. *International Journal of Legal Medicine*, 1-6. doi: 10.1007/s00414-014-1073-2

Chen, D.-L., Yang, P.-F., & Lai, Y.-S. (2012). A review of three-dimensional viscoelastic models with an application to viscoelasticity characterization using nanoindentation. *Microelectronics Reliability, 52*(3), 541-558. doi: 10.1016/j.microrel.2011.10.001

Constantin von See, Majeed Rana, M. S., Horst Kokemueller, & Martin Ruecker, N.-C. G. (2012). Designing the ideal model for assessment of wound contamination after gunshot injuries a comparative experimental study. *von See et al. BMC Surgery 2012, 12:6*.

Davidson, P. L., Taylor, M. C., Wilson, S. J., Walsh, K. A., & Kieser, J. A. (2012). Physical components of soft-tissue ballistic wounding and their involvement in the generation of blood backspatter. *J Forensic Sci, 57*(5), 1339-1342. doi: 10.1111/j.1556-4029.2012.02143.x

Dring, R. P. (1982). Sizing Criteria for Laser Anemometry Particles. *Journal of Fluids Engineering-Transactions of the Asme, 104*(1), 15-17.

Fackler, M., Surinchak, J. S., Malinowski, J. A., & Bowen, R. E. (1984). Bullet Fragmentation: A Major Cause of Tissue Disruption. *The Journal of Trauma and Acute Care Surgery, 24*(1), 35-39.

Fackler, M. L. (1988). Wound ballistics. *JAMA, 260*(22), 3277-3277. doi: 10.1001/jama.1988.03410220061022

Fackler, M. L., Bellamy, R. F., & Malinovski, J. A. (1988). The Wound Profile: Illustration of the Missile-tissue Interaction. *Journal of Trauma- Injury, Infection, and Critical Care, 28*(1), S21-S29.

Fackler, M. L., & Malinovski, J. A. (1988). Ordnance gelatin for ballistic studies. Detrimental effect of excess heat used in gelatin preparation. *The American Journal of Forensic Medicine and Pathology*.

Fackler, M. L., & Malinowski, J. A. (1985). The wound profile: a visual method for quantifying gunshot wound components. *The Journal of trauma, 25*(6), 522-529.

Faller, A., & Schuenke, M. (2004). *The Human Body. An Introduction to Structure and Function* (1st edition ed.). New York USA: Thieme.

Farjo, L. A., & Miclau, T. (1997). Ballistics and mechanisms of tissue wounding. *Injury, 28, Supplement 3*(0), C12-C17. doi: 10.1016/s0020-1383(97)90088-7

Frank, M., Schönekeß, H., Jäger, F., Hertel, H., Ekkernkamp, A., & Bockholdt, B. (2012). Temporary cavity created by free-flying projectiles propelled from a powder-actuated nail gun. *International Journal of Legal Medicine, 126*(5), 801-805. doi: 10.1007/s00414-012-0742-2

Gu, L., Chafi, M. S., Ganpule, S., & Chandra, N. (2012). The influence of heterogeneous meninges on the brain mechanics under primary blast loading. *Composites Part B: Engineering*. doi: 10.1016/j.compositesb.2012.04.014

Hinz, B. J., & Muci-Küchler, K. H. (2012). Study of Air Flow Into Ballistic Wounds Using Flow Visualization Experiments and Numerical Simulations. *ASME 2012 International Mechanical Engineering Congress and Exposition Volume 2: Biomedical and Biotechnology*, 771-778.

Jena, A., Sun, E., & Prasad, V. (2014). Does the Declining Lethality of Gunshot Injuries Mask a Rising Epidemic of Gun Violence in the United States? *Journal of General Internal Medicine*, 1-5. doi: 10.1007/s11606-014-2779-z

Jussila, J. (2004). Preparing ballistic gelatine--review and proposal for a standard method. *Forensic Sci Int, 141*(2-3), 91-98. doi: 10.1016/j.forsciint.2003.11.036

Jussila, J. (2005). Measurement of kinetic energy dissipation with gelatine fissure formation with special reference to gelatine validation. *Forensic Sci Int, 150*(1), 53-62. doi: 10.1016/j.forsciint.2004.06.038

Jussila, J., Kjellström, B. T., & Leppäniemi, A. (2005). Ballistic variables and tissue devitalisation in penetrating injury—establishing relationship through meta-analysis of a number of pig tests. *Injury, 36*(2), 282-292. doi: http://dx.doi.org/10.1016/j.injury.2004.09.010

Jussila, J., Leppaniemi, A., Paronen, M., & Kulomaki, E. (2005). Ballistic skin simulant. *Forensic Sci Int, 150*(1), 63-71. doi: 10.1016/j.forsciint.2004.06.039

Kabaliuk, N. (2014). Dynamics of Blood Drop Formation and Flight.Ph.D. Thesis University of Canterbury New Zealand.

Kneubuehl, B. P., M. J. Thali, R. M. Coupland, & Rothschild, M. A. (2012). Wound Ballistics: basics and applications. *International Journal of Legal Medicine, 126*(6), 979-980. doi: 10.1007/s00414-012-0744-0

Kneubuehl, B. P., & Thali, M. J. (2003). The evaluation of a synthetic long bone structure as a substitute for human tissue in gunshot experiments. *Forensic Sci Int, 138*(1–3), 44-49. doi: 10.1016/j.forsciint.2003.08.003

Knudsen, P. T., Vigsnæs, J., Rasmussen, R., & Nissen, P. (1995). Terminal ballistics of 7.62 mm NATO bullets: experiments in ordnance gelatin. *International Journal of Legal Medicine, 108*(2), 62-67. doi: 10.1007/bf01369906

Korac, Z. (2001). Substitute ellipse of the permanent cavity in gelatin blocks and debridement of gunshot wounds. *Military Medicine, 166*(8), 689-694.

Kunz, S. N., Brandtner, H., & Meyer, H. (2013). Unusual blood spatter patterns on the firearm and hand: A backspatter analysis to reconstruct the position and orientation of a firearm. *Forensic Sci Int, 228*(1–3), e54-e57. doi: http://dx.doi.org/10.1016/j.forsciint.2013.02.012

Kwon, J., & Subhash, G. (2010). Compressive strain rate sensitivity of ballistic gelatin. *J Biomech, 43*(3), 420-425. doi: http://dx.doi.org/10.1016/j.jbiomech.2009.10.008

Lazarjan, M. S., Geoghegan, P. H., Jermy, M. C., & Taylor, M. (2014). Experimental investigation of the mechanical properties of brain simulants used for cranial gunshot simulation. *Forensic Sci Int, 239*(0), 73-78. doi: http://dx.doi.org/10.1016/j.forsciint.2014.03.022

Li, J., Tan, H.-N.-S., & Seng, K. Y. (2010). A Biomechanical Computational Study of the Role of Helmet Pads in Mitigating Blast-Induced Traumatic Brain Injury

6th World Congress of Biomechanics (WCB 2010). August 1-6, 2010 Singapore. In C. T. Lim & J. C. H. Goh (Eds.), (Vol. 31, pp. 1518-1521): Springer Berlin Heidelberg.

M. Hrapko, J.A.W. van Dommelen, G.W.M. Peters, & Wismans, J. S. H. M. (2006). The mechanical behaviour of brain tissue: Large strain response and constitutive modelling. *Biorheology, Volume 43, Number 5/2006,* 623-636.

Melling, A. (1997). Tracer particles and seeding for particle image velocimetry. *Measurement Science and Technology, 8*(12), 1406-1416. doi: 10.1088/0957-0233/8/12/005

Miller, K., & Chinzei, K. (2002). Mechanical properties of brain tissue in tension. *J Biomech, 35*(4), 483-490. doi: http://dx.doi.org/10.1016/S0021-9290(01)00234-2

Mota, A., Klug, W. S., Ortiz, M., & Pandolfi, A. (2003). Finite-element simulation of firearm injury to the human cranium. *Computational Mechanics, 31*(1-2), 115-121. doi: 10.1007/s00466-002-0398-8

Munson, B. R., Young, D. F., Okiishi , T. H., & por Hugo, T. (2006). *Fundamentos de mecánica de fluidos / B.R. Munson, D.F. Young, T.H. Okiishi ; tr. por Hugo Villagómez Velázquez* (Y. Okiishi Ed.): México : Limusa-Wiley.

Nicolas, N. C., & R, W. J. (2004). Ballistic Gelatine (Institute for Non-Lethal Defense Technologies Report). *Applied Research Laboratory The Pennsylvania State University*, 28.

Nicolle, S., Lounis, M., Willinger, R., & Palierne, J. F. (2005). Shear linear behavior of brain tissue over a large frequency range. *Biorheology, 42*(3), 209-223.

Nie, X., Sanborn, B., Weerasooriya, T., & Chen, W. (2012). High-rate bulk and shear responses of bovine brain tissue

International Journal of Impact Engineering

doi: 10.1016/j.ijimpeng.2012.07.012

Pervin, F., & Chen, W. W. (2009). Dynamic mechanical response of bovine gray matter and white matter brain tissues under compression. *J Biomech, 42*(6), 731-735. doi: http://dx.doi.org/10.1016/j.jbiomech.2009.01.023

Pervin, F., & Chen, W. W. (2011). Effect of inter-species, gender, and breeding on the mechanical behavior of brain tissue. *NeuroImage, 54, Supplement 1*(0), S98-S102. doi: 10.1016/j.neuroimage.2010.03.077

Peschel, O., Kunz, S. N., Rothschild, M. A., & Mützel, E. (2011). Blood stain pattern analysis. *Forensic Science, Medicine, and Pathology, 7*(3), 257-270. doi: 10.1007/s12024-010-9198-1

Prange, M. T., Meaney, D. F., & Margulies, S. S. (2000). Defining brain mechanical properties: effects of region, direction, and species. *Stapp Car Crash J. 44, 205–213.*

Ragsdale, B., & Josselson, A. (1988). Predicting temporary cavity size from radial fissure measurment in ordenance gelatine. *The Journal of trauma, 28*, 5.

Rashid, B., Destrade, M., & Gilchrist, M. D. (2012). Mechanical characterization of brain tissue in compression at dynamic strain rates. *Journal of the Mechanical Behavior of Biomedical Materials, 10*(0), 23-38. doi: http://dx.doi.org/10.1016/j.jmbbm.2012.01.022

Rashid, B., Destrade, M., & Gilchrist, M. D. (2013). Influence of preservation temperature on the measured mechanical properties of brain tissue. *J Biomech, 46*(7), 1276-1281. doi: http://dx.doi.org/10.1016/j.jbiomech.2013.02.014

Rosenberg, Z., & Dekel, E. (2012). Terminal ballistic *Book*. doi: DOI 10.1007/978-3-642-25305-8

Rutty, G., Boyce, P., Robinson, C., Jeffery, A., & Morgan, B. (2008). The role of computed tomography in terminal ballistic analysis. *International Journal of Legal Medicine, 122*(1), 1-5. doi: 10.1007/s00414-006-0145-3

Samuel, A. L., Elizabeth, M. R., & Michele, J. G. (2004). The high frequency properties of brain tissue. *Biorheology, 41*(6), 681-691.

Schyma, C., & Madea, B. (2012). Evaluation of the temporary cavity in ordnance gelatine. *Forensic Sci Int, 214*(1–3), 82-87. doi: http://dx.doi.org/10.1016/j.forsciint.2011.07.021

Schyma, C. W. (2010). Colour contrast in ballistic gelatine. *Forensic Sci Int, 197*(1-3), 114-118. doi: 10.1016/j.forsciint.2010.01.002

Schyma, C. W. A. (2010). Colour contrast in ballistic gelatine. *Forensic Sci Int, 197*(1–3), 114-118. doi: 10.1016/j.forsciint.2010.01.002

Sheppard, S. E., & Sweet, S. S. (1921). THE ELASTIC PROPERTIES OF GELATIN JELLIES. *Journal of the American Chemical Society, 43*(3), 539-547. doi: 10.1021/ja01436a017

Szabo, T. L. (2005). Chapter 7 - Viscoelastic behaviour *Plastics (3rd)* (pp. 203-227). Oxford: Butterworth-Heinemann.

Takhounts, E. G., Crandall, J. R., & Darvish, K. (2003). On the Importance of Nonlinearity of Brain Tissue Under Large Deformations. *Stapp Car Crash J. 47, 79–92.*

Tamura, A., Hayashi, S., Nagayama, K., & Matsumoto, T. (2008). Mechanical Characterization of Brain Tissue in High-Rate Extension. *Journal of Biomechanical Science and Engineering, 3*(2), 263-274. doi: 10.1299/jbse.3.263

Taylor, P. A., & Ford, C. C. (2009). Simulation of Blast-Induced Early-Time Intracranial Wave Physics leading to Traumatic Brain Injury. *Journal of Biomechanical Engineering, 131*(6), 061007.

Thali, M. J., Kneubuehl, B. P., Dirnhofer, R., & Zollinger, U. (2001). Body models in forensic ballistics: reconstruction of a gunshot injury to the chest by bullet fragmentation after shooting through a finger. *Forensic Sci Int, 123*(1), 54-57. doi: http://dx.doi.org/10.1016/S0379-0738(01)00519-9

Thali, M. J., Kneubuehl, B. P., Zollinger, U., & Dirnhofer, R. (2002). The "Skin–skull–brain model": a new instrument for the study of gunshot effects. *Forensic Sci Int, 125*(2–3), 178-189. doi: 10.1016/s0379-0738(01)00637-5

Thoroddsen, S. T., Etoh, T. G., & Takehara, K. (2008). High-Speed Imaging of Drops and Bubbles. *Annual Review of Fluid Mechanics, 40*(1), 257-285. doi: doi:10.1146/annurev.fluid.40.111406.102215

Tortora, J. G., & Grabowsk, i. R. S. (1996). *Principles of Anatomy and Physiology* (Eighth Edition ed.). Menlo Park, California. Reading, Massachusetts. Harlow, England. New Yourk. Don Mills. Sydny. Amesterdam. Mardrid. Mexico.: HarperCollins College.

Werner, K. (2003). *Color Atlas and Textbook of Human Anatomy: Nervous system and sensory organs* (5th Revised edition ed. Vol. 3). New York Thieme

Zhang, J., Yoganandan, N., Pintar, F. A., & Gennarelli, T. A. (2005). Temporal Cavity and Pressure Distribution in a Brain Simulant following Ballistic Penetration. *Journal of Neurotrauma, 22*(11), 1335-1347. doi: 10.1089/neu.2005.22.1335

Zhang, J., Yoganandan, N., Pintar, F. A., Guan, Y., & Gennarelli, T. A. (2007). Experimental model for civilian ballistic brain injury biomechanics quantification. *J Biomech, 40*(10), 2341-2346. doi: 10.1016/j.jbiomech.2006.10.021

Zhang, J., Yoganandan, N., Pintar, F. A., Guan, Y., Shender, B., Paskoff, G., & Laud, P. (2011). Effects of tissue preservation temperature on high strain-rate material properties of brain. *J Biomech, 44*(3), 391-396. doi: 10.1016/j.jbiomech.2010.10.024

Zhang, L., Makwana, R., & Sharma, S. (2013). Brain response to primary blast wave using validated finite element models of human head and advanced combat helmet. *Frontiers in Neurology, 4*. doi: 10.3389/fneur.2013.00088

Zhang, L., Yang, K. H., & King, A. I. (2001). Comparison of Brain Responses Between Frontal and Lateral Impacts by Finite Element Modeling. *Journal of Neurotrauma, 18*(1), 21-30. doi: http://dx.doi.org/10.1089/089771501750055749